High Resolution Mass Spectrometry Based Quantification In Metabolomics

Thesis Submitted to AcSIR For the Award of
the Degree of
DOCTOR OF PHILOSOPHY
in Chemical Sciences

By
Dharmeshkumar S Parmar
10CC12A26031

Under the guidance of
Dr. Venkateswarlu Panchagnula

CSIR-National Chemical Laboratory, Pune-411008

Thesis Certificate

This is to certify that the work incorporated in this Ph.D. thesis entitled "**High Resolution Mass Spectrometry Based Quantification In Metabolomics"** submitted by **Mr**. **Dharmeshkumar Parmar** to Academy of Scientific and Innovative Research (AcSIR) in fulfillment of the requirements for the award of the Degree of **Doctor of Philosophy**, embodies original research work under my supervision. I further certify that this work has not been submitted to any other University or Institution in part or full for the award of any degree or diploma. Research material obtained from other sources has been duly acknowledged in the thesis. Any text, illustration, table etc., used in the thesis from other sources, have been duly cited and acknowledged.

_____   _____

Dharmeshkumar S Parmar   Dr. Venkateswarlu Panchagnula

(Student)   (Supervisor)

Place:

Date:

Declaration of Authorship

I hereby declare that this Ph.D. thesis entitled **"High Resolution Mass Spectrometry Based Quantification In Metabolomics"** was carried out by me for the degree of **Doctor of Philosophy** in Chemical Sciences under the guidance and supervision of Dr. Venkateswarlu Panchagnula, Senior Scientist, CSIR-National Chemical Laboratory, Pune, INDIA. I confirm that this work was done wholly by me while in candidature for a research degree at this institution. I also affirm that no part of this thesis has previously been submitted for a degree or any other qualification at this institution or any other institution. Also, the interpretations put forth are based on my knowledge and understanding of the original research articles and all resources and researchers have been duly cited and acknowledged as and when appropriate.

Place:
Date:

Dharmeshkumar S Parmar
CEPD Division
CSIR-National Chemical Laboratory

Foreword

Metabolic profile of a system collectively reflects the phenotypic expression resulting from a complex interplay of genetic, epigenetic, nutritional, and environmental factors along with exposure to various stresses. In the post genomic era, mass spectrometry (MS)-based approaches have become the mainstay in metabolomics research contributing significantly to the fundamental understanding of disease biology, diagnostics and therapy. MS-based metabolomics complements genomic and transcriptomic data towards integrative systems-based understanding and predictive modelling. Concurrently, the increasing use of MS in clinical metabolomics, and as a complementary tool for diagnostics have begun demonstrating the prowess of MS in impacting early disease prediction and patient care.

Over the past decade, high resolution mass spectrometry (HRMS) has been the most significant instrumental advancement that has revolutionized bioanalysis and continues to carve a niche in metabolomics analysis. HRMS is capable of separating analyte ions with high mass accuracies (up to the fifth decimal exact mass) whereas low resolution triple quadrupole (QqQ) MS is limited to unit mass resolution. A single HR full-scan analysis provides far more detailed metabolic profiles in comparison to conventional lower resolution analysis. This has made comprehensive metabolic profiling of complex biological system a possibility.

HR-accurate mass (HR-AM) quantitation is steadily gaining acceptance for comprehensive qual/quant metabolomics analysis. This is a departure from existing approaches where a HRMS qualitative analysis is generally followed by a QqQ MS quantitation with a smaller scope using selected single or multiple ion monitoring schemes. However, LC HR-AM methodologies are process intensive and few studies have explored the breadth of complexities involved for use in metabolomics. Specifically, the performance evaluation of LC HR-AM analysis over an extended metabolomics workflow execution, as is usually the case in indepth metabolomics studies has not been examined before.

In this dissertation, aspects of LC HR-AM MS methods have been investigated from metabolomics contexts using specific mammalian and microbial model systems. Firstly, the analytical robustness of LC HR-AM MS was evaluated for estimating the metabolic consumption and release (CORE) profiles in two sub populations of glioblastoma at various drug concentrations. Thereafter, hydrophilic interaction liquid chromatography (HILIC) coupled to HRMS as a method was demonstrated for two separate systems respectively for relative metabolic profiling and tracing intracellular polar metabolites using stable isotope labelling (SIL). The final part of the dissertation highlights the translational aspects of LC-HRMS and chromatography-free MS for the determination of isomeric dimethyl arginines (DMA) from diabetic urine samples.

This thesis is dedicated to my parents,

Who shared every tough terrain I chose to travel upon.

For their ceaseless patience and support,

Which in spite of arduous times remains unwavered.

Acknowledgement

"Il a fallu se battre, mais on a fini par y arriver."

(Translation: It was a battle, but we managed in the end.)

Abbreviations

ADMA	Asymmetric Dimethylarginine
AGC	Automated Gain Control
AP-MALDI	Atmospheric Pressure-MALDI
ASR	Asymmetric To Symmetric Dimethylarginine Ratio
ATCC	American Type Culture Collection
BCAA	Branched Chain Amino Acids
CHCA	2-Cyano-4-Hydroxycinnamic Acid
CI	Chemical Ionization
CID	Collision Induced Dissociation
CKD	Chronic Kidney Disorders
CMS	Colony Mass Spectrometry
CVD	Cardiovascular Disease
DART	Direct Analysis In Real Time
DDAH	Dimethylarginine Dimethylamino Hydrolase
DE	Delayed Extraction
DESI	Desorption Electrospray Ionization
DHB	2,5-Dihydroxybenzoic Acid
DMA	Dimethylarginine
EI	Electron Impact
ESI	Electrospray Ionization
ESRD	End-Stage Renal Diseases
FA	Formic Acid
FAB	Fast Atom Bombardment
FDA	Food And Drug Association
FWHM	Full Width At Half Maxima
G3P	Glyceraldehyde-3-Phosphate
GC	Gas Chromatographyxiv
GFR	Glomerular Filtration Rate
HPLC	High Performance Liquid Chromatography

HRMS	High Resolution Mass Spectrometry
IGT	Impaired Glucose Tolerant
IR	Infra-Red
LB	Luria Bertani
LC	Liquid Chromatography
LOD	Limit Of Detection
LOQ	Limit Of Quantitation
m/z	Mass To Charge Ratio
MA	Mass Accuracy
MAC	Macroalbuminuria
MALDI	Matrix-Assisted Laser Desorption/Ionization
MAP	Mass Accuracy Precision
MAV	Mass Accuracy Variability
MEW	Mass Extraction Window
MIC	Microalbuminuria
MMA	Methylmalonic Acid
MRM	Multiple Reaction Monitoring
MS	Mass Spectrometry
MS/MS	Tandem Mass Spectrometry
Nd:YAG	Neodymium-Doped Yttrium Aluminium Garnet
NDD	Newly Diagnosed Diabetic
NGT	Normal Glucose Tolerant
NMR	Nuclear Magnetic Resonance
NO	Nitric Oxide
NOS	Nitric Oxide Synthase
PCA	Principal Component Analysis
PEG	Polyethylene Glycol
PLS-DA	Partial Least Squares-Discriminant Analysis
PPM	Parts Per Million
PRMT	Protein Arginine Methyl Transferases

PSD	Post-Source Decay
QC	Quality Control
Q-TOF	Quadrupole-Time Of Flight
RSD	Relative Standard Deviation
S/N	Signal To Noise Ratio
SA	Succinic Acid
SD	Standard Deviation
SDMA	Symmetric Dimethylarginine
SIM	Selected Ion Monitoring
SRM	Single Reaction Monitoring
TCA	Tricarboxylic Acid
TFA	Trifluoroacetic Acid
THAP	2',4',6'-Trihydroxyacetophenone
TOF	Time Of Flight
UHPLC	Ultra-High Performance Liquid Chromatography
UV	Ultraviolet
XIC	Extracted Ion Chromatogram

Note: Nomenclature of amino acid in the dissertation is according to IUPAC and IUB guidelines.

TABLE OF CONTENTS

LIST OF FIGURES

LIST OF TABLES

Chapter 1

Introduction

1.1 Metabolomics, its analytical challenges, and high-resolution mass spectrometry

Metabolites are low molecular weight (< 1500 Da) molecular components that represent the phenotypical expression of functional machinery in a biological system.[1–4] Metabolomics – the study of a collection of systemic metabolites - provides crucial insights into the state and dynamics of a system under consideration. Metabolomics has a wide gamut of current and potential applications in diverse fields such as healthcare (clinical and pharmaceuticals), nutriomics, industrial biotechnology, biofuels, ecological and plant research. For example, metabolomics in clinical investigations holds immense potential for understanding disease, its progression, identification of biomarkers, establishing standards for diagnosis, development of therapeutic interventions and finally addressing therapeutic challenges in patient care through personalized medicine.[5] Study of biological modification in various disease states allows us to explore and understand the dynamics of molecular change with respect to etiology and epidemiology. So far different biomarkers have been identified and assigned to diagnose diseases like diabetes, hypertension, cancers, kidney dysfunction, neurological diseases, tuberculosis and oxidative stress in multiple disease states.[6–9] Metabolomics investigations can be broadly classified into targeted or untargeted approaches. These approaches are governed by fundamental knowledge of the biological system and aim of the study. The untargeted approach is usually a comprehensive and global search for a wide range of metabolic features. Untargeted metabolomics can be used to attain a broader view of metabolic changes in response to disease, environmental or genetic perturbations. Various algorithmic and database resources such as software such as XCMS, MetaboAnalyst, MZmine, MAVEN, AMDORAP are available for aiding untargeted metabolomics analysis.[10–16] Often, the untargeted analysis is followed by targeted profiling for more confident quantitation of relevant metabolites.[17] The targeted approach focuses on the analysis of the predefined list of metabolites pertaining to specific groups such as chemical class, interconnected pathways or unique metabolite(s).[18,19] Targeted analysis is often used for quantitative measurement of specific metabolites using calibration curves from metabolite reference standards and/or isotopically labelled standards. Instrumental analytical approaches and methods to accurately detect and quantitatively measure metabolites are of paramount importance in metabolomics pursuits.

There are several levels of complexities involved in the analysis of metabolomics samples. In samples of biological origin, analyte(s) of interest coexist with a large number of compounds with distinct chemical properties, often referred to as a matrix. Biological matrices influence various stages of sample preprocessing and analyses.[20] Inefficient extraction, ion suppression/enhancements, and interferences from background signals are the key influences of matrices.[21,22] These contributions make detection, qualification and/or quantification, a challenging task. This is even more evident in metabolomics as the comprehensive metabolome consists of hundreds of metabolites that could be present within relatively narrow molecular weight regions. Unlike proteins that are made up of repetitive units, metabolites are structurally unique molecules with vast chemo diversity. It is also noteworthy that many metabolites undergo biotransformation, susceptible to environmental degradations and are extremely difficult to detect owing to their complexation with bio-macromolecules. Limited availability of synthetic standards further contributes in reducing the odds of identification and confirmation of many classes of metabolites. Metabolites often manifest in diverse abundances, making a direct simultaneous measurement challenging.[23] Therefore, optimization of the analytical methodologies is essential in order to distinguish between the analyte and background signal for reliable and accurate measurements of metabolites. Evidently, the efficiency of an analytical instrument to distinguish between closely related analyte – analytical resolution - constitutes a factor of primary interest for analysts in various fields with metabolomics applications.

Various chromatographic and electro-separation techniques have traditionally been used for analytical resolution of metabolites from complex biological samples. These have been extensively used in tandem with mass spectrometry (MS), and occasionally with nuclear magnetic resonance (NMR) to resolve metabolites from each other as well as from background matrix signals.[24–33] Hyphenated and tandem analytical methodologies have proven to be promising in many applications as they offer synergistic advantages of both dimensions. Advancements in separation science that include development of novel stationary phases, new ultra-high pressure liquid chromatography systems, minimization of batch to batch variability of columns and introduction of microfluidic separations have significantly enhanced the bioanalytical toolbox in general and mass spectrometry-based metabolomics, in particular.[34,35] In spite of the significant progress in the analytical methodologies, there is still scope for improvement towards accurate and reliable assessment of individual metabolite(s) and of

comprehensive metabolome from a biological system. Further explanation on reversed phase and hydrophilic interaction chromatography has been provided in the latter part of this chapter.

Mass spectrometry is a separation technique, in gas phase albeit, capable of achieving significantly higher separation efficiencies than liquid/gas phase chromatography. MS instrumentation has undergone significant evolution in the last two decades with highly efficient and soft ionization sources, various combinations of precise mass analyzers, and most prominently accompanying algorithmic advancements. Electrospray (ESI)[36–38] and matrix-assisted laser desorption ionization (MALDI)[39–41] among ionization sources, and time-of-flight (TOF)[42,43] and Orbitrap®[44–46] among high-resolution mass analyzers (HRMS) are prominent in this regard. These developments have broadened the areas of application of MS as trace level metabolites can be accurately and efficiently measured with high throughput and sensitivity.[47,48] HRMS has revolutionized metabolomics research (witnessed in the duration of this dissertation work) and is now being used on a large scale. A mass spectrometer that offers a resolution of more than 10,000 FWHM is considered as HRMS. Currently available HRMS analyzers include furrier-transform ion cyclotron resonance (FT-ICR), TOF, and Orbitrap®. Resolution more than 200,000 FWHM is achievable with Orbitrap and FT-ICR HRMS.[49,50] Apart from major applications in qualitative analysis like metabolite identification and structure elucidation, latest HRMS instrument possesses desirable specifications such as high scan speed compatible for LC-MS, wide dynamic range and MS/MS capabilities essential for any quantitative metabolomics investigations.

In conventional workflows, liquid chromatography (LC) coupled with unit resolution triple quadrupole (QqQ) MS has been the most preferred platform for quantitative analysis. There were two main reasons behind the success of LC-QqQ MS. First, the ability of chromatography technique to retain analyte and elute them based on polarity provided primary separation and reduced the complexity of analytes being injected into MS. The highly specific, sensitive, and reproducible monitoring of precursor to product transition using MS/MS, was the second. At present, QqQ-based quantitation using selective precursor-to-product ion monitoring, for single or multiple ions (SRM and MRM), is generally accepted as an industry gold standard by regulatory agencies in food and pharma industry. However, QqQ MS can only generate low-resolution data, which poses significant limitation for discovery metabolomics.[51] For high specificity, it requires monitoring of individual molecular transitions (single/multiple reaction monitoring) during the analysis. Also, the maximum number of ion

transition that can be monitored within a chromatographic peak lasting for few seconds is limited.[52] This places a major constraint on the total number of molecules that can be analyzed in a given sample through a single analytical run, significantly limiting the 'systems level' metabolic measurements.[53]

High-resolution mass spectrometry (HRMS), largely used only for qualitative metabolomics analysis, on the other hand, overcomes the limitations of conventional QqQ MS. HRMS-based analysis, with simultaneous qualitative and quantitative (Qual/Quan), is a viable alternative to QqQ MS (or TQ MS). Various groups have evaluated the quantitative performance of HRMS against TQ MS as a standalone platform for analyzing samples belonging to a diverse set of matrices such as mammalian tissue (kidney)[54], honey,[55,56] urine, rat and human plasma,[31,57–60], dried blood spots[61], hair[62], food[63–65]. It was observed that the sensitivity of MS/MS is better only if small numbers of analytes are being monitored. This occurs mainly because of reduction in the dwell time per analyte with an increase in the number of ions monitored. HRMS (especially the Orbitrap®) was found to be more sensitive in monitoring a large number of compounds in a full-scan mode. Additionally, the HRMS method was found to be more generic and applicable to all reproducibly detected compounds for untargeted profiling of samples. But an era of full-fledged utilization of HRMS for qual/quant analyses is yet to come.

Accurate mass HRMS metabolomics analysis (HR-AM) in most biological model systems, as well as clinical specimens, encounter significant process complexities. These have neither been fully evaluated nor optimized with a process analytical perspective. Field or clinical translation of important outcomes of discovery metabolomics presents further scale-up challenges as well. In certain scenarios to validate established metabolite disease markers, direct HRMS or HR-AM devoid of chromatographic front end might be a viable alternative for larger-scale clinical validation. This again remains relatively unexplored.

This thesis explores the use of HRMS based qualitative and quantitative analysis for specific biological and translational applications with a focus on the performance evaluation and analytical process optimization. The *introductory chapter* provides an overview of mass spectrometry instrumentation, various aspects and MS terminologies relevant to metabolomics and a general description of the methodology that forms the basis of the remaining chapters. *Chapter two* describes the method development and performance evaluation of accurate mass – extracted ion chromatogram (AM-XIC) based targeted metabolomics analysis in a model

mammalian cell culture system. In this, the analytical robustness of the LC HR-AM analysis workflow to profile consumption and release of metabolites from differentially expressed sub-populations of glioblastoma cell cultures with various sampling time points and anti-cancer drug concentrations was evaluated. *Chapter three* describes the use of hydrophilic interaction liquid chromatography (HILIC) in combination with HR-AM analysis for profiling of polar intracellular metabolites. Metabolic changes in *Chromobacterium violaceum (CV)* between wild-type and two adapted laboratory evolution (ALE) developed chloramphenicol resistant (ChlR) and streptomycin resistant (StpR) strains were investigated (3A). In the subsequent section, an extension of HILIC HR-AM analysis to ^{13}C-glucose labeled polar metabolites from Chinese hamster ovary (CHO) culture is described (3B). *Chapter four and five* describe the evaluation and translational application of chromatography free HRMS analysis. These chapters demonstrates the application of MALDI HR-AM analysis for the determination of isomeric dimethylarginine ratio from diabetic urine samples in a clinical study involving 555 individuals.

1.2 Overview of mass spectrometry

Mass spectrometry is an analytical technique capable of distinguishing ions based upon mass to acquired charge ratio (*m/z*). A mass spectrometer mainly consists of four different parts namely (i) sample inlet (ii) ionization source, (iii) analyzer, and (iv) detector. A schematic representation of a mass spectrometer is portrayed in figure 1.1. In the first step, the sample inlet is used to introduce the sample, from a chromatograph or a direct insertion probe or crystallized bed of matrix as per the ionization technique employed in the analysis. Subsequently, an ionization source ionizes the chemical moieties present in the samples, eventually producing gas phase ions from the sample. After ionization, the ions are directed into the analyzer, where they are separated based on mass to charge ratio (*m/z*). In a contemporary mass spectrometer, a single or multiple mass analyzers in combination are being used are used to separate the ions. Finally, ions are detected by a detector, and a processing system produces the mass spectrum as a plot of ions and their respective intensities.
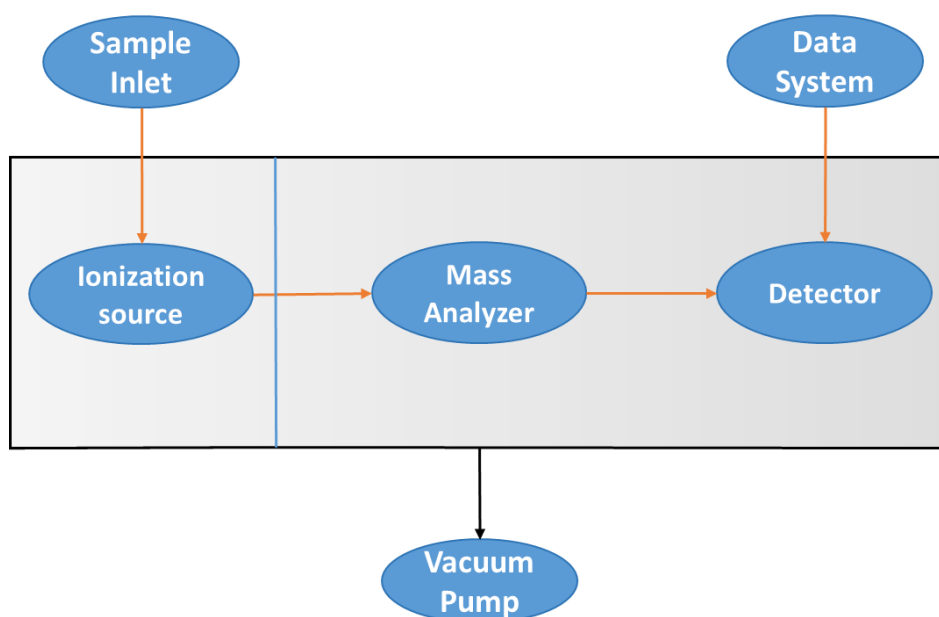
Figure 1.1 Schematic of the mass spectrometer

1.2.1 Ionization source

The instrumental part used to generate ions is called an ionization source. A variety of commercial ionization techniques are available for use in mass spectrometry. The most commonly used ionization sources are electrospray ionization (ESI), matrix-assisted laser desorption ionization (MALDI), electron Ionization (EI) and chemical ionization (CI).[66] EI, which generates ions using a beam of high energy electrons, is only suitable for gas-phase ionization and thus, its use is limited to ionize compounds that are sufficiently volatile and thermally stable. EI also causes substantial fragmentation as a result of high energy electrons.[67] A CI source produces ions through a collision of the analyte molecule in the gas phase with primary gaseous ions present in the ionization chamber.[68] The commonly used gases in chemical ionization are methane, ammonia, and isobutene.[69,70] MALDI and ESI are two soft ionization techniques, preferably used in metabolomics and proteomics research, are described in details in following paragraphs.

1.2.1.1 Electrospray ionization

Electrospray ionization, more commonly referred as ESI, is a liquid phase ionization technique operating at atmospheric pressure. The schematic of ESI has is represented below in

figure 1.2. Electrospray ionization is obtained by applying a high electric potential (up to 8 kV) on capillary through which the liquid containing analyte is flowing.[36,38] The electric potential induces charge accumulation on liquid surface passing through capillary. Liquid leaves the end of the capillary forming a Taylor's cone, which subsequently breaks into the highly charged droplets. A gas injected coaxially allows the dispersion of the droplets in a limited space. These droplets then passes through a sheath of heated inert gas, most often nitrogen, to vaporize and remove solvent molecules.[71] The process of evaporation ends up generating a singly/multiply charged analyte ion that are introduced into MS using a capillary inlet.[72] The accumulation of charge on an ion is governed by the polarity of solvent, surface area, and proton affinity of analyte.[37] Formation of multiply charged ions is advantageous as it enables the analysis of high-molecular weight ions using analyzers with a lower *m/z* scan range.
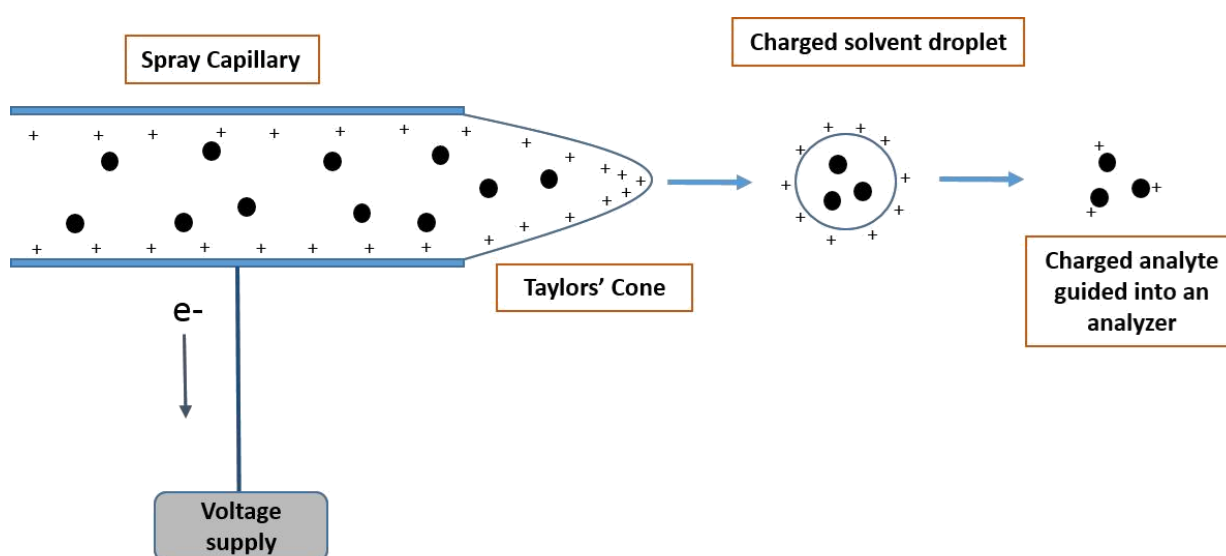
Figure 1.2 Schematic representation of an electrospray ionization (ESI) source

1.2.1.2 Matrix Assisted Laser Desorption/Ionization (MALDI)

Matrix Assisted Laser Desorption/Ionization, uses a laser as a source of energy to produce gaseous phase ions (Figure 1.3). Generally, a UV or IR laser is used in the process.[73,74] Many molecules do not possess chromophores for UV absorption. Therefore, UV absorbing small organic acids commonly known as "MALDI matrix", are used to facilitate desorption/ionization process. The most commonly used MALDI matrices are 2,5-

dihydroxybenzoic acid (DHB), α-cyano-4-hydroxycinnamic acid (CHCA), sinapic acid or sinapinic acid (SA), 2′,4′,6′-trihydroxyacetophenone (THAP), and 9-aminoacridine (9AA). For analyses, the matrix solution is either premixed or applied in layer-by-layer pattern with sample solution on a stainless steel plate, known as "MALDI target plate". Post application the spots are allowed to dry. Drying process leaves a bed of matrix crystals containing sample molecules on the plate. Subsequently, the plate is placed in the ionization source chamber and subjected to repetitive laser shots. Exposure to laser generates singly charged ions.
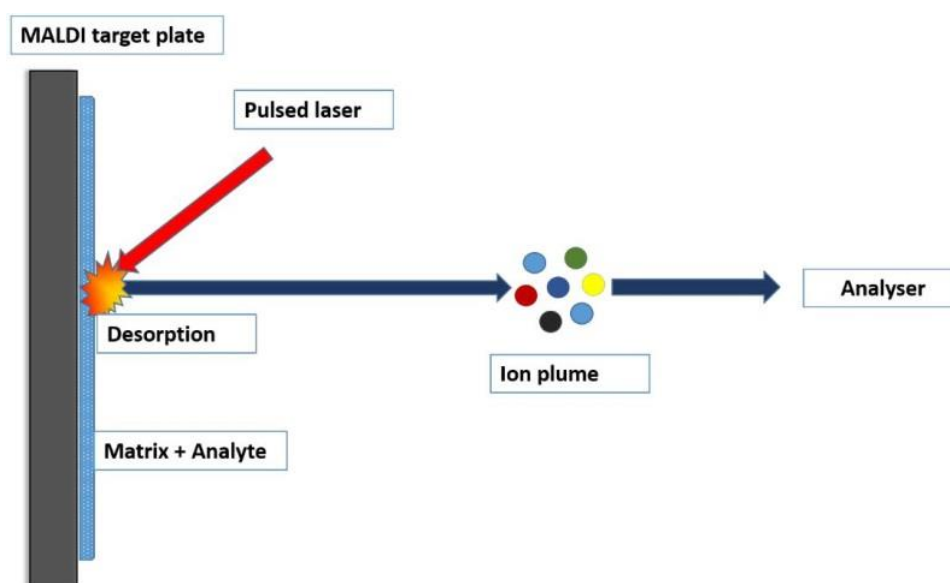
Figure 1.3 Schematic representation of matrix-assisted laser desorption/ionization (MALDI).

The exact mechanism of desorption and ionization is not yet fully understood, but several theories are available explaining the possible underlying mechanism in ionization.[75,76] MALDI is a sensitive ionization technique, which is high-throughput in nature and has a high tolerance to salts, buffers, and detergents. MALDI can be operated in both vacuum and atmospheric pressure conditions.

1.2.2 Mass analyzers

After the ions are produced by ionization source, the charged gaseous plume is pushed into the next part of the mass spectrometer, an analyzer. Using an analyzer, the ions are separated based upon their mass to charge (m/z) ratio rather than their masses alone. Hence, a multiply charged ions' effective mass in terms of m/z will be a fraction of its original mass

according to its charge state.[66] Several mass analyzers have been developed based upon various principles of discriminating ions from each other according to *m/z*. All analyzers use either electric or magnetic field or both in combination to discriminate between the ions. The ability of an analyzer to distinguish between ions is called as resolving power. As mentioned earlier, use of the electric or magnetic field is an essential requirement for the analyzer to work. In practice, it is very difficult to generate and maintain a spatially uniform magnetic field. Hence, uses of electric field based analyzers have gained popularity over magnetic field based sector analyzers. Most widely used analyzers in mass spectrometry namely, quadrupole, time of flight (TOF) and Orbitrap™ analyzer are explained here in details.

1.2.2.1 Quadrupole mass analyzer

Quadrupole, as the name suggests, is an analyzer consisting of four poles made of conducting rods. The four rods are of circular or hyperbolic geometry placed in parallel alignment with perfectly similar dimensions (figure 1.4a). Each pair of oppositely aligned rods is connected to a DC voltage of opposite polarity. Ions are made to travel in an axis passing right through the quadrupole.[77] Additionally, an AC voltage is superposed over the constantly applied DC voltage. This causes ions passing through quadrupole to oscillate. A voltage ratio between DC and AC potential determines the stability of the path. A representation of the relationship between the stability of path and the applied voltage is given below in figure 1.4b.
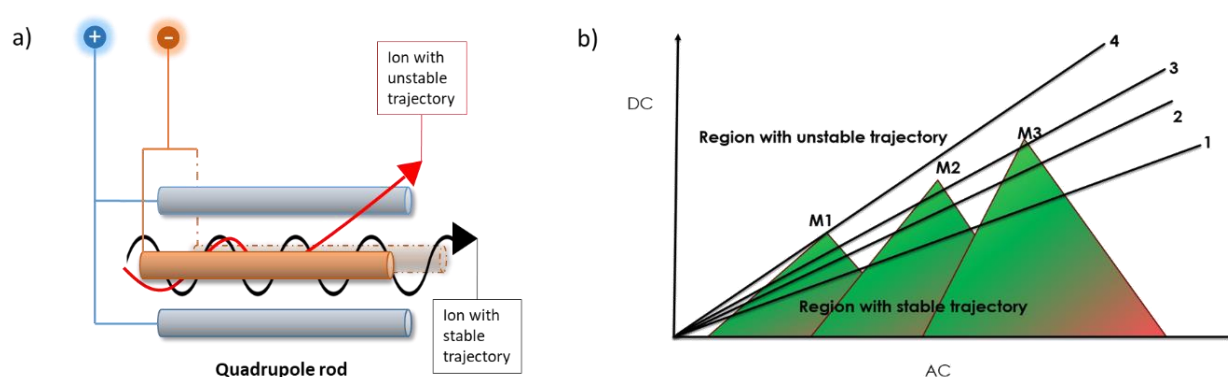
Figure 1.4 a) Schematic representation of quadrupole analyzer and ion trajectories; b) Stable trajectory areas for ions with different masses (M1<M2<M3) as a function of DC and AC voltage.

During scanning, the oscillating voltage resonates the ions. While passing the poles, lighter and heavier ions hit the rods because of the unstable trajectory, determined using Pauls'

and Mathews' equations.[78] According to their equation of trajectory, the relation between DC and AC determines the stable trajectory of an ion. Changing DC linearly as a function of AC, we obtain a straight operating line that allows us to observe those ions successively. A line with a higher slope would give us a higher resolution, so long as it passes through the stability areas. Changing DC and AC voltage along of the operating line (1, 2, 3, and 4) enables a stable trajectory for selected ions with variable resolution and ion intensities. Quadrupole mass spectrometer offers "unit resolution" i.e. it can effectively distinguish two peaks with at least 1 Da mass difference between them.[79] The resolution normally obtained is not sufficient to deduce the elemental composition. Despite low resolution offered by quadrupole mass analyzer, it's popular because of selectivity it offers in triple-quadruple setup via various reaction monitoring schemes. It can simultaneously monitor transition of one or more ions through single reaction monitoring (SRM) or multiple reaction monitoring (MRM), respectively. In these schemes, first and third quadruple acts as ion filter, while the second quadruple performs the collision-induced dissociation (CID).

1.2.2.2 Time of flight (TOF)

The TOF analyzer separates ions based upon the time taken to travel from one end to another end of a tube in a free-field region, called a flight tube (Figure 1.5). The ions are uniformly accelerated by an electric field. This process occurs in bundles of ions. Because of uniform acceleration, all ions acquire the same kinetic energy. However, because of the difference in their masses, they exhibit different acceleration and velocities. This can be explained by the equation of kinetic energy mentioned below.

$$E = \frac{1}{2}.mV^2$$

Where, E represents Kinetic energy; M is mass of the ion, and V is velocity. The lighter ions (lower *m/z*) acquire higher velocity as compared to heavier ions (higher *m/z*). Therefore, the lighter ions require less time to travel to another end of the flight tube as compared to heavier ions.[42] Time taken to reach from one end of flight-tube to another end is correlated with the mass to generate the ion profiles. The TOF analyzer offers high-resolution power as compared to previously described quadrupole mass analyzers.[53] Further, the resolution is improved in proportion to the flight distance, which is theoretically doubled by using the analyzer in reflector mode. Virtually, the upper mass range of a TOF instrument has no limit.[43]

This makes it especially suitable for analyses of molecules with high masses up to 300,000 Da.[80]

1.2.2.3 Orbitrap mass analyzer

Orbitrap® mass analyzer is based on the principle of ion trapping technique.[45] It utilizes electrostatic field for trapping ions in small space between a central and peripheral/coaxial cylindrical electrode. Ions are injected into the Orbitrap from an offset to its equator using a voltage potential at the inlet end. Once ion pack enters the Orbitrap, under the influence of the electric field applied by two electrodes, they start coherent axial oscillations. This rotational motion around central electrode is balanced in terms of centrifugal and centripetal force, for all the ions irrespective of their masses.[44] Schematic of Orbitrap mass analyzer is provided in figure 1.6.
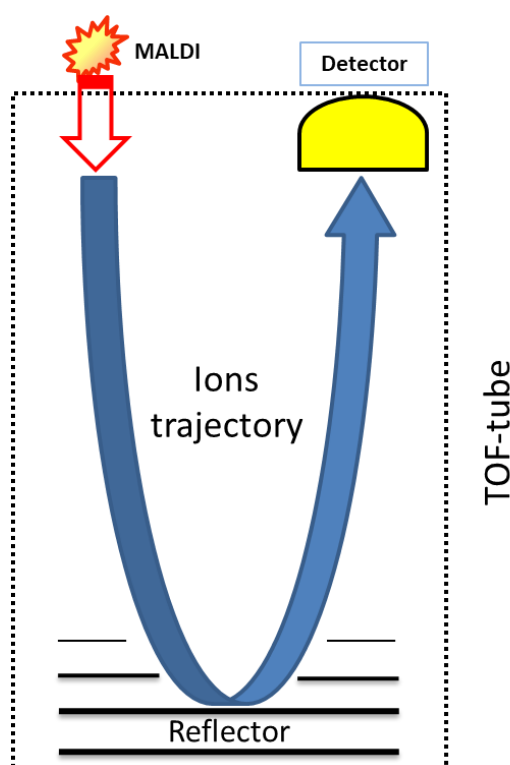
Figure 1.5 Schematic representation of TOF analyzer (reflector mode).The ions are generated using an ionization source, such as MALDI and guided into TOF-tube. TOF-tube is a field-free drift region with mean free path equivalent to length of the tube. The analyzer can be operated in linear and reflector mode (showcased here). The distance travelled in reflector mode is double the distance in linear mode. Reflector mode provide higher resolution as compared to linear mode.
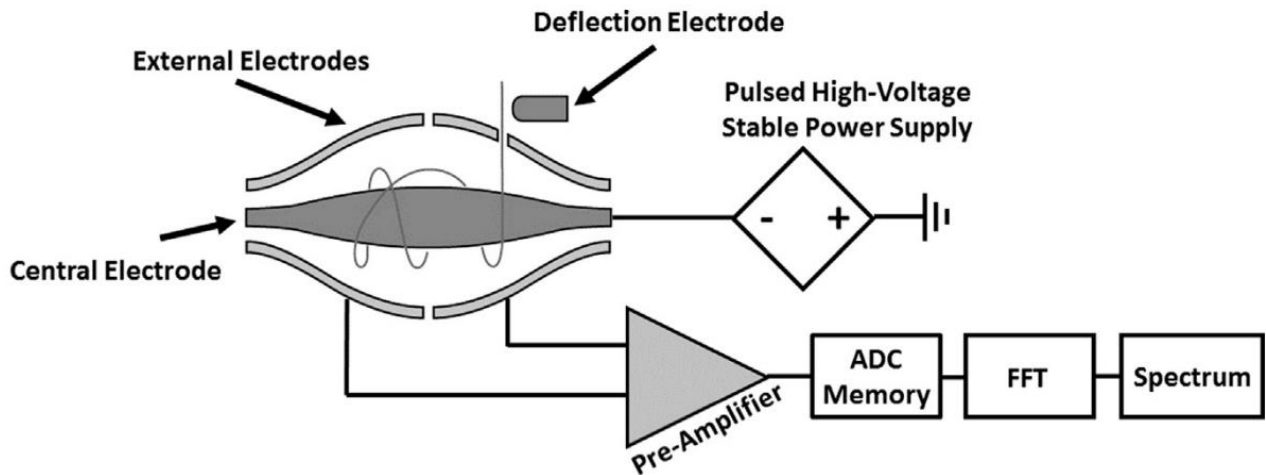
Figure 1.6 Schematic representation of Orbitrap mass analyzer (reproduced with permission from Briois et. al., Planetary and Space Science 131 (2016) 33–45)

Initially, when an ion packet enters the Orbitrap, the kinetic energy of ions is poorly matched with the radial electrical field component. Because of this, ions follow a random non circular orbit around the central electrode for initial few hundred revolutions. In subsequent revolutions, ions align themselves in eccentric motion circles around the central electrode, matching closely to a doughnut shape.[81] During this period of each ion align itself to a nearly circular path with different radii. The radius is a factor of *m/z* of an ion. According to the equation of a centripetal force, mentioned below, ions with higher *m/z* tends to acquire larger radius whereas ions with small *m/z* have relatively smaller radius. The maximum radius of ion trajectory is controlled by the outer cylindrical electrode to avoid loss of ions.

$$W_z = \sqrt{\frac{K}{m/z}}$$

Where W_z is a frequency of oscillation, K is field curvature and *m/z* mass by charge ratio.[82]

In terms of angular velocity with respect to the centripetal force, lighter ions move with higher angular velocity than heavier ions. The radius of circular motion and angular velocity determines the frequency of rotation of an ion in an Orbitrap. An ion follows the motion along the axial electrode from one half of Orbitrap to another. Movement from one half of the outer electrode to the other generates an image current, thus creating a signal that is detected by

differential amplification and Fourier transform. Because each ion has characteristic velocity and axial movement, ions can be differentiated from each other with a high degree of specificity. This provides the basis of high resolution offered by Orbitrap mass analyzer. A comparison of mass resolution offered by various instruments is provided in table 1.1.

Table 1.1 Currently used HRMS instruments[83]

Instrument type	Mass Range (m/z)	Resolution (in thousands, FWHM)	Mass accuracy	Manufacturers
TOF	Upto 20000	10-20	<3ppm	AB Sciex, Agilent, Bruker-Daltonics, Waters, Leco, Perkin-Elmer. Shimadzu
Q-TOF	Upto 60000	15-40	<3ppm	AB Sciex, Bruker-Daltonics, Waters, Agilent,
Q-Orbitrap®	50-6000	35-140	<1ppm	Thermo Fisher Scientific
LTQ-Orbitrap XL™	50-4000	7.5->100	<1 ppm	Thermo Fisher Scientific

1.2.3 Analytical significance of resolution, mass accuracy and mass extraction window (MEW)

1.2.3.1 Mass resolution

Mass resolution is an outcome of resolving power of a mass spectrometer, expressed as [m/Δm]. Higher the resolution more efficient is the separation between the ions with smaller mass difference. Table 1.1 and 1.2 represents a range of resolution offered by an instrument and amount of information which is accessible through it, respectively. High resolution offered by HRMS can resolve interference observed in case of nominally equal masses, as compared to a low-resolution quadrupole instrument where it is necessary to identify and track diagnostic product ion for qualification and/or quantification. HRMS such as Orbitrap® can accurately measure *m/z* with less than 2 ppm error. Such high mass accuracy drastically reduces the number of possible chemical formulae to be assigned to the observed ion.[84,85] Thus, higher mass accuracy enables assignment of molecular formula and consequent database search.

Higher resolution also offers better ground for identification or characterization of analytes as it removes the interference of closely related molecules and reduces the chance of false positive or false negative result.[86]

HRMS can accurately measure the *m/z* values up to 6 decimals. In such cases, it is essential to use exact masses (monoisotopic) in order to avoid errors in identification.[53,63,81] Figure 1.7 represents the role of resolution in the analysis of benzophenone. At 50,000 FWHM benzophenone is resolved from an unknown interfering peak.[87] Mass analyzers which offer >10,000 units of resolution are considered as high-resolution mass analyzers. Fourier transform ion cyclotron resonance (FT-ICR), Reflector-time of flight (TOF) and Fourier transform Orbitrap are high-resolution mass analyzers used in today's scenario. These are compatible with Electrospray ionization (ESI), matrix-assisted laser desorption (MALDI) and other atmospheric direct ionization sources. They are also available with a quadrupole and/or ion trap (IT) at preface as Q-TOF or Q-orbitrap or Q-IT-Orbitrap, which acts as mass filters for initial screening of ions.

HRMS instruments can be operated at various mass resolutions. However, the choice of appropriate operational resolution is dependent on the differences of *m/z* values between two ions. Minimum resolution or R_{min} is resolution required to separate two closely spaced ions. This is of practical significance especially when the two analytes have a very small difference in exact masses.

Table 1.2 Resolution and its potential implications in the metabolomics analysis.

Resolution	Outcome	Inference
Unit resolution (Quadruple)	Separation of ions with a mass difference of one Da and unit charge	Isotopic peaks can be differentiated
>10,000 FWHM (ion trap, TOF)	Separation of ions with mass difference up to three decimal points (mDa)	Analytes with mDa mass differences can be distinguished
>100,000 FWHM (Orbitrap, FT-ICR)	Separation ions with less than 1 mDa differences	Isolation of nominally isobaric analytes

For example, among the amino acids, hydroxyproline and leucine have *m/z* of 132.06552 (m_1) and 132.10191 (m_2) respectively. The formula to calculate R_{min} is as follows.

$$R_{min} = 2 \times \frac{m_1}{m_1 - m_2}$$

Which returns R_{min} for these amino acids as 7000 FWHM. Whereas pipecolic acid (*m/z* 130.08626) has an isotopic peak at 132.09050 and to resolve hydroxyproline from potential interference from the isotopic peak, R_{min} of 23,000 FWHM is necessary.[85]
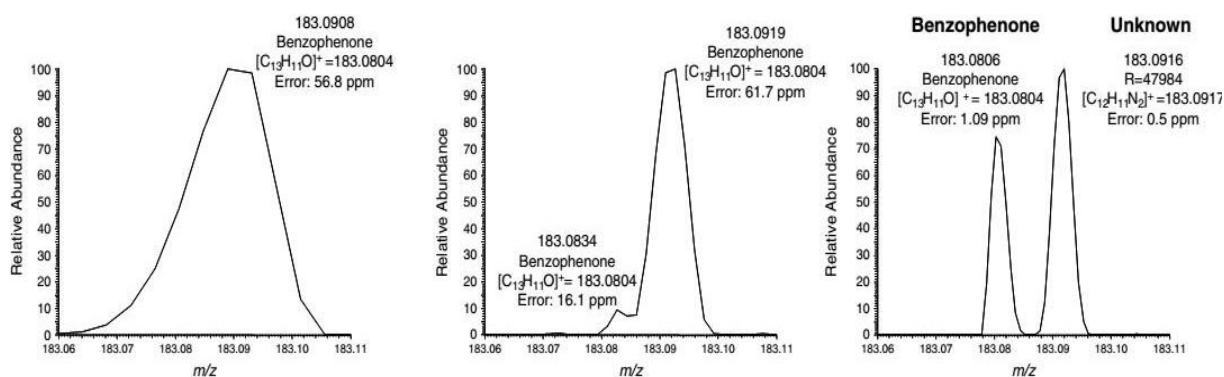
Figure 1.7 sample analyzed by LC/HRMS at three different mass resolving powers: (A) 10 000 FWHM, (B) 25 000 FWHM, and (C) 50 000 FWHM. *(Reproduced with permission from H. Gallart-Ayala et. al. Rapid Commun. Mass Spectrom. 2011, 25, 3161–3166)*

1.2.3.2 Mass accuracy

Mass accuracy is closeness to correct mass value generated using exact masses of each element present in the compound. It is essential to have high mass accuracy or low mass error in order to avoid any false positive or false negative identification.[87,88] Therefore, periodic calibration of the instrument using a set of standards (with *m/z* in working ranges) is crucial in generating reliable data with acceptable accuracy and precision. In order to maintain a constant state of accurate mass measurement, few systems also provide an in-line infusion of calibration standards along with sample runs.

There are various parameters that influence the accuracy of MS. These include, the temperature of the instrumental facility, instrument temperature (internal), calibration interval, and purity of calibration standards. Among these, room temperature is an external parameter, and should be regularly monitored to achieve consistent mass accuracy, post calibration. Rochat *et. al.* reports the impact of room temperature on the accurate mass measurement of caffeine using HRMS.[89]

1.2.3.3 Mass extraction window (MEW)

Analyte specific information from a high-resolution full-scan data (total ion chromatogram) is represented by the construction of an accurate mass – extracted ion chromatogram (AM-XIC). XIC is generated using a narrow window around theoretical *m/z* known as mass-extraction-window (MEW).[20,89,90] MEW is carefully selected based on mass accuracy, mass resolution, and mass accuracy precision (MAP) to avoid any false positive or false negative outcomes. It is advisable to consider the fixed width at half maximum (FWHM) of *m/z* peak before selecting a window of extraction, as the wider window more than FWHM may lead to false positive results. Also, the too narrow window should be avoided as in case of shifts in MA may lead to false negative results. MEW can be chosen as an absolute window around the mass (+/-mDa) or relative to *m/z* as ppm. As a general correlation with the increase in resolution FWHM decreases, so is the MEW. Typical MEW values for different resolution is mentioned below in table 1.3.[87,91,92]

Table 1.3 Mass resolution and corresponding MEW

Sr. No	Resolution @ 200 *m/z*	Absolute MEW (mDa)	Relative MEW (ppm)
1	10,000	25-50	25-50
2	25,000	25-10	25-10
3	50,000	10-5	10-5
4	>75,000	<5	<5

1.2.4 Difference between data acquisition schemes of quadruple Vs HRMS analyzers

HRMS application in the field of clinical and biological research has been restricted to qualitative analyses, while quadrupole analyzers have been extensively used in day to day quantitative analyses. This was owing to the reproducible ion transition monitoring and fast scanning speeds. Triple-quadrupole (TQ) has been proven excellent for single reaction monitoring (SRM) as well as multiple reaction monitoring (MRM) with good reproducibility and high sensitivity. SRM/MRM carried out using three quadrupoles in series (QqQ), where quadrupole at each end acts as a mass filter (ion selection in narrow *m/z* window), while one in the center acts as a collision cell. Because of the above mentioned desirable attributes, LC-TQ MS has entered most clinical research and industrial setup. Analysts have been rigorously

trained on LC-TQ MS instruments on setting up the precursor to product ion transition(s) using standards and perform quantitative assay. Thus, LC-TQ MS has become the gold standard in quantitative analysis analysis.

On the other hand, HRMS instrument generates a full-scan high-resolution spectra. The data is represented as total ion chromatogram (TIC), which is a plot of total ion count of every single acquisition versus time or scan number. A single full-scan contains the details of all detected ions in terms of *m/z* values and their respective intensities. Data of each individual ion can be further extracted using MEW to generate AM-XIC and peak area can be determined.[89,93,94] since the introduction of hybrid Orbitrap® (Q-Exactive™, LTQ-Orbitrap XL™) and TOF analyzers (Q-TOF, Q-IT-TOF), HRMS instrument have been re-evaluated for its quantitative nature. By now, various groups have reported quantification using high-resolution instruments which were found to be comparable with TQ-MS in terms of sensitivity, level of accuracy and throughput capabilities.[79,95,96] Recently introduced hybrid TOF-MS have shown improved resolution for ions having low *m/z* and increased dynamic range. Additionally, the TOF dynamic range has been significantly improved due to analogue to digital conversion protocol rather than previously used less efficient time to digital conversion protocol.[89] The use of above mentioned HRMS(S) allows simultaneous qualitative and quantitative analysis along with the acquisition of high quality FS data for profiling and data mining in later stages. It is noteworthy that the triple-quadruple data contains limited information acquired via preset reaction monitoring schemes, whereas HRMS which generates full-scan data has a potential to facilitate re-evaluation of data for extended metabolite search and untargeted analysis. A figure comparing the scan modes in low resolution and high resolution MS is mentioned in the figure. 1.8.

It is essential to follow fragmentation using collision-induced dissociation in case of quadrupole based analysis for targeted studies involving single or multiple ions. Quadrupole can be used in mainly three modes each involving filtration with the help of narrow range mass filter which is likely to be followed by fragmentation. These three modes are SIM (selected ion monitoring), SRM (selected reaction monitoring) or MRM (multiple reaction monitoring).[79,97] A major drawback of SIM/SRM/MRM is the loss of vital information during runs. While a particular ion(s) is/are being monitored, information on other ions is completely lost. This could be of great importance while carrying out global profiling studies in metabolomics, proteomics, and lipidomics. On other hand, HRMS can be used in full scan mode or SRM/MRM mode with

the possibility to perform MS^n.[98] This enhances the extent of information which can be obtained over a single run. A comparison of Triple Quad based mass spectra and HRMS has been given in figure 1.8.

- Apart from the advantages of full-scan MS analysis with high resolution, HRMS instrument can monitor product ion transitions like triple-quad analyzer with high mass accuracy. Various modes of product ion monitoring are mentioned below.

- Parallel reaction monitoring: Just like TQ-MS acquisition, HRMS instrument can select ions within single mass isolation windows and perform SRM or MRM studies with high spectral resolution.[97,99,100]

- All ion fragmentation: Non-selective all ion fragmentation can also be performed.[26]

- SWATH™: HRMS instrument also offers sequential fragmentation in a larger window of 20-50 *m/z*.[101]

- The rate of acquisition of high-resolution full-scan (HR-FS) is compatible with UPLC runs. The scan rate is more than 4Hz performed at >20,000 resolution. Because of high-resolution full-scan, there is no need of experimentally determining collision energy as it is must for SRM. Most HRMS instrument can record HR-FS, MS^{ALL}, and MS^{SWATH} in sequential scans as well. This makes simultaneous acquisition of data for both quantitative and qualitative analysis.[102,103]HRMS, as a result of full-scan mode, provides a much detailed picture of the co-eluting compound, adducts, contaminants and matrix peaks. This can potentially advantageous in a holistic approach such as systems biology.[55,104]
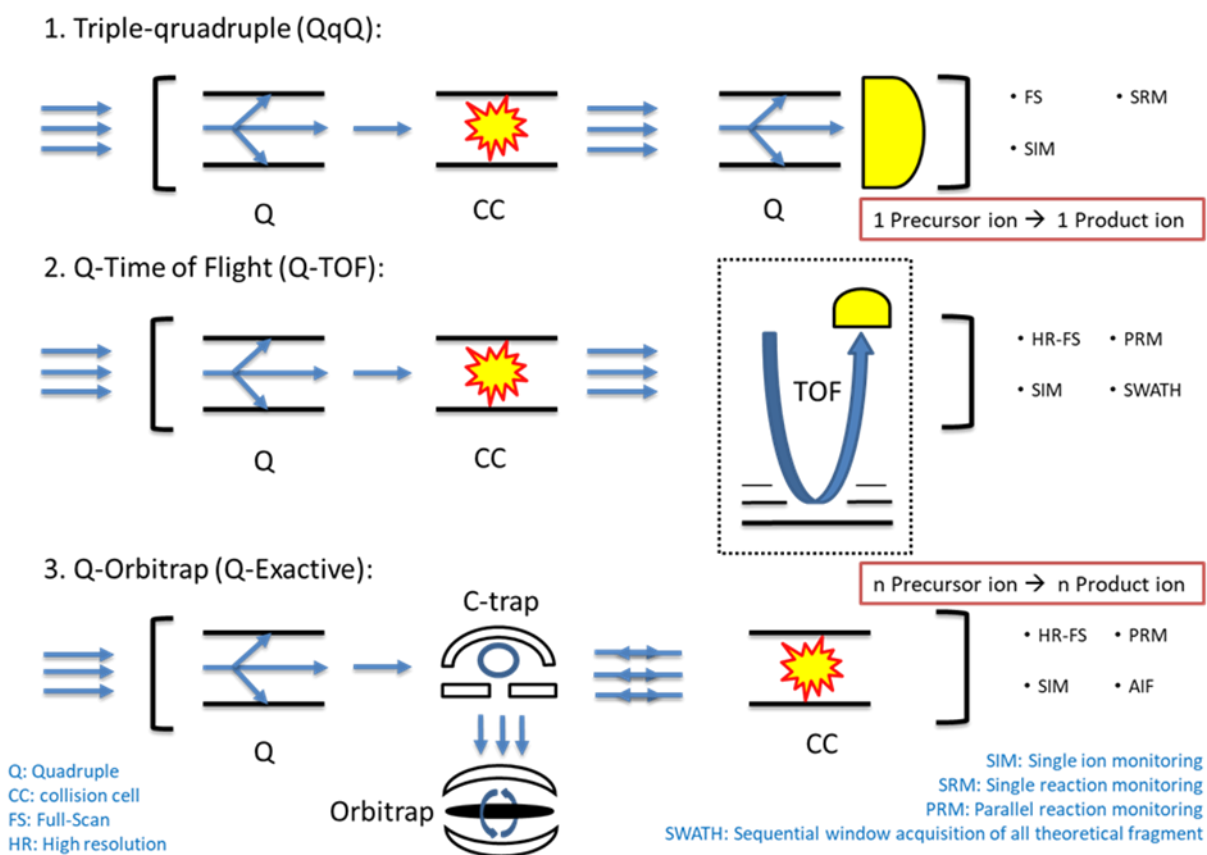
Figure 1.8 Scan modes in low (QqQ-MS) versus high resolution (Q-TOF, Q-Orbitrap®) mass spectrometer *(Adapted from Rochat et. al. Bioanalysis* **4,** *2939–2958 (2012))*

1.3 Maintenance and Calibration of HRMS

As explained earlier (Page 25-26), HRMS is sensitive to various environmental conditions and usage. Over extended period of usage, it is likely to display signs of deposition of sample residue on ionization interface, carryover, and carbon deposition on internal parts exposed to ion trajectories. Therefore, it is necessary to perform a routine evaluation and maintenance procedure to ensure the best performance of MS instruments. The maintenance is carried out either by the user through software operated bake-out cycle as well as by cleaning of some internal parts, such as ion guide, by authorized personnel. Bake-out is a procedure involving the selective heating of internal parts to remove the organic deposits. Bake-out is followed by vacuum stabilization to preset levels.

Bake-out is followed by mandatory mass calibration using calibration standard mix to ensure accuracy and precision of the MS instrument. The calibration standard set as well

technique may differ as per the analyzer. For example, in case of AB Sciex MALDI TOF/TOF 5800 instrument, a mixture of peptides namely, des-Arg1-bradykinin, Angiotensin I, Glu-Fibrinopeptide B, and adrenocorticotropic hormone (1-17 clip, 18-39 clip, and 7-38 clip) is used to perform the calibration. Briefly, CHCA is mixed with calibration standard mix and applied onto the MALDI target plate. The spots are allowed to dry. Laser energy and the number of shots are optimized followed by optimization of the X and Y deflector parameters. Whereas, in the case of Thermo Q-Exactive™ HRMS (Quadruple-Orbitrap analyzer) calibration is performed by direct infusion of calibration mix using a syringe and piston pump. The calibration mix, in this case, contains Caffeine, MRFA peptide (Met-Arg-Phe-Ala), Ultramark 1621(fluorinated phosphazines)[105], sodium dodecyl sulfate, sodium taurocholate and n-Butyl-amine.

1.4 Liquid chromatography techniques

1.4.1 Reversed-phase chromatography

Reversed phase chromatography (RPC) is one of the most widely used modes of chromatography techniques. The term reversed phase is used because of the reversed polarity of stationary and mobile phase in comparison to normal phase chromatography (NPC), where the polar stationary phase is used along with non-polar mobile phase. Stationary phases in RPC are comprised of silica particles grafted with non-polar alkyl chains ranging in length from 1 to 18 carbons. The most prevalent example of RPC stationary phase is octadecylsilane; consisting of 18 carbon length alkyl chain. The mobile phase consists of polar aqueous phase mixed with the organic phase. Analyte retention in RPC could occur by two mechanisms, namely adsorption of the analyte molecules on alkyl chains, or by partitioning into the micro-environment of alkyl chains, or both. RPC has widespread application in the analyses of a broad range of molecular structures with hydrophobic functional groups.[106] As compared to its counterpart NPC, RPC eliminates limited solubility and potential toxicity issues encountered with NPC mobile phases/solvents by allowing the combined use of aqueous phase and less toxic organic phases such as methanol and acetonitrile. Reliability, robustness, repeatability, stability and well-understood mechanism of analytical separation efficiencies in RPC have made it widely acceptable for use in both LC and LC-MS.[107] However, polar analytes are poorly retained on RP stationary phases significantly limiting its application in metabolomics,

especially with polar/semi-polar extracts derived from aqueous biofluids or tissue that comprises of a wealth of polar molecules.[108–110] Use of ion-pairing agents (fluorinated carboxylic acids) has in part addressed retention of polar metabolites in RPC. Conversely, the traditional normal phase is capable of retaining and separating polar analytes. However, it suffers from poor reproducibility and column bleeding issues. Additionally, routinely used mobile phases such as hexane is MS incompatible and impose yet another limitation that has hampered the full-fledged tandem application of NPC with MS platforms.[111] This void in polar analyte separation has been aptly filled by hydrophilic interaction liquid chromatography that was initially developed for carbohydrate separation now widely used for the separation of polar metabolites using aqueous mobile phases.[112]

1.4.2 Hydrophilic interaction liquid chromatography and it's retention mechanisms

The HILIC retention mechanism is not completely elucidated and the availability of diverse stationary phases makes it an even more complex process with multiple possibilities. However, as per the current understanding, the separation is achieved through two major phenomena: (1) hydrophilic partitioning of analytes in aqueous surface/pockets formed by water and buffer, and (2) weak electrostatic interactions on charged stationary phase material.[112–114] The first is evident by the fact that upon interaction with aqueous mobile phase, the polar surface of the stationary phase is known to strongly retain water. This forms a semi-immobilized phase of the water-rich layer in the vicinity of the stationary phase with increasing gradient of acetonitrile-rich phase away from the stationary phase material towards the bulk. This formation of a 'water-rich layer' has been experimentally shown by Wikberg and colleagues using nuclear magnetic resonance (NMR) spectroscopy.[115] The two phases of different polarity made up of acetonitrile-rich bulk and the water-rich layer can be considered as a biphasic liquid-liquid separation system. A minimum of 2-3% water content in the mobile phase is essential to allow the formation of this biphasic system.[116] Hydrogen bonding has frequently been cited as a causal in this regard. Polar analytes are partitioned into the semi-immobilized water-rich surface layer with stronger retention than the non-polar analytes, and thus eluting in the later stages of aqueous rich gradient.[117]

Influence and contribution of electrostatic interaction in retention of polar metabolites is controlled by the presence of buffers, organic solvent content and acidity/basicity of analytes.[118,119] While hydrogen bonding does play a role in some cases, most such postulations

are not accompanied by evidence to distinguish this from the dipole-dipole interactions that are probably responsible for the generation of the immobilized aqueous layer. For effective separation in HILIC mode, charged state of analytes is generally considered an ideal state as compared to their uncharged state as it renders analytes comparatively more hydrophilic in nature. In the presence of stationary phase with ionizable groups, for example, phosphate/ammonium/zwitterions, can enable electrostatic interactions with charged analytes. These interactions can be either attractive or repulsive, depending on the charged state of stationary phase and analyte ion. As expected, electrostatic attractions produce the increase of retention times, whereas electrostatic repulsion has the opposite effect on retention. Interestingly, in the case of repulsion, analytes can still be retained through hydrophilic interactions, owing to a proper orientation of the molecule, which aids in the reduction of the electrostatic repulsions. This combination has been described by Alpert as electrostatic repulsion–hydrophilic interaction chromatography (ERLIC).[120,121]

Quantitative structure-retention relationship (QSRR) approaches have been employed by various groups to understand the role of different contributing factors in HILIC mechanisms.[122] Among different QSSR models, the linear solvation energy relationship (LSER) model has been widely used to investigate the factors affecting retention in chromatographic systems.[123] LSER relates the retention of a given analyte to its physicochemical and structural parameters, using the solvato-chromic descriptors provided by Abraham *et al.*, which include hydrogen bond acidity and basicity parameters.[124] The high values found for these parameters have proved that molecules with hydrogen donor or hydrogen acceptor functionalities can interact through the hydrogen bond formation with the stationary phase. This kind of interaction is however dependent on the possibility of the phase to create hydrogen bonds and becomes particularly important in case of uncharged analytes when electrostatic interactions are absent.

1.5 References

(1)   Patti, G. J.; Yanes, O.; Siuzdak, G. Innovation: Metabolomics: The Apogee of the Omics Trilogy. *Nat. Publ. Gr.* **2012**, *13* (4), 263–269.

(2)   Nicholson, J. K.; Wilson, I. D. Understanding "global" Systems Biology: Metabonomics and the Continuum of Metabolism. *Nat. Rev. Drug Discov.* **2003**, *2* (8), 668–676.

(3)   Fiehn, O. Metabolomics - the Link between Genotypes and Phenotypes. In *Plant molecular biology*; 2002; pp 155–171.

(4)   Ramautar, R.; Berger, R.; van der Greef, J.; Hankemeier, T. Human Metabolomics: Strategies to Understand Biology. *Curr. Opin. Chem. Biol.* **2013**, *17* (5), 841–846.

(5)   Xia, J.; Broadhurst, D. I.; Wilson, M.; Wishart, D. S. Translational Biomarker Discovery in Clinical Metabolomics: An Introductory Tutorial. *Metabolomics* **2013**, *9* (2), 280–299.

(6)   Pepe, M. S.; Etzioni, R.; Feng, Z.; Potter, J. D.; Lou, M.; Thornquist, M.; Winget, M.; Yasui, Y.; Ntroduction, I. Phases of Biomarker Development for Early Detection of Cancer OF. *J. Natl. cancer Inst.* **2001**, *93* (14), 1054–1061.

(7)   Talat, N.; Shahid, F.; Dawood, G.; Hussain, R. Dynamic Changes in Biomarker Profiles Associated with Clinical and Subclinical Tuberculosis in a High Transmission Setting: A Four-Year Follow-up Study. *Scand. J. Immunol.* **2009**, *69* (6), 537–546.

(8)   Mayeux, R. Biomarkers : Potential Uses and Limitations. *NeuroRx* **2004**, *1* (April), 182–188.

(9)   Mayne, S. T. Biomarkers of Nutritional Exposure and Nutritional Status Antioxidant Nutrients and Chronic Disease : Use of Biomarkers of Exposure and Oxidative Stress Status in Epidemiologic Research 1. *Am. Soc. Nutr. Sci.* **2003**, No. 2, 933–940.

(10)   Ruiz-aracama, A.; Peijnenburg, A.; Kleinjans, J.; Jennen, D.; Delft, J. Van; Hellfrisch, C.; Lommen, A. An Untargeted Multi-Technique Metabolomics Approach to Studying Intracellular Metabolites Of. **2011**.

(11)   Velenosi, T. J.; Hennop, A.; Feere, D. A.; Tieu, A.; Kucey, A. S.; Kyriacou, P.; Mccuaig, L. E.; Nevison, S. E.; Kerr, M. A.; Urquhart, B. L. Untargeted Plasma and Tissue Metabolomics in Rats with Chronic Kidney Disease given AST-120. *Nat. Publ. Gr.* **2016**.

(12)   Tautenhahn, R.; Patti, G. J.; Rinehart, D.; Siuzdak, G. XCMS Online: A Web-Based Platform to Process Untargeted Metabolomic Data. *Anal. Chem.* **2012**, *84* (11), 5035–5039.

(13)   Xia, J.; Mandal, R.; Sinelnikov, I. V; Broadhurst, D.; Wishart, D. S. MetaboAnalyst 2.0—a Comprehensive Server for Metabolomic Data Analysis. *Nucleic Acids Res.* **2012**, *40*, 127–133.

(14)   Takahashi, H.; Morimoto, T.; Ogasawara, N.; Kanaya, S. AMDORAP: Non-Targeted Metabolic Profiling Based on High-Resolution LC-MS. *BMC Bioinformatics* **2011**, *12* (1), 259.

(15)   Pluskal, T.; Castillo, S.; Villar-Briones, A.; Oresic, M. MZmine 2: Modular Framework for Processing, Visualizing, and Analyzing Mass Spectrometry-Based Molecular Profile Data. *BMC*

Bioinformatics **2010**, *11*, 395.

(16)   Clasquin, M. F.; Melamud, E.; Rabinowitz, J. D. LC-MS Data Processing with MAVEN: A Metabolomic Analysis and Visualization Engine. *Curr. Protoc. Bioinforma.* **2012**, *Chapter 14*, Unit14.11.

(17)   Wang, M.; Lamers, R. A. N.; Korthout, H. A. A. J.; Nesselrooij, J. H. J. Van; Witkamp, R. F.; Heijden, R. Van Der; Voshol, P. J.; Havekes, L. M.; Verpoorte, R.; Greef, J. Van Der. Metabolomics in the Context of Systems Biology : Bridging Traditional Chinese Medicine and Molecular Pharmacology. *Physiother. Res.* **2005**, *19*, 173–182.

(18)   Garcia-Canaveras, J. C.; Donato, M. T.; Castell, J. V.; Lahoz, a. Targeted Profiling of Circulating and Hepatic Bile Acids in Human, Mouse, and Rat Using a UPLC-MRM-MS-Validated Method. *J. Lipid Res.* **2012**, *53* (10), 2231–2241.

(19)   Hu, S.; Wang, J.; Ji, E. H.; Christison, T.; Lopez, L.; Huang, Y. Targeted Metabolomic Analysis of Head and Neck Cancer Cells Using High Performance Ion Chromatography Coupled with a Q Exactive HF Mass Spectrometer. *Anal. Chem.* **2015**, 150522130556009.

(20)   Wolfender, J.-L.; Marti, G.; Thomas, A.; Bertrand, S. Current Approaches and Challenges for the Metabolite Profiling of Complex Natural Extracts. *J. Chromatogr. A* **2015**, *1382*, 136–164.

(21)   Smeraglia, J.; Baldrey, S. F.; Watson, D. Matrix Effects and Selectivity Issues in LC-MS-MS. *Chromatographia* **2002**, *55* (1), 95–99.

(22)   Matuszewski, B. K.; Constanzer, M. L. Matrix Effect in Quantitative LC / MS / MS Analyses of Biological Fluids : A Method for Determination of Finasteride in Human Plasma at Picogram Per Milliliter Concentrations Matrix Effect in Quantitative LC / MS / MS Analyses of Biological Fluids : A Met. *Anallytical Chem.* **1998**, *70* (10), 882–889.

(23)   Fraser, W. D.; Milan, A. M. Vitamin D Assays: Past and Present Debates, Difficulties, and Developments. *Calcif. Tissue Int.* **2013**, *92* (2), 118–127.

(24)   Comstock, K.; Stratton, T.; Wang, H. J.; Huang, Y.; Scientific, T. F.; Jose, S. Simultaneous , Fast Analysis of Melamine and Analogues in Pharmaceutical Components Using Q Exactive - Benchtop Orbitrap LC-MS / MS. 25.

(25)   Lutz, U.; Lutz, R. W.; Lutz, W. K. Metabolic Profiling of Glucuronides in Human Urine by LC-MS/MS and Partial Least-Squares Discriminant Analysis for Classification and Prediction of Gender. *Anal. Chem.* **2006**, *78* (13), 4564–4571.

(26)   Scheibner, O.; Baar, P. Van; Wode, F.; Dünnbier, U.; Akervik, K.; Humphrie, J.; Bromirski, M. A Strategy for an Unknown Screening Approach on Environmental Samples Using HRAM Mass Spectrometry. *Thermo Appl. note* **2013**, 1–7.

(27)   Tang, J. K.; You, L.; Blankenship, R. E.; Tang, Y. J. Recent Advances in Mapping Environmental Microbial Metabolisms through 13 C Isotopic Fingerprints. *J. R. Soc. Interface*

2012, *9*, 2767–2780.

(28)   Luraschi, P. Heavy Chain Disease Can Be Detected by Capillary Zone Electrophoresis. *Clin. Chem.* **2004**, *51* (1), 247–249.

(29)   Hommerson, P.; Khan, A. M.; Jong, G. J. De; Somsen, G. W. Ionization Techniques In Capillary Electrophoresis-Mass Spectrometry : Principles , Design , And Application. *Mass Spectrom. Rev.* **2011**, *30*, 1096–1120.

(30)   Peterson, A. C.; Mcalister, G. C.; Quarmby, S. T.; Griep-raming, J.; Coon, J. J. Development and Characterization of a GC-Enabled QLT-Orbitrap for High-Resolution and High-Mass Accuracy GC / MS. **2010**, *82* (20), 8618–8628.

(31)   Müller, D. C.; Degen, C.; Scherer, G.; Jahreis, G.; Niessner, R.; Scherer, M. Metabolomics Using GC-TOF-MS Followed by Subsequent GC-FID and HILIC-MS/MS Analysis Revealed Significantly Altered Fatty Acid and Phospholipid Species Profiles in Plasma of Smokers. *J. Chromatogr. B* **2014**, *966*, 117–126.

(32)   Lanza, I. R.; Zhang, S.; Ward, L. E.; Karakelides, H.; Raftery, D.; Sreekumaran Nair, K. Quantitative Metabolomics by 1H-NMR and LC-MS/MS Confirms Altered Metabolic Pathways in Diabetes. *PLoS One* **2010**, *5* (5).

(33)   Goudar, C.; Biener, R.; Boisart, C.; Heidemann, R.; Piret, J.; de Graaf, A.; Konstantinov, K. Metabolic Flux Analysis of CHO Cells in Perfusion Culture by Metabolite Balancing and 2D [13C,1H] COSY NMR Spectroscopy. *Metab. Eng.* **2010**, *12* (2), 138–149.

(34)   Jandera, P.; Janás, P. Recent Advances in Stationary Phases and Understanding of Retention in Hydrophilic Interaction Chromatography. A Review. *Anal. Chim. Acta* **2017**, *967*, 12–32.

(35)   Qiao, L.; Shi, X.; Xu, G. Recent Advances in Development and Characterization of Stationary Phases for Hydrophilic Interaction Chromatography. *TrAC - Trends Anal. Chem.* **2016**, *81*, 23–33.

(36)   Banerjee, S.; Mazumdar, S. Electrospray Ionization Mass Spectrometry: A Technique to Access the Information beyond the Molecular Weight of the Analyte. *Int. J. Anal. Chem.* **2012**, *2012*, 282574.

(37)   Ho, C. S.; Lam, C. W. K.; Chan, M. H. M.; Cheung, R. C. K.; Law, L. K.; Lit, L. C. W.; Ng, K. F.; Suen, M. W. M.; Tai, H. L. Electrospray Ionisation Mass Spectrometry: Principles and Clinical Applications. *Clin. Biochem. Rev.* **2003**, *24* (1), 3–12.

(38)   Fenn, J. B.; Mann, M.; Meng, C. K. A. I.; Wong, S. F.; Whitehouse, C. M. Electrospray Ionization for Mass Spectrometry of Large Biomolecules. *Science (80-.).* **1989**, *246* (6), 64–71.

(39)   Karas, M.; Hillenkamp, F. Laser Desorption Ionization of Proteins with Molecular Masses Exceeding 10 000 Daltons. *Anal. Chem.* **1988**, *60* (20), 2299–2301.

(40)   Merchant, M.; Weinberger, S. R. Recent Advancements in Surface-Enhanced Laser

Desorption/Ionization-Time of Flight-Mass Spectrometry. *Electrophoresis* **2000**, *21* (6), 1164–1177.

(41)   Hillenkamp, F.; Karas, M.; Beavis, R. C.; Chait, B. T. Matrix-Assisted Laser Desorption/Lonization Mass Spectrometry of Biopolymers. *Anal. Chem.* **1991**, *63* (24), 1193 A-1202 A.

(42)   Wiley, W. C.; McLaren, I. H. Time-of-Flight Mass Spectrometer with Improved Resolution. *Rev. Sci. Instrum.* **1955**, *26* (12), 1150–1157.

(43)   Vestal, M. L. Modern MALDI Time-of-Flight Mass Spectrometry. *J. Mass Spectrom.* **2009**, *44* (3), 303–317.

(44)   Makarov, A. Electrostatic Axially Harmonic Orbital Trapping: A High-Performance Technique of Mass Analysis. *Anal. Chem.* **2000**, *72* (6), 1156–1162.

(45)   Hu, Q.; Noll, R. J.; Li, H.; Makarov, A.; Hardman, M.; Graham Cooks, R. The Orbitrap: A New Mass Spectrometer. *J. Mass Spectrom.* **2005**, *40* (4), 430–443.

(46)   Scigelova, M.; Hornshaw, M.; Giannakopulos, A.; Makarov, A. Fourier Transform Mass Spectrometry. *Mol. Cell. Proteomics* **2011**, *10* (7), M111.009431.

(47)   Goeddel, L.; Patti, G. Maximizing the Value of Metabolomic Data. *Bioanalysis* **2012**, *4* (18), 2199–2201.

(48)   Nicholls, A. W. Realising the Potential of Metabolomics. *Bioanalysis* **2012**, *4* (18), 2195–2197.

(49)   Pomerantz, A. E.; Mullins, O. C.; Paul, G.; Ruzicka, J.; Sanders, M. Orbitrap Mass Spectrometry : A Proposal for Routine Analysis of Nonvolatile Components of Petroleum. *Energy Fuels* **2011**, *25*, 3077–3082.

(50)   Ghaste, M.; Mistrik, R.; Shulaev, V. Applications of Fourier Transform Ion Cyclotron Resonance (FT-ICR) and Orbitrap Based High Resolution Mass Spectrometry in Metabolomics and Lipidomics. *Int. J. Mol. Sci.* **2016**, *17* (6).

(51)   Ramanathan, R.; Jemal, M.; Ramagiri, S.; Xia, Y. Q.; Humpreys, W. G.; Olah, T.; Korfmacher, W. a. It Is Time for a Paradigm Shift in Drug Discovery Bioanalysis: From SRM to HRMS. *J. Mass Spectrom.* **2011**, *46* (6), 595–601.

(52)   Churchwell, M. I.; Twaddle, N. C.; Meeker, L. R.; Doerge, D. R. Improving LC-MS Sensitivity through Increases in Chromatographic Performance: Comparisons of UPLC-ES/MS/MS to HPLC-ES/MS/MS. *J. Chromatogr. B Anal. Technol. Biomed. Life Sci.* **2005**, *825* (2), 134–143.

(53)   Kadar, H.; Veyrand, B.; Antignac, J.-P.; Durand, S.; Monteau, F.; Le Bizec, B. Comparative Study of Low- versus High-Resolution Liquid Chromatography-Mass Spectrometric Strategies for Measuring Perfluorinated Contaminants in Fish. *Food Addit. Contam. Part A. Chem. Anal. Control. Expo. Risk Assess.* **2011**, *28* (9), 1261–1273.

(54)   Prentice, B. M.; Chumbley, C. W.; Caprioli, R. M. High-Speed MALDI MS/MS Imaging Mass

Spectrometry Using Continuous Raster Sampling. *J. Mass Spectrom.* **2015**, *50* (4), 703–710.

(55)   Mol, H. G. J.; Van Dam, R. C. J.; Zomer, P.; Mulder, P. P. J. Screening of Plant Toxins in Food, Feed and Botanicals Using Full-Scan High-Resolution (Orbitrap) Mass Spectrometry. *Food Addit. Contam. Part A. Chem. Anal. Control. Expo. Risk Assess.* **2011**, *28* (10), 1405–1423.

(56)   Kaufmann, A.; Butcher, P.; Maden, K.; Walker, S.; Widmer, M. Quantitative and Confirmative Performance of Liquid Chromatography Coupled to High-Resolution Mass Spectrometry Compared to Tandem Mass Spectrometry. *Rapid Commun. Mass Spectrom.* **2011**, *25* (7), 979–992.

(57)   MacAllister, R. J.; Rambausek, M. H.; Vallance, P.; Williams, D.; Hoffmann, K. H.; Ritz, E. Concentration of Dimethyl-L-Arginine in the Plasma of Patients with End-Stage Renal Failure. *Nephrol. Dial. Transplant* **1996**, *11* (12), 2449–2452.

(58)   Boelaert, J.; Lynen, F.; Glorieux, G.; Schepers, E.; Neirynck, N.; Vanholder, R. Metabolic Profiling of Human Plasma and Urine in Chronic Kidney Disease by Hydrophilic Interaction Liquid Chromatography Coupled with Time-of-Flight Mass Spectrometry: A Pilot Study. *Anal. Bioanal. Chem.* **2017**, *409* (8), 2201–2211.

(59)   Dunn, W. B.; Broadhurst, D.; Begley, P.; Zelena, E.; Francis-McIntyre, S.; Anderson, N.; Brown, M.; Knowles, J. D.; Halsall, A.; Haselden, J. N.; et al. Procedures for Large-Scale Metabolic Profiling of Serum and Plasma Using Gas Chromatography and Liquid Chromatography Coupled to Mass Spectrometry. *Nat. Protoc.* **2011**, *6* (7), 1060–1083.

(60)   Martens-Lobenhoffer, J.; Bode-Böger, S. M. Measurement of Asymmetric Dimethylarginine (ADMA) in Human Plasma: From Liquid Chromatography Estimation to Liquid Chromatography-Mass Spectrometry Quantification. *Eur. J. Clin. Pharmacol.* **2006**, *62* (SUPPL. 13), 61–68.

(61)   Thomas, A.; Geyer, H.; Schänzer, W.; Crone, C.; Kellmann, M.; Moehring, T.; Thevis, M. Sensitive Determination of Prohibited Drugs in Dried Blood Spots (DBS) for Doping Controls by Means of a Benchtop Quadrupole/Orbitrap Mass Spectrometer. *Anal. Bioanal. Chem.* **2012**, *403* (5), 1279–1289.

(62)   Vogliardi, S.; Favretto, D.; Tucci, M.; Stocchero, G.; Ferrara, S. D. Simultaneous LC-HRMS Determination of 28 Benzodiazepines and Metabolites in Hair. *Anal. Bioanal. Chem.* **2011**, *400* (1), 51–67.

(63)   Kaufmann, A. The Current Role of High-Resolution Mass Spectrometry in Food Analysis. *Anal. Bioanal. Chem.* **2012**, *403* (5), 1233–1249.

(64)   Lattanzio, V. M. T. Mycotoxin Analysis in Cereal Foods by Collision Cell Fragmentation – High Resolution Mass Spectrometry. **2012**.

(65)   Botitsi, H. V; Garbis, S. D.; Economou, A.; Tsipi, D. F. Current Mass Spectrometry Strategies

for the Analysis of Pesticides and Their Metabolites in Food and Water Matrices. *Mass Spectrom. Rev.* **2011**, *30* (5), 907–939.

(66)   SIUZDAK, G. An Introduction to Mass Spectrometry Ionization: An Excerpt from The Expanding Role of Mass Spectrometry in Biotechnology, 2nd Ed.; MCC Press: San Diego, 2005. *J. Assoc. Lab. Autom.* **2004**, *9* (2), 50–63.

(67)   Yang, S.; Brereton, S. M.; Wheeler, M. D.; Ellis, A. M. Electron Impact Ionization of Haloalkanes in Helium Nanodroplets. *J. Phys. Chem. A* **2006**, *110* (5), 1791–1797.

(68)   Field, F. H. Chemical Ionization Mass Spectrometry. *Acc. Chem. Res.* **1968**, *1* (2), 42–49.

(69)   Munson, M. S. B.; Field, F. H. Chemical Ionization Mass Spectrometry. I. General Introduction. *J. Am. Chem. Soc.* **1966**, *88* (12), 2621–2630.

(70)   Biemann, K. Gas Chromatography-Chemical Ionization Mass Spectrometry. *Chem. Commun.* **1970**, *944*, 1542–1543.

(71)   Lu, W.; Bennett, B. D.; Rabinowitz, J. D. Analytical Strategies for LC-MS-Based Targeted Metabolomics. *J. Chromatogr. B. Analyt. Technol. Biomed. Life Sci.* **2008**, *871* (2), 236–242.

(72)   Cole, R. Book Review: Electrospray Ionization Mass Spectrometry: Fundamentals, Instrumentation, and Applications. *Am. Soc. Mass Spectrom.* **1997**, *8* (11), 1191–1194.

(73)   Eriksson, C.; Masaki, N.; Yao, I.; Hayasaka, T.; Setou, M. MALDI Imaging Mass Spectrometry—A Mini Review of Methods and Recent Developments. *Mass Spectrom.* **2013**, *2* (Special_Issue), S0022--S0022.

(74)   Nordhoff, E.; Kirpekar, F.; Karas, M.; Cramer, R.; Hahner, S.; Hillenkamp, F.; Kristiansen, K.; Roepstorff, P.; Lezius, A. Comparison of IR- and UV-Matrix-Assisted Laser Desorption/Ionization Mass Spectrometry of Oligodeoxynucleotides. *Nucleic Acids Res.* **1994**, *22* (13), 2460–2465.

(75)   Karas, M.; Krüger, R. Ion Formation in MALDI: The Cluster Ionization Mechanism. *Chem. Rev.* **2003**, *103* (2), 427–440.

(76)   Knochenmuss, R.; Zenobi, R. MALDI Ionization : The Role of In-Plume Processes. *Chem. Rev.* **2003**, *103*, 441–452.

(77)   Uthe, P. M. QUADRUPOLE MASS ANALYZER, 1969.

(78)   Dawson, P. H. Quadrupole Mass Analyzers: Performance, Design and Some Recent Applications. *Mass Spectrom. Rev.* **1986**, *5* (1), 1–37.

(79)   Henry, H.; Sobhi, H. R.; Scheibner, O.; Bromirski, M.; Nimkar, S. B.; Rochat, B. Comparison between a High-Resolution Single-Stage Orbitrap and a Triple Quadrupole Mass Spectrometer for Quantitative Analyses of Drugs. *Rapid Commun. Mass Spectrom.* **2012**, *26* (5), 499–509.

(80)   Spengler, B. Mass Spectrometry Imaging of Biomolecular Information. *Anal. Chem.* **2015**, *87*, 64–82.

(81) Thevis, M.; Makarov, A. a; Horning, S.; Schänzer, W. Mass Spectrometry of Stanozolol and Its Analogues Using Electrospray Ionization and Collision-Induced Dissociation with Quadrupole-Linear Ion Trap and Linear Ion Trap-Orbitrap Hybrid Mass Analyzers. *Rapid Commun. Mass Spectrom.* **2005**, *19* (22), 3369–3378.

(82) Makarov, A.; Denisov, E.; Kholomeev, A.; Balschun, W.; Lange, O.; Strupat, K.; Horning, S. Performance Evaluation of a Hybrid Linear Ion Trap / Orbitrap Mass Spectrometer. *Anal. Chem.* **2006**, *78* (7), 2113–2120.

(83) van Dongen, W. D.; Niessen, W. M. LC–MS Systems for Quantitative Bioanalysis. *Bioanalysis* **2012**, *4* (19), 2391–2399.

(84) Xian, F.; Hendrickson, C. L.; Marshall, A. G. High Resolution Mass Spectrometry. *Anal. Chem.* **2012**, *84*, 708–719.

(85) Marshall, A. G.; Hendrickson, C. L. High-Resolution Mass Spectrometers. *Annu. Rev. Anal. Chem. (Palo Alto. Calif).* **2008**, *1*, 579–599.

(86) Bruce, S. J.; Rochat, B.; Béguin, A.; Pesse, B.; Guessous, I.; Boulat, O.; Henry, H. Analysis and Quantification of Vitamin D Metabolites in Serum by Ultra-Performance Liquid Chromatography Coupled to Tandem Mass Spectrometry and High-Resolution Mass Spectrometry--a Method Comparison and Validation. *Rapid Commun. Mass Spectrom.* **2013**, *27*, 200–206.

(87) Gallart-Ayala, H.; Nuñez, O.; Moyano, E.; Galceran, M. T.; Martins, C. P. B. Preventing False Negatives with High-Resolution Mass Spectrometry: The Benzophenone Case. *Rapid Commun. Mass Spectrom.* **2011**, *25* (20), 3161–3166.

(88) Shahidi-latham, S. K.; Dutta, S. M.; Conaway, M. C. P.; Rudewicz, P. J. Evaluation of an Accurate Mass Approach for the Simultaneous Detection of Drug and Metabolite Distributions via Whole-Body Mass Spectrometric Imaging. *Anal. Chem.* **2012**, *84*, 7158–7165.

(89) Rochat, B.; Kottelat, E. The Future Key Role of LC – High-Resolution-MS Analyses in Clinical Laboratories : A Focus on Quantification. *Bioanalysis* **2012**, *4* (24), 2939–2958.

(90) Koulman, A.; Woffendin, G.; Narayana, V. K.; Welchman, H.; Crone, C.; Volmer, D. A. High-Resolution Extracted Ion Chromatography , a New Tool for Metabolomics and Lipidomics Using a Second- Generation Orbitrap Mass Spectrometer. *Rapid Commun. mass Spectrom.* **2009**, *23*, 1411–1418.

(91) Pinhancos, R.; Maass, S.; Ramanathan, D. M. High-Resolution Mass Spectrometry Method for the Detection, Characterization and Quantitation of Pharmaceuticals in Water. *J. Mass Spectrom.* **2011**, *46* (11), 1175–1181.

(92) Xia, Y.-Q.; Lau, J.; Olah, T.; Jemal, M. Targeted Quantitative Bioanalysis in Plasma Using Liquid Chromatography/High-Resolution Accurate Mass Spectrometry: An Evaluation of

Global Selectivity as a Function of Mass Resolving Power and Extraction Window, with Comparison of Centroid and Profile Mo. *Rapid Commun. Mass Spectrom.* **2011**, *25* (19), 2863–2878.

(93)   Ruan, Q.; Peterman, S.; Szewc, M. a; Ma, L.; Cui, D.; Humphreys, W. G.; Zhu, M. An Integrated Method for Metabolite Detection and Identification Using a Linear Ion Trap/Orbitrap Mass Spectrometer and Multiple Data Processing Techniques: Application to Indinavir Metabolite Detection. *J. Mass Spectrom.* **2008**, *43* (2), 251–261.

(94)   Franke, A. a; Custer, L. J.; Morimoto, Y.; Nordt, F. J.; Maskarinec, G. Analysis of Urinary Estrogens, Their Oxidized Metabolites, and Other Endogenous Steroids by Benchtop Orbitrap LCMS versus Traditional Quadrupole GCMS. *Anal. Bioanal. Chem.* **2011**, *401* (4), 1319–1330.

(95)   Zhang, N. R.; Sean Yu; Tiller, P.; Yeh, S.; Mahan, E.; Emary, W. B. Quantitation of Small Molecules Using High-Resolution Accurate Mass Spectrometers – a Different Approach for Analysis of Biological Samples. *Rapid Commun. Mass Spectrom.* **2009**, *23*, 1085–1094.

(96)   Kaufmann, A.; Butcher, P.; Maden, K.; Walker, S.; Widmer, M. Semi-Targeted Residue Screening in Complex Matrices with Liquid Chromatography Coupled to High Resolution Mass Spectrometry: Current Possibilities and Limitations. *Analyst* **2011**, *136* (9), 1898–1909.

(97)   Henry, H.; Sobhi, H. R.; Scheibner, O.; Bromirski, M.; Nimkar, S. B.; Rochat, B. Comparison between a High-Resolution Single-Stage Orbitrap and a Triple Quadrupole Mass Spectrometer for Quantitative Analyses of Drugs. *Rapid Commun. Mass Spectrom.* **2012**, *26* (5), 499–509.

(98)   Lim, H.; Chen, J.; Cook, K.; Sensenhauser, C.; Silva, J.; Evans, D. C. A Generic Method to Detect Electrophilic Intermediates Using Isotopic Pattern Triggered Data-Dependent High-Resolution Accurate Mass Spectrometry. *Rapid Commun. mass Spectrom.* **2008**, *22*, 1295–1311.

(99)   Lim, H.; Chen, J.; Sensenhauser, C.; Cook, K. Metabolite Identification by Data-Dependent Accurate Mass Spectrometric Analysis at Resolving Power of 60 000 in External Calibration Mode Using an LTQ / Orbitrap. **2007**, 1821–1832.

(100) Scheibner, O.; Bromirski, M.; Scientific, T. F. Qualitative and Quantitative Analysis of Pesticides in Horse Feed Matrix Using Orbitrap MS. *Thermo Appl. note* No. 573, 1–6.

(101) Zhu, X.; Chen, Y.; Subramanian, R. Comparison of Information-Dependent Acquisition, SWATH, and MS. *Anal. Chem.* **2014**, *86* (1202–1209).

(102) Shahidi-latham, S. K.; Dutta, S. M.; Conaway, M. C. P.; Rudewicz, P. J. Evaluation of an Accurate Mass Approach for the Simultaneous Detection of Drug and Metabolite Distributions via Whole-Body Mass Spectrometric Imaging. **2012**.

(103) Sanders, M.; Hnatyshy, S.; Robertson, D.; Reily, M.; Mcclure, T.; Athanas, M.; Wang, J.; Yang, P. Metabolomic Profiling in Drug Discovery : Understanding the Factors That Influence a Metabolomics Study and Strategies to Reduce Biochemical and Chemical Noise. *Thermo Appl.*

note No. 562, 1–5.

(104) Athanas, M.; Peake, D. A.; Dreyer, M.; Sanders, M.; Wang, J.; Huang, Y.; Scientific, T. F.; Parkway, R. O.; Jose, S. Applying Q Exactive Benchtop Orbitrap LC-MS / MS and SIEVE Software for Cutting Edge Metabolomics and Lipidomics Research. 95134.

(105) Jiang, L.; Moini, M. Ultramark 1621 as a Reference Compound for Positive and Negative Ion Fast-Atom Bombardment High-Resolution Mass Spectrometry. *J. Am. Soc. Mass Spectrom.* **1992**, *3* (8), 842–846.

(106) Molnar, I.; Horvath, C. Reverse Phase Chromatography of Polar Biological Substances: Separation of Catechol Compounds by High Performance Liquid Chromatography. *Clin. Chem.* **1976**, *22* (9), 1497–1502.

(107) Cubbon, S.; Antonio, C.; Wilson, J.; Thomas-oates, J. METABOLOMIC APPLICATIONS OF HILIC – LC – MS. **2010**, No. November 2008, 671–684.

(108) Dunn, W. B.; Ellis, D. I. Metabolomics: Current Analytical Platforms and Methodologies. *TrAC Trends Anal. Chem.* **2005**, *24* (4), 285–294.

(109) Armirotti, A.; Basit, A.; Realini, N.; Caltagirone, C.; Bossù, P.; Spalletta, G.; Piomelli, D. Sample Preparation and Orthogonal Chromatography for Broad Polarity Range Plasma Metabolomics: Application to Human Subjects with Neurodegenerative Dementia. *Anal. Biochem.* **2014**, *455* (1), 48–54.

(110) Skov, K.; Hadrup, N.; Smedsgaard, J.; Frandsen, H. LC-MS Analysis of the Plasma Metabolome-A Novel Sample Preparation Strategy. *J. Chromatogr. B Anal. Technol. Biomed. Life Sci.* **2015**, *978–979*, 83–88.

(111) Strege, M. A. Hydrophilic Interaction Chromatography-Electrospray Mass Spectrometry Analysis of Polar Compounds for Natural Product Drug Discovery. *Anal. Chem.* **1998**, *70* (13), 2439–2445.

(112) Alpert, A. J.; Shukla, M.; Shukla, A. K.; Zieske, L. R.; Yuen, S. W.; Ferguson, M. A. J.; Mehlert, A.; Pauly, M.; Orlando, R. Hydrophilic-Interaction Chromatography of Complex Carbohydrates. *J. Chromatogr. A* **1994**, *676* (1), 191–202.

(113) Kawachi, Y.; Ikegami, T.; Takubo, H.; Ikegami, Y.; Miyamoto, M.; Tanaka, N. Chromatographic Characterization of Hydrophilic Interaction Liquid Chromatography Stationary Phases: Hydrophilicity, Charge Effects, Structural Selectivity, and Separation Efficiency. *J. Chromatogr. A* **2011**, *1218* (35), 5903–5919.

(114) Alpert, A. J. Hydrophilic-Interaction Chromatography for the Separation of Peptides, Nucleic Acids and Other Polar Compounds. *J. Chromatogr. A* **1990**, *499* (C), 177–196.

(115) Wikberg, E.; Sparrman, T.; Viklund, C.; Jonsson, T.; Irgum, K. A2H Nuclear Magnetic Resonance Study of the State of Water in Neat Silica and Zwitterionic Stationary Phases and Its

Influence on the Chromatographic Retention Characteristics in Hydrophilic Interaction High-Performance Liquid Chromatography. *J. Chromatogr. A* **2011**, *1218* (38), 6630–6638.

(116) Dinh, N. P.; Jonsson, T.; Irgum, K. Water Uptake on Polar Stationary Phases under Conditions for Hydrophilic Interaction Chromatography and Its Relation to Solute Retention. *J. Chromatogr. A* **2013**, *1320*, 33–47.

(117) Hemström, P.; Irgum, K. *Hydrophilic Interaction Chromatography*; 2006; Vol. 29.

(118) Buszewski, B.; Noga, S. Hydrophilic Interaction Liquid Chromatography (HILIC) — a Powerful Separation Technique. *Anal Bioanal Chem* **2012**, *402*, 231–247.

(119) McCalley, D. V. Effect of Mobile Phase Additives on Solute Retention at Low Aqueous PH in Hydrophilic Interaction Liquid Chromatography. *J. Chromatogr. A* **2017**, *1483*, 71–79.

(120) Alpert, A. J. Electrostatic Repulsion Hydrophilic Interaction Chromatography for Isocratic Separation of Charged Solutes and Selective Isolation of Phosphopeptides. *Anal. Chem.* **2008**, *80* (1), 62–76.

(121) Hao, P.; Guo, T.; Li, X.; Adav, S. S.; Yang, J.; Wei, M.; Sze, S. K. Novel Application of Electrostatic Repulsion-Hydrophilic Interaction Chromatography (ERLIC) in Shotgun Proteomics: Comprehensive Profiling of Rat Kidney Proteome. *J. Proteome Res.* **2010**, *9* (7), 3520–3526.

(122) Chirita, R. I.; West, C.; Zubrzycki, S.; Finaru, A. L.; Elfakir, C. Investigations on the Chromatographic Behaviour of Zwitterionic Stationary Phases Used in Hydrophilic Interaction Chromatography. *J. Chromatogr. A* **2011**, *1218* (35), 5939–5963.

(123) Vitha, M.; Carr, P. W. The Chemical Interpretation and Practice of Linear Solvation Energy Relationships in Chromatography. *J. Chromatogr. A* **2006**, *1126* (1–2), 143–194.

(124) Abraham, M. H.; Ibrahim, A.; Zissimos, A. M. Determination of Sets of Solute Descriptors from Chromatographic Measurements. *J. Chromatogr. A* **2004**, *1037* (1–2), 29–47.

Chapter 2

High Resolution-Accurate Mass Quantitation of Targeted Endo and Exo Metabolites in Glioblastoma Sub Populations

2.1 Introduction

Liquid chromatography-mass spectrometry (LC-MS) is an invaluable tool for low molecular weight metabolite analysis from in vitro model systems.[1,2] Metabolomic workflows generally employ high-resolution mass spectrometry (LC-HRMS) for qualitative profiling while triple-quadrupole (QqQ or TQ-MS) based low-resolution MS is separately used for quantitative measurements.[3,4] There is an increasing shift away from viewing LC-HRMS as a stand-alone qualitative platform. Simultaneous accurate mass-based (HR-AM) qualitative and quantitative (qual/quant) metabolite measurements further enhance the ability to comprehensively evaluate biochemical pathways.[3–6] For example, HRMS allows profiling of metabolites, from native pathways that could be impacted in drug metabolism investigations, beyond the traditional metabolized drug or degraded drug products alone.[7–11] HR-AM quantitation is particularly useful in eliminating any potential m/z interferences from closely spaced metabolites. Data from such metabolic profiling can also be advantageously used in integrative systems biology approaches towards predictive metabolic modeling .[12–15]

HRMS analysis of metabolites from mammalian and microbial samples, including quantitation, has been reported in several publications. Table 2.1 summarizes these and highlights the method aspects of these publications. However, relatively few studies have evaluated the performance of HR-AM quantitation specifically for metabolic consumption and release (CORE) analysis for study contexts that present analytical complexities of sample and scale. Often in vitro studies investigate differentially expressed biological systems. Various nutritional, drug and other environmental conditions and resultant phenotypic changes are probed.[16] LC HR-AM workflows for the measurement of CORE in such scenarios can be process intensive potentially involving hundreds of analytical runs. Thus, in addition to the sample preparation strategies, it is crucial to optimize several method and instrumental parameters to establish the quantitative performance of HR-AM analysis in large-scale metabolic workflows. It is of utmost importance that these parameters remain unaltered over the course of the metabolomics study. To ensure the reliability of the results and reduce the possibilities of artifacts, it is also important to plan batches of sample, control and blank LC analytical runs interlaced with QC samples.

In this work, we report an elaborate workflow implemented for the LC-HRAM quantitative analysis of metabolic CORE in two differentially expressed subpopulations of

glioblastoma cells. Intra and extra-cellular metabolites extracted at various time points and with the cells grown under different concentrations of the anti-cancer drug temozolomide were analyzed. The analysis focused on a set of metabolites for screening and quantitation according to their significance in cell growth and proliferation in culture media. A simple reverse phase LC-ESI-Orbitrap HRMS method was evaluated for quantitation of 34 metabolites (mainly amino acids, organic acids and carbohydrate) identified uniformly from the culture samples. The samples were analyzed in both positive and negative modes. Figure 2.1 shows the detailed experimental workflow from which samples were drawn resulting in 988 LC-HRAM analyses executed over 15 days. Principal component analysis was performed using the quantitative metabolomics data to obtain insights into the differentially expressed cell populations. [17]

Table 2.1 Previous reports of quantitative analysis using HRMS

Sr. No.	System	RP/HILIC	HRMS	Absolute quantitation	Focus	Ref.
1	*C. autoethanogenum*	HILIC	Q-Orbitrap	Yes (LOD, LOQ, linearity, Accuracy, Precision)	Novel method for LC-IDMS	[18]
2	*S. cerevisiae*	RP (ion pairing agent)	Orbitrap	Yes (LOD, linearity, Accuracy, Precision)	Quantification of metabolites Identification of unknown peaks	[19]
3	*Lymphoblastic leukemia*	HILIC	Q-TOF	Yes (LOD, linearity, intra and inter-batch variation, pooled QC)	CORE profile	[20]
4	*Aortic endothelial cells (HAECs)*	Silica	LTQ-Orbitrap	Yes	Absolute quantification using isobaric tags (DiART)	[21]
5	*Colon cancer cells (HT29)*	HILIC	Q-TOF	No (pooled QC)	Untargeted metabolomics to identify effects of polyphenols	[22]
6	*Pluripotent stem cells (iPSCs)*	RP	Q-TOF	No (Relative)	Untargeted metabolomics	[23]
7	*Human plasma*	HILIC	Qq-TOF	Yes (Linearity, LOD, LLOQ, accuracy, Precision, sample stability, matrix effect, carry over)	Quantification of kynurenine pathway metabolites	[24]
8	*Human plasma & microsomes*	RP	Q-TOF	Yes (LLOQ, Linearity, accuracy)	SWATH, qual/quant of bosentan and its metabolites	[5]
9	*Mice Liver*	HILIC	TOF	Yes (LOD, LLOQ, linearity, recoveries, reproducibility)	Quantification of ethionine pathway metabolites	[25]
10	*Mouse hypothalamus*	RP	Q-Orbitrap	Yes (LOD, LOQ, linearity, accuracy, precision,	Quantification of neurotransmitters/metabolites	[26]
11	*fibrosarcoma cell line (HT1080M)*	HILIC	Orbitrap	Yes (isotope-based approach)	Quantification of methionine metabolism	[27]
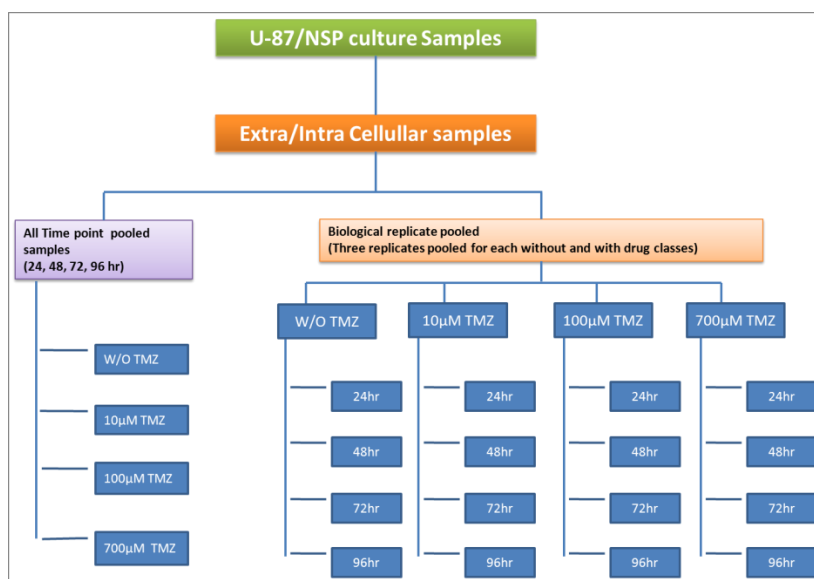
Intra and extracellular (N1=2) metabolites from two cell culture samples (U87 and NSP; N2=2) were used. Each sample was run in triplicate in positive and negative ion modes; along with calibration levels (10 each) + QCs. Intermittent QC samples were also used during sample runs at the interval of 9hrs respectively. The total analysis was completed in 17 days.

- Total number of time point pooled samples (a) = 12*N1*N2 = 48
- Total number of biological replicate pooled samples (b) = 16*N1*N2 = 64
- Common Zero hour samples (C) = 2
- Total number of sample injections = (48+64+2)*3= 342
- Total number of samples run in two modes (d) = 684
- Total number of calibration runs (e) = 160
- Total number of QC run during calibration (f) = 16
- Total number of QCs run during sample run (g) = 112
- Total number of runs for the experiment (a+b+c+d+e+f+g) =988

Figure 2.1 Classification of glioblastoma samples. Details of analytical runs on LC-HRMS. The total number of runs includes standards, quality control (QC) samples, pooled representative samples, two modes of ionization and intra/extra-cellular samples. A total of 988 analytical runs were made in the span of 15 days. The cell lines were grown in four different conditions, one without temozolomide (Drug used in chemotherapy) and at three different concentration of temozolomide i.e. 10 µM, 100 µM and 700 µM. For each experiment, samples were collected at an interval of 24 hrs for four days.

2.2 Materials and methods

2.2.1 Materials

All amino acids, glucose, L-ascorbic acid, citric acid, glyceraldehyde-3-phosphate, ketoglutaric acid, lactic acid, citrulline, ornithine, malic acid, maleic acid, methylmalonic acid, malonic acid, oxo-adipic acid, pyruvic acid, sorbitol, non-essential amino acids (NEA) medium, bovine serum albumin (BSA) and LC-MS grade formic acid were procured from Sigma Aldrich. LC-MS grade acetonitrile and methanol were purchased from J T Baker. Deionized water (specific resistivity 18.2 MΩ) was obtained from Millipore Milli-Q water purification system. Verapamil and atorvastatin, used as internal standards, were received as gratis samples from Mylan, Hyderabad, India. Dulbecco's Modified Eagle's Medium having minimal essential media (MEM) composition was acquired from HiMedia (India). 10% Fetal Bovine Serum (FBS, Gibco™) were purchased from ThermoFisher Scientific. LC vials (200 µL) vials with screw caps were purchased from Amkette analytics (India)

2.2.2 Preparation of reference standards, calibrants, QCs, sample preprocessing and LC-HRMS

10 mg of L-ascorbic acid, citric acid, glyceraldehyde-3-phosphate, ketoglutaric acid, lactate, L-citrulline, L-ornithine, D-malic acid, maleic acid, methylmalonic acid, malonic acid, oxoadipic acid, pyruvate, and d-sorbitol was individually weighed and 10 mg each of the metabolite standards were dissolved in 1 mL of DI water. The metabolite concentrations in the respective stock solutions were as follows: L-ascorbic acid (2.84 mM), citric acid (5.20 mM), glyceraldehyde-3-Phosphate (11.76 mM), ketoglutaric acid (6.84 mM), lactate (111.01 mM), L-citrulline (28.54 mM), L-ornithine (1.48 mM), D-malic acid (14.92 mM), maleic acid (0.86 mM), methylmalonic acid (25.40 mM), malonic acid (96.10 M), oxoadipic acid (62.45 mM), pyruvate (56.78 mM), D-sorbitol (10.98 mM). The standard mixture was 100 fold diluted using 50 % acetonitrile (diluent).

Subsequently, chemically defined media components; 445 µL MEM, 5µl of NEA and 50 µL of water were thoroughly mixed in a clean 1.5ml centrifuge tube using vortex mixer. The mixture was subjected to cold methanol to remove any potential protein content. 100 µL of above solution was withdrawn and transferred to a fresh 1.5 mL tube. 400 µL of chilled methanol was added to the above-mentioned aliquot. The mixture was thoroughly mixed for ~1

min using a vortex mixer. The solution was allowed to stand on ice bath for 5 mins, followed by centrifugation for 15 min at 5000 rpm. 300 µL supernatant volume was carefully withdrawn. The supernatant was 20 fold diluted using the diluent. The solution was stored at -80 °C until further use.

The above metabolite standard solution and mentioned media extract were mixed in equal volumes to prepare the primary stock solution. Subsequently, the stock was serially diluted to prepare different calibration levels as represented in table 2.2. These were subsequently diluted to obtain calibrants and QC samples at concentration ranges/concentrations described in the rest of the manuscript. Standard QCs (QC1 and QC2) were prepared at intermediate concentration levels by mixing 85 µL + 15 µL (higher), and 25 µL + 75 µL (lower), of stock solution and diluent, respectively. Whereas, Spiked QCs (QC3 and QC4) were prepared in similar fashion with a solution containing 10 % albumin.

2.2.3 Cell culture

Cells were cultured in Dubelco's MEM containing glucose (1 mg/mL), L-glutamine (0.584mg/ml), and 10% Fetal Bovine Serum and 1% non-essential amino acids (NEA) was used. Cells lines were maintained at 37°C in a humidified atmosphere of 5% CO2/95% air. All the cells cultures and intracellular extractions were carried out by Selva Rupa Immanuel as part of a collaboration with Dr. Anu Raghunathan, NCL Pune. Detailed information is available elsewhere.[16]

Table 2.2 Dilution chart for preparation of calibration levels.

Sr. No	Dilution factor	Volm of stock (µL)	Volm of diluent (ACN:H$_2$0, 1:1)	IS solution (µL)	Diluent	Total vol. (µL)
1	1	100	0	100	200	400
2	1.1	90	10	100	200	400
3	1.3	80	20	100	200	400
4	1.4	70	30	100	200	400
5	1.7	60	40	100	200	400
6	2	50	50	100	200	400
7	2.5	40	60	100	200	400
8	3.3	30	70	100	200	400
9	5	20	80	100	200	400
10	10	10	90	100	200	400
11	15.4	6.5	93.5	100	200	400
12	20	5	95	100	200	400

2.2.4 Extraction of media sample

The samples were removed from -80°C and were allowed to thaw on an ice bath. Post-thawing, the samples were thoroughly mixed to ensure content uniformity. In a fresh 1.5 mL tube, 100 µL of extracellular sample was mixed with 400 µL of chilled methanol followed by thorough mixing of samples for ~1 min. Subsequently, the mixture was subjected to centrifugation for 15 min at 5000 rpm in a temperature controlled centrifuge (4°C). 300 µL supernatant was collected at the end of the extraction procedure. The samples were further diluted 10 and 5 times in consecutive two steps. 50 µL extract was mixed with equal volume of internal standard (4.399 µM verapamil in 50% acetonitrile) solution prior to LC-HRMS run.

2.2.5 LC-HRMS analysis

Samples were analyzed on reverse-phase C18-hypersil gold column (10cm * 2.1mm * 3.0µm, Thermo) with a flow rate of 1ml per min. The mobile phase consisted of 0.1% formic acid in deionized water (mobile phase A) and 0.1% formic acid in acetonitrile (mobile phase B). The mobile phase gradient was set to 30% 'B' (0-2.5 min), 90% 'B' (3.5-5.5 min), 30% 'B' (5.6-8.0 min). Liquid chromatograph was coupled with Q-Exactive™ (Thermo) high-resolution mass spectrometer using a heated-ESI source. The instrument was operated using Xcalibur™ (Thermo) software version 2.2. The data was acquired in 60-900 *m/z* range at 70,000 FWHM resolution with AGC target 1e6 ions, maximum injection time 50 mSec, sheath gas 35, auxiliary gas 15 and ionization voltage 3.5 kV. Standard and sample data was acquired in triplicates in both positive and negative ion mode. MS data analysis was done following Qual/Quan approach. Initial qualification of metabolites of interest from biological matrix was based on following two tests of merits. First, the generation of accurate mass extracted ion chromatogram (AM-XIC) of individual analytes, and subsequent structural confirmation using tandem MS based signature fragment identification. Mass Frontier™ version 7.0.3.1 (developed by High Chem™) was used for structural fragment evaluation of tandem MS data. The metabolites confirmed through the qualitative analysis were quantitated from various intra/extra-cellular samples. Accurate mass extracted ion chromatogram (AM-XIC) was used for generating calibration curve as well in quantitation of metabolites from samples with mass extraction window 20 ppm. The accuracy and precision of the method was checked using various standard and spiked QC samples. The reproducibility of the method was periodically monitored using intermittent QC runs. Raw data was processed using Thermo Xcalibur™

version 2.2 SP1, build 48 (Modules: Qual browser, Quan browser). An average response for triplicate sample run was used for quantitation.

2.3 Results and Discussion

2.3.1 HRAM full scan and MS/MS analysis

Figures 2.1 gives an overview of the scale of the qual/quant analytical workflow described in this work that necessitates detailed performance evaluation. Figure 2.2 describes the sequence of the quantitative workflow for investigating the CORE of metabolites in the differentially expressed sub populations of glioblastoma samples (U87 and NSP). Tentative times for the sample extraction and the entire quantitative LC-HRMS analysis subsequent to method optimization are indicated in figure 2.2. This did not include the time involved in data processing and interpretation. The entire sample extraction for this study was carried out in multiple steps, each performed discretely on a sample lot basis. The extra-cellular and intra-cellular samples were extracted using two different protocols. Care was taken to prevent any sample degradation during the extraction and the samples were stored at -80°C prior to LC-HRMS analysis.

Figure 2.3 illustrates high-resolution data obtained for two representative intracellular metabolites from a pooled sample in the negative and positive ion modes respectively. The metabolites, (a) glutamine $[M+H]^+$ and (b) lactic acid $[M-H]^-$, were detected well within a mass accuracy of 5 ppm. The rest of the metabolites were detected within 10 ppm mass accuracy as well in the full scan mode. All the 34 targeted metabolites, which included amino acids, carbohydrates, and small organic acids, were subsequently qualified using MS/MS. A precursor ion selection window of ±0.5 *m/z* was used. Table 2.3 summarizes all the respective product ions detected for the metabolites. This data was in agreement with the respective libraries (METLIN and MASSBANK) confirming the presence of the metabolites in the samples under investigation. In case the MS/MS data for particular metabolites was not available in METLIN, the data was matched with the theoretical fragmentation pattern generated by MassFrontier^{TM} (Thermo).
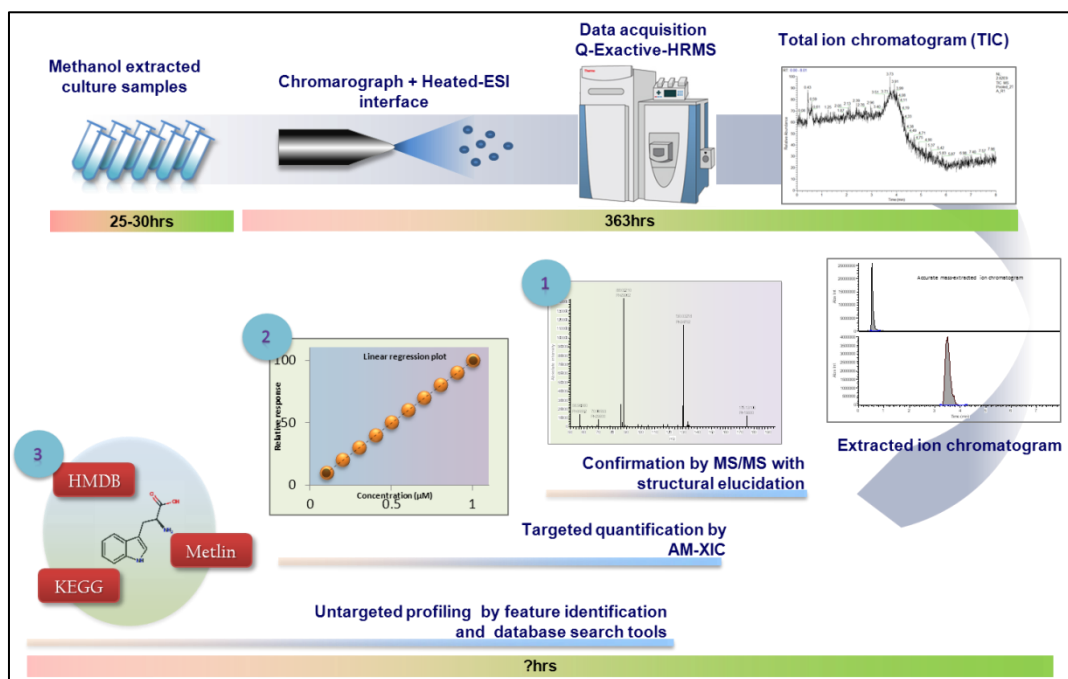
Figure 2.2 Overview of the qual/quant analytical workflow used for the LC-HRMS analysis of the glioblastoma metabolic CORE investigations. (http://planetorbitrap.com/q-exactive)

a)
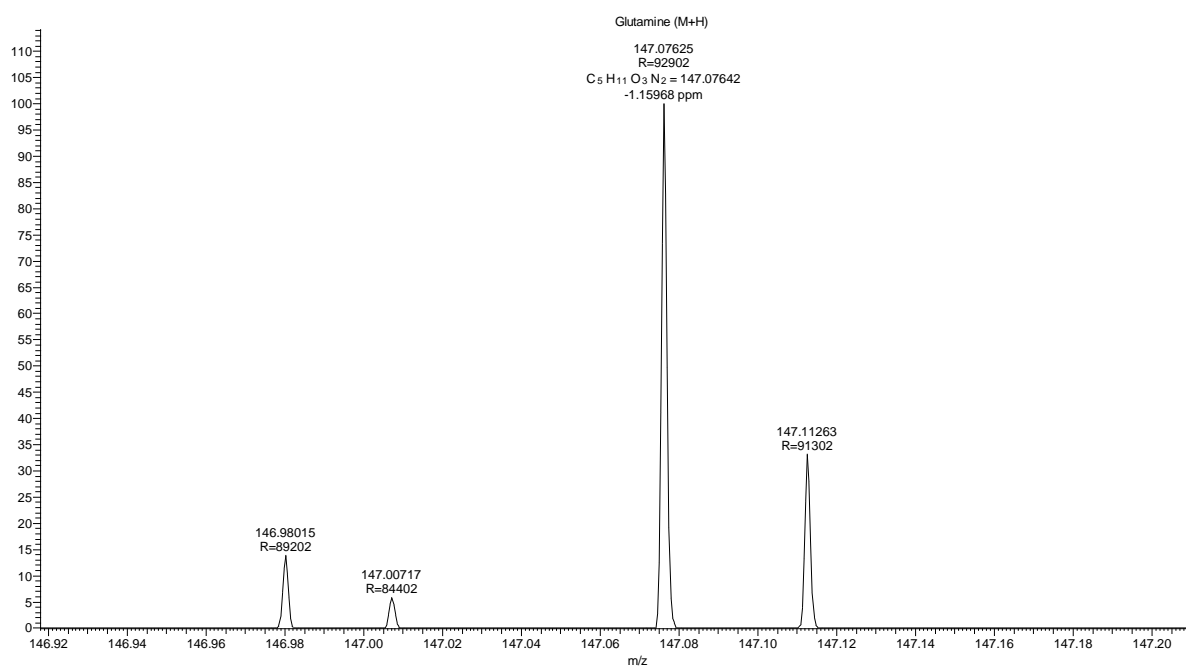
b)
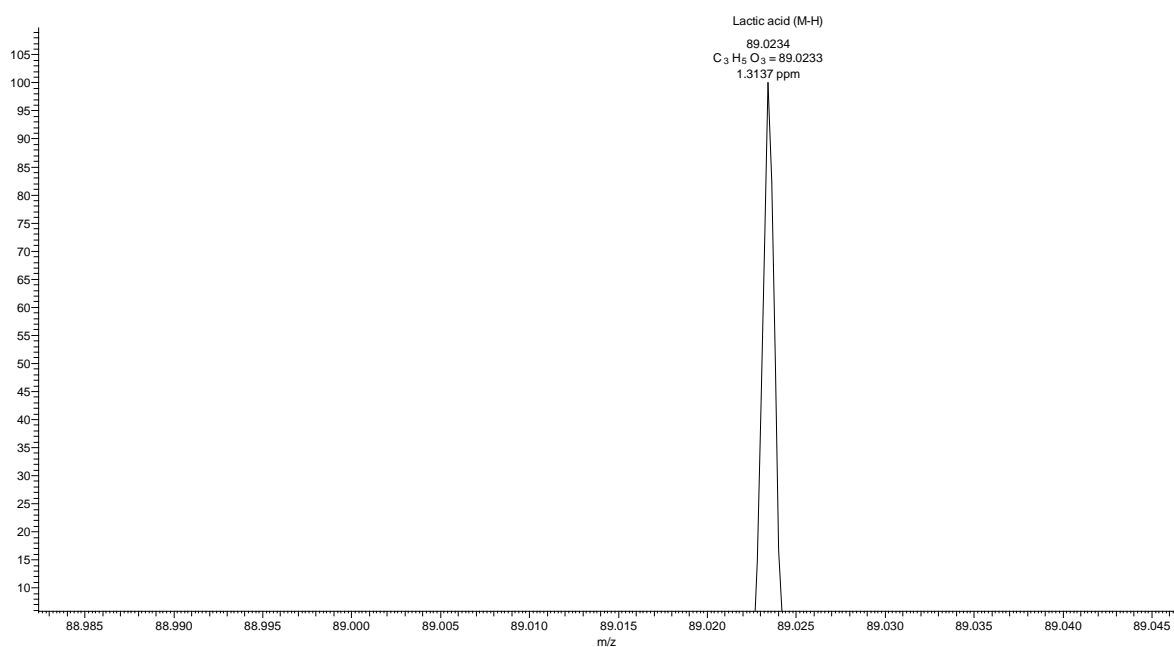
Figure 2.3 High-resolution mass spectrum of (a) glutamine and (b) lactic acid at 70,000 resolution (at m/z 200) in positive and negative ion mode respectively.

Table 2.3 MS/MS confirmation of 34 metabolites

Metabolites	Precursor *m/z*	Matched product ions in MS/MS
Alanine	90.0557	73.0292, 61.0293, 60.0453
Arginine	175.1192	60.0565, 158.09272, 157.1086, 116.071, 112.0874
Asparagine	133.06	99.0067
Aspartic acid	134.0450	116.0347, 88.04, 74.0245, 90.00148
Cysteine	241.0311	74.0244, 120.0118
Glutamic acid	148.0607	130.0502, 101.0238, 84.0451, 102.0556, 116.0368
Glutamine	147.0767	101.0715, 84.04515, 102.0556, 60.0453, 70.0659, 74.0244
Glycine	76.04	Below lowest *m/z* range of instrument
Histidine	156.077	110.071, 138.066, 115.0558, 95.061, 93.045, 83.061, 82.053,
Leucine/Isoleucine	132.1021	114.0667, 114.0917, 86.0971, 84.0452, 69.0707, 56.0502
Lysine	147.113	130.0866, 129.1026, 101.1078, 94.0658, 84.0815, 82.0658, 74.0243
Methionine	150.0577	118.0297, 73.0655
Phenylalanine	166.0864	120.0811, 149.0598, 107.0496, 103.0547, 56.0503
Proline	116.071	70.0659, 81.0339, 72.0816, 72.0455
Serine	106.0504	60.0453, 56.0504, 88.04, 89.0108
Threonine	120.0659	102.0556, 74.0608, 56.0504, 84.0451, 57.0344, 75.0448
Tryptophan	205.0966	188.0711, 170.0603, 159.092, 146.0604, 144.0811, 143.0732, 118.0656
Tyrosine	182.0816	165.055, 150.0553, 136.076, 147.0444, 123.0445, 119.0496, 103.0549, 56.0504
Valine	118.0868	72.0816, 84.08016, 59.0501
Ornithine	133.1056	116.0711, 72.0816, 70.066
Citrulline	176.1072	156.0772, 102.0555, 72.0816, 70.0659, 59.05
D-sorbitol	183.095	147.0645, 73.0293
Ascorbic acid	175.0239	59.0125,87.0075,115.0025
Citric acid	173.0082	73.0281,117.0181,129.0182
Lactic Acid	89.0231	59.0125,71.0124,72.9918
Malic acid	133.0142	89.0231,131.0131,59.0125
Glucose	179.0561	59.0125
Maleic acid	115.0025	68.9944, 71.0125
Malonate	103.0026	59.0125
Methymalonate	117.0182	55.0176, 73.0281
G3P	150.9793	138.9784
ketoglutarate	145.0144	57.0333,72.0281,101.0231
Oxoadipate	159.0291	87.0439,115.0389,141.0183

2.3.2 Accuracy, precision, and reproducibility of LC-HRAM analysis

Calibration ranges for various metabolites were selected following the comparison between the responses from the samples and the reference standards. The extracellular sample at the zeroth time point was essentially the culture media, which was subsequently used up by the cells to grow. However, the intracellular sample extracts had metabolite concentrations that were much lower than those for the extracellular samples. A suitable range to accommodate both the extra and intracellular metabolite sample concentrations was chosen. Samples were diluted accordingly to bring the signal responses within this working calibration range. A 10-fold dilution for the intra-cellular samples and a 500-fold dilution for the extracellular samples were used and subsequently factored in. 10 point calibration curves were generated using the internal standard normalized peak area derived from AM-XIC. Details of calibration curves and QCs are showcased in table 2.4. R^2 ~0.94-0.99 was reproducibly obtained with the calibration curves for 31 of 34 metabolites establishing linearity across the respective concentration ranges. However, R^2 for two metabolites, glucose, and lactic acid, was found to be 0.84 and 0.66, respectively. The lower correlation coefficient was a result of irregular peak shape observed for the two analytes.

Consistency in instrumental behavior and reliable data generation necessitates evaluation of the LC-HRMS platform at regular intervals. Incorporating quality control (QC) sample runs and the use of an internal reference standard (IS) spiked in the sample are two widely accepted approaches to monitor the long-term reproducibility of the method. The assessment was carried out in terms of mass accuracy, AM-XIC peak shape, and AM-XIC peak intensity/area for individual analytes. QC samples generally are a representative set of standards or sample (or pooled samples) containing analytes of interest within the working concentration ranges. IS(s), when added to a sample in known concentration, facilitates the qualitative identification (for example peak matching). It also aids in normalization of data across samples to account for instrumental response variations towards the quantitative determination of the sample components.[28] Although structurally similar or isotopically labeled IS are generally preferred, other non-endogenous IS have also been successfully used before.[29,30] IS was uniformly spiked in the entire sample set. Unlike QC samples, IS was incorporated in the sample and hence observed in every single run. IS helps in monitoring any possible variation in consecutive sample runs. The instrumental performance was monitored during the span of sample analysis by measuring the reproducibility of an intermediate

calibration level, containing all the metabolites along with an internal standard (verapamil) was measured.

Figure 2.4 illustrates the QC regime implemented in this work during calibrations and alongside sample data acquisition. Three levels of QC were used in the workflow to establish the accuracy, precision and long-term reproducibility of the LC HRAM method. Two technical QC samples, QC 1 and QC 2, consisted of reference standards from the combined metabolite mixture with concentrations intermittent to the calibrants. Two separate matrix matched sample QCs (QC3 and QC4) with known concentration spiked into a representative matrix were also prepared and used. QC 1 through 4 were analyzed along with the calibrants and the corresponding metabolite recoveries were used to validate the calibration curves. Additionally, a time-point pooled sample (extract of U87; extracellular) QC5 was prepared and subsequently analyzed intermittently to the sample runs at 9-hour intervals throughout the 17 days. All the QCs were analyzed both in the negative and positive ion modes.

Metabolite concentrations in all the QC samples were measured and % recovery {(measured concentration/known concentration)*100} was estimated. The % recoveries for all the metabolites in the QC 1 through QC 4 were found to be within 85-115 % (figure 2.5 and 2.6) indicating acceptable recoveries within 15% of the expected values. Glucose and lactic acid for QC1 and QC3 showed recoveries of 150%. Intermittently, QC5 injected at intervals of 9 hr. in both positive and negative ion mode analysis was followed by a cleaning run at the same intervals. Thus, a total of 26 combined analysis runs for positive and negative ion mode for QC5 were accomplished through the 17 days. Reproducibility across QC samples was measured as the IS normalized-peak area for each of the 34 metabolites under consideration. The peak area distribution was found to be within ±15 % RSD throughout the 26 runs/17 days. The variation in QC5 data has been represented using SD error bars in figure 2.7.

Quantitative TQ-MS workflows are established and the issues affecting quantitative analysis are well understood. TQ-MS approaches generally use a predefined targeted set of single or multiple precursor-to-product (ion) reaction monitoring (SRM, MRM) schemes for selective and sensitive quantitation.[31–33] Calibrations from low resolution extracted ion chromatograms of reference standards are used for absolute quantitation of targeted metabolites from samples. In contrast, HRMS quantitation employs accurate-mass extracted ion chromatograms (HR-AM) in the full-scan mode (FS) or parallel reaction monitoring (PRM MS

or MS/MS) modes.[34–37] Quantitative measurements can be performed on metabolic features identified with high mass accuracy in a targeted fashion on the same platform without having to setup separate LC TQ- MS analytical runs. Sensitive high-resolution measurements are susceptible to a method and instrumental variations. Performance of the analysis could be influenced by mobile phase flow rate, solvent volatility, ionization cone temperature, voltage, distance as well as angle between ESI source and the inlet capillary, sheath and auxiliary gas flow rates.[38–40] Reproducible signal responses devoid of matrix interferences and linearity across variable concentration ranges for a diverse set of metabolites are also vital for establishing HR-AM quantitative analysis. The precision, accuracy and longer-term reliability demonstrated by the results in this study indicate full-scan mode HR-AM quantitative analysis to be analytically robust for quantifying a diverse set of metabolites.

Table 2.4 Calibration statistics and recoveries of quality control samples

Analyte	Calibration range (µM)	R^2	Slope	Quality control sample			
				QC1	QC2	QC3	QC4
Alanine	0.02 - 0.50	0.942	0.24	97.9	110.6	102.7	100.2
Arginine	0.10 - 1.99	0.986	0.52	104.4	98.1	101.2	89.8
Asparagine	0.02 - 0.50	0.978	0.21	102.1	118.5	103.0	86.0
Aspartic acid	0.02 - 0.50	0.960	0.30	113.6	101.4	113.7	88.2
Cysteine	0.05 - 1.00	0.981	0.17	105.1	102.5	106.2	90.7
Glutamic acid	0.02 - 0.50	0.979	0.35	115.9	111.6	100.3	93.1
Glutamine	1.00 - 19.98	0.983	0.15	105.9	101.3	104.1	91.6
Glycine	0.12 - 2.50	0.977	0.10	95.5	105.6	102.1	92.2
Histidine	0.05 - 1.00	0.975	0.50	108.3	100.8	97.7	85.7
Leucine/isoleucine	0.20 - 4.00	0.993	2.33	102.4	101.1	99.4	95.7
Lysine	0.20 - 4.00	0.985	0.39	103.5	97.5	100.8	89.0
Methionine	0.05 - 1.01	0.983	0.69	96.8	99.3	92.7	98.0
Phenylalanine	0.10 - 2.00	0.986	0.96	100.3	101.6	96.4	94.9
Proline	0.02 - 0.50	0.968	4.00	105.6	94.3	101.4	83.2
Serine	0.12 - 2.50	0.974	0.15	112.1	100.5	109.9	91.5
Threonine	0.20 - 3.95	0.983	0.35	103.6	100.1	101.6	90.1
Tryptophan	0.02 - 0.39	0.979	0.48	102.3	110.1	97.3	108.0
Tyrosine	0.12 - 2.30	0.979	0.40	95.1	99.8	93.3	99.0
Valine	0.20 - 4.01	0.970	0.98	114.2	99.5	112.7	88.3
Ascorbic acid	0.03 - 0.51	0.953	0.37	113.2	114.8	87.4	113.3
Citric acid	0.05 - 0.93	0.956	0.31	111.6	110.3	101.2	109.3
G3P	0.11 - 2.10	0.992	0.49	105.6	108.1	103.3	104.2
Glucose	1.39 - 27.75	0.842	0.01	150.6	88.3	141.3	92.4
Ketoglutarate	0.06 - 1.22	0.991	0.64	113.5	108.2	107.7	104.2
Lactic acid	0.27 - 5.36	0.661	0.01	158.3	91.9	155.4	118.5
Citrulline	0.25 - 5.10	0.983	0.09	116.7	105.5	117.9	104.5
Ornithine	0.01 - 0.26	0.987	13.96	112.0	108.5	106.4	106.6
Malic acid	0.13 - 2.66	0.974	0.44	106.1	112.0	102.0	102.6
Maleic acid	0.01 - 0.15	0.991	2.65	112.8	112.1	104.0	106.0
Methyl-MA	0.23 - 4.54	0.998	0.40	115.2	106.4	108.6	104.0
Malonic acid	0.86 - 17.16	0.991	0.23	126.8	106.0	112.3	102.4
Oxoadipic acid	0.56 - 11.15	0.988	0.44	115.2	106.4	108.6	104.0
Pyruvic acid	0.51 - 10.14	0.967	0.09	126.8	106.0	112.3	102.4
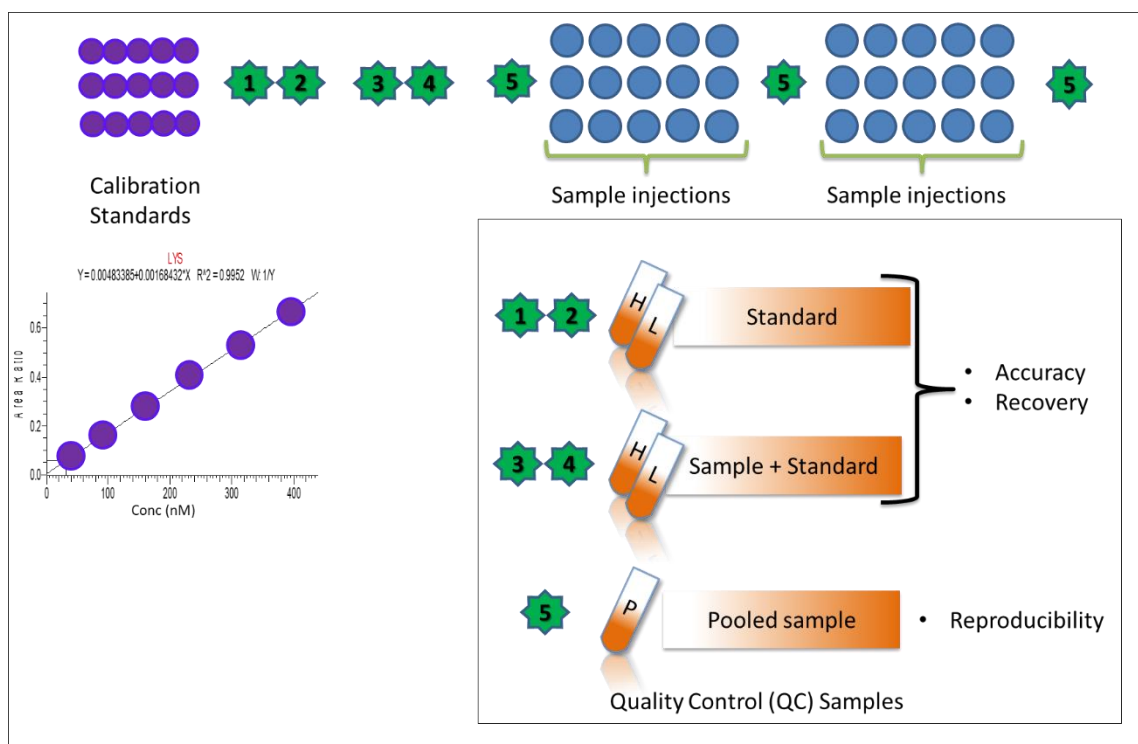
Fig. 2.4. Schematic representation of the data acquisition sequence during sample analysis. The standard calibration runs were followed by QC samples, sample injections and intermittent quality control samples, respectively.
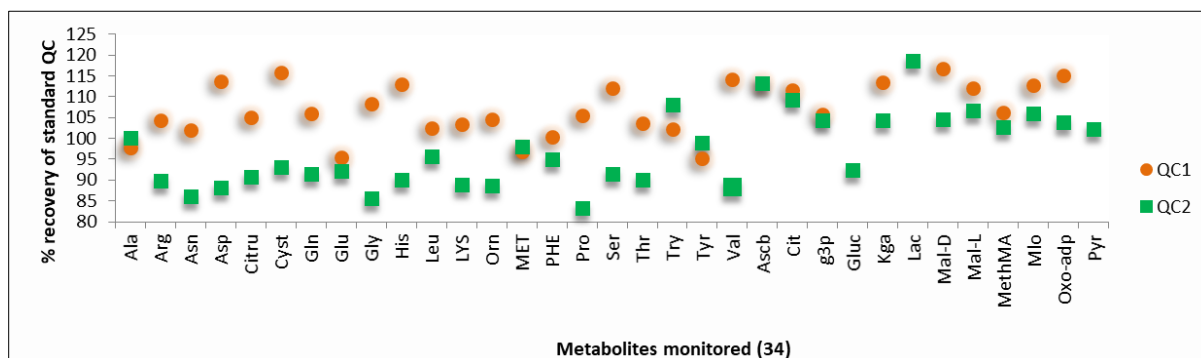
Fig. 1.5. Percentage recovery of standard quality control (QC1 and QC2) samples.
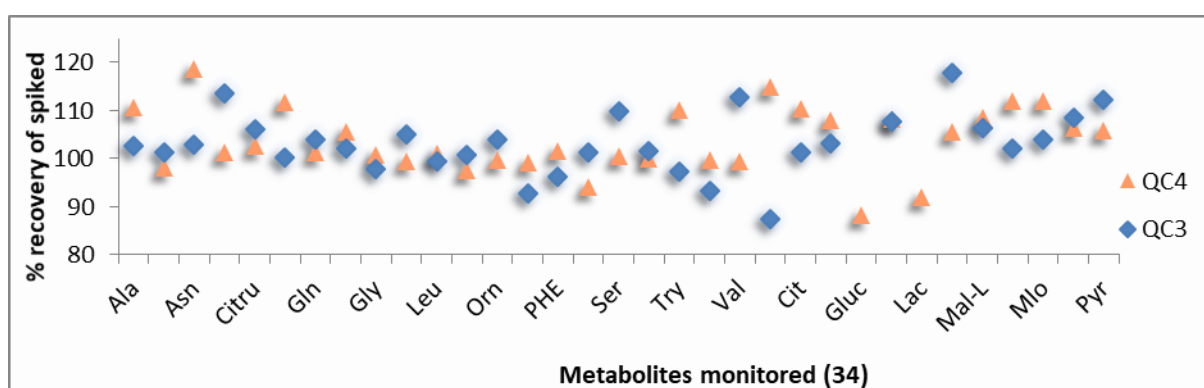
Fig. 2.6. Percentage recovery of matrix matched quality control (QC4 and QC 3) samples.
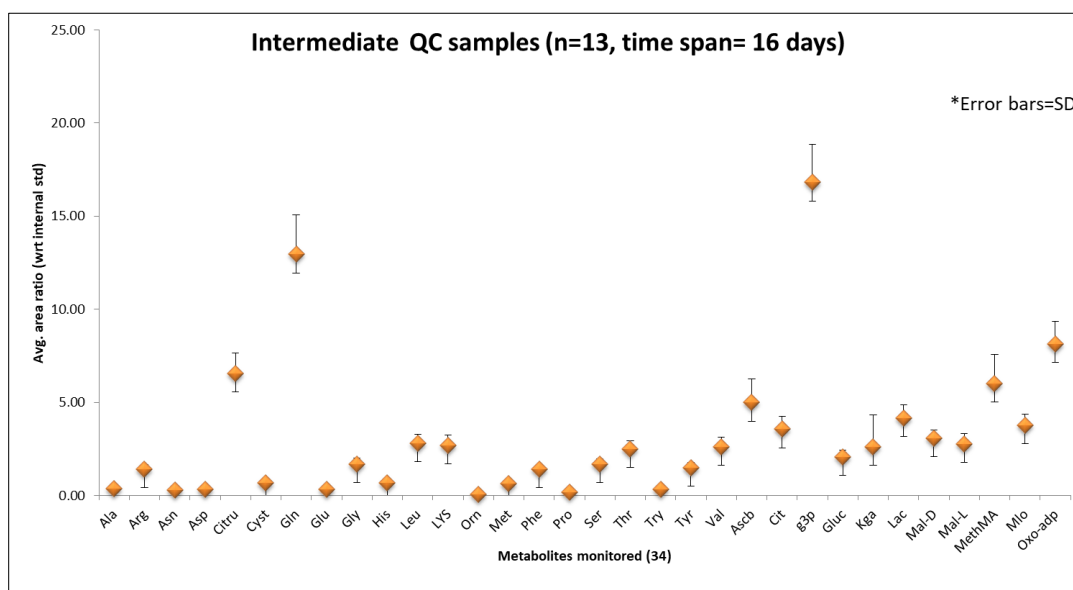
Fig. 2.7. Intermittent QC samples (QC5) were injected at an interval of 9 hours. The internal standard normalized data with standard deviation (SD) error bar is represented.

2.3.3 Targeted metabolomics of glioblastoma cell culture

Quantitative profiles of the 34 metabolites were measured for the intra and extracellular samples using LC-HRMS.[16] The sample set consisted of two glioblastoma cell lines, namely U87 (control) and NSP (differentiated) cells. The U87 is an adherent primary glioblastoma cell line whereas, NSP is a non-adherent differentiated cell line from U87. The cells were treated with a chemotherapeutic agent, temozolomide. The metabolomics expression of cell lines at three different levels of the drug was studied in order to understand the respective fold changes in the metabolite profiles (figure 2.1). To perform unsupervised principal component analysis (PCA), the metabolite concentrations in U87 and NSP were normalized using the internal standard to account for any instrumental variation. The IS normalized data was then subjected to feature scaling using maximum value normalization to obtain the data within 0 to 1 range. Maximum value normalization was carried out to avoid weightage based on concentration levels rather than the extent of variation observed across and within the sample set. The PCA plots were generated before and after the drug treatment of U87 and NSP cells. Untreated U87 and NSP time points sample were distinctly grouped indicating clear metabolic difference between these sample types (figure 2.8). There is a clear time-point dependent divergence in the two sub populations as seen in the figure 2.8.
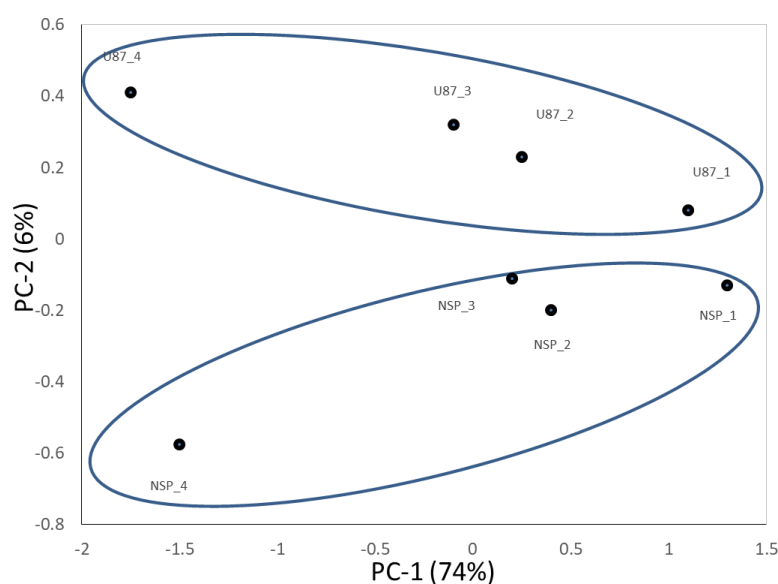
Figure 2.8 PCA plot of untreated U87 VS NSP. The suffix 1, 2, 3, and 4 represents 24, 48, 72, and 96 hrs.
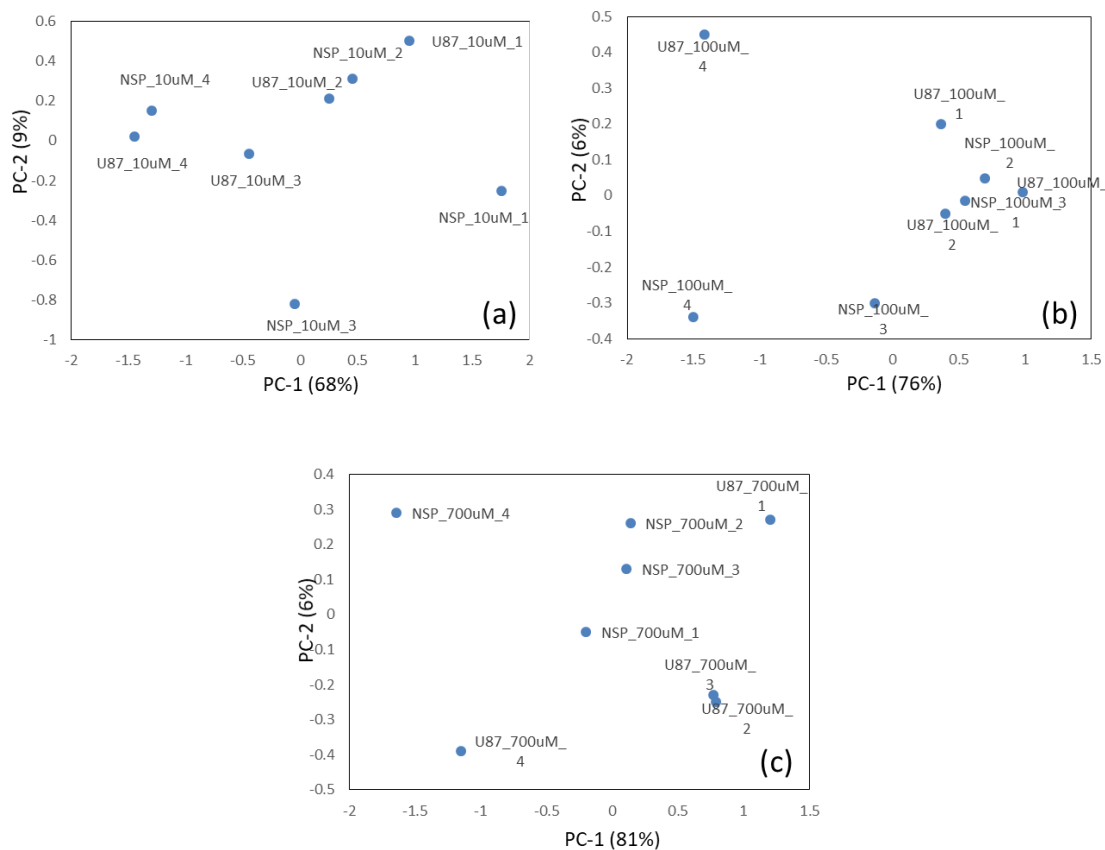
Figure 2.9 PCA plot of drug-treated U87 and NSP samples. The samples were treated at three drug concentration levels i.e. 10, 100, and 700μM temozolomide. The suffix 1, 2, 3, and 4 represents 24, 48, 72, and 96 hrs. Maximum contributing metabolites in PCA scores were found to be glucose, glutamine, serine, tryptophan, and pyruvate.

Metabolic reprogramming is considered one of the hallmarks of carcinogenesis, which represents the dynamics of beginning and advancement of cancer.[41] Cancer has been associated with specific changes in the cellular metabolism that are not simply byproducts of the disease, but rather deliberately drive the disease using alternative routes in the metabolic pathway. In this study, cultures of two (glioblastoma) cell lines were analyzed to identify differential profiles of metabolites as a part of their phenotypic expression. During the cell culture experiments clear differences between U87 and NSP were observed in terms of cell morphology, growth rate, and LD_{50} values.[16] NSP had higher LD_{50} values as compared to U87 cells. Subsequent PCA analysis (figure 2.9) of metabolic data from U87 and NSP under drug treatment groups revealed metabolic differences between these cells post drug treatment. Maximum contributing metabolites in PCA scores were found to be glucose, glutamine, serine, tryptophan, and pyruvate.

2.4 Conclusions and future scope

Comparative evaluation of HRMS-based full-scan methodologies for quantification of drugs vis-à-vis LC-QqQ MS has been investigated before.[42–45] However, acquisition of large-scale metabolomics data using LC-HRMS involves multiple analytical operations with significant complexity that can potentially propagate inaccuracies of measurement.[46] Analysis of metabolic CORE in glioblastoma cells investigated in this work is an illustrative example in this regard and involved large-scale analytical experimentation. Various levels of QC checks were necessary in order to monitor any potential variation in the HR-AM quantitation for ensuring confidence in the data generated. Precision, accuracy, and reproducibility of the HR-AM method, as established, meet the US FDA guidelines for bioanalytical method validation.[47] Metabolic profiles of the two glioblastoma cell lines were successfully measured using the developed method. PCA revealed differential grouping and changes in metabolic expression changes between U87 and NSP cells.

Measurement of biochemical pathways metabolite concentrations alone is often not sufficient in delineating cellular metabolic fluxes.[1,48] Probing metabolic flux using isotopically labeled tracers, usually accompanied by low-resolution LC-MS measurements, has been resourceful in this pursuit.[18,27,48] Extension of this work using isotopic tracer based CORE profiling for glioblastoma sub population would further delineate metabolic pathway fluxes. Improved separation of polar metabolites achieved using HILIC additionally resolves isomeric interferences. Quantitative analysis using a parallel reaction monitoring (PRM) in the MS/MS has been suggested for eliminating isomeric interferences.[49] To enhance metabolite confirmation for targeted/untargeted analyses, quantitation in the MS/MS mode, and fragmentation-based approaches can be employed.[50,51]

2.5 References

(1)   Jain, M.; Nilsson, R.; Sharma, S.; Madhusudhan, N.; Kitami, T.; Souza, a. L.; Kafri, R.; Kirschner, M. W.; Clish, C. B.; Mootha, V. K. Metabolite Profiling Identifies a Key Role for Glycine in Rapid Cancer Cell Proliferation. *Science (80-.).* **2012**, *336* (6084), 1040–1044.

(2)   Wang, J.; Zhou, L.; Lei, H.; Hao, F.; Liu, X.; Wang, Y.; Tang, H. Simultaneous Quantification of Amino Metabolites in Multiple Metabolic Pathways Using Ultra-High Performance Liquid Chromatography with Tandem-Mass Spectrometry. *Sci. Rep.* **2017**, *7* (1), 1–16.

(3)   Ramanathan, R.; Jemal, M.; Ramagiri, S.; Xia, Y. Q.; Humpreys, W. G.; Olah, T.; Korfmacher, W. a. It Is Time for a Paradigm Shift in Drug Discovery Bioanalysis: From SRM to HRMS. *J. Mass Spectrom.* **2011**, *46* (6), 595–601.

(4)   Rochat, B.; Kottelat, E. The Future Key Role of LC – High-Resolution-MS Analyses in Clinical Laboratories : A Focus on Quantification. *Bioanalysis* **2012**, *4* (24), 2939–2958.

(5)   Hopfgartner, G.; Tonoli, D.; Varesio, E. High-Resolution Mass Spectrometry for Integrated Qualitative and Quantitative Analysis of Pharmaceuticals in Biological Matrices. *Anal Bioanal Chem* **2012**, *402*, 2587–2596.

(6)   Gertsman, I.; Gangoiti, J. A.; Barshop, B. A. Validation of a Dual LC–HRMS Platform for Clinical Metabolic Diagnosis in Serum, Bridging Quantitative Analysis and Untargeted Metabolomics. *Metabolomics* **2014**, *10* (2), 312–323.

(7)   Zhang, H.; Zhang, D.; Ray, K.; Zhu, M. Mass Defect Filter Technique and Its Applications to Drug Metabolite Identification by High-Resolution Mass Spectrometry. *J. Mass Spectrom.* **2009**, *44* (7), 999–1016.

(8)   Zhu, M.; Zhang, H.; Humphreys, W. G. Drug Metabolite Profiling and Identification by High-Resolution Mass Spectrometry. *J. Biol. Chem.* **2011**, *286* (29), 25419–25425.

(9)   Ojanperä, I.; Kolmonen, M.; Pelander, A. Current Use of High-Resolution Mass Spectrometry in Drug Screening Relevant to Clinical and Forensic Toxicology and Doping Control. *Anal. Bioanal. Chem.* **2012**, *403* (5), 1203–1220.

(10)   Lommen, A. MetAlign: Interface-Driven, Versatile Metabolomics Tool for Hyphenated Full-Scan Mass Spectrometry Data Preprocessing. **2009**, *81* (8), 3079–3086.

(11)   Fung, E. N.; Xia, Y. Q.; Aubry, A. F.; Zeng, J.; Olah, T.; Jemal, M. Full-Scan High Resolution Accurate Mass Spectrometry (HRMS) in Regulated Bioanalysis: LC-HRMS for the Quantitation of Prednisone and Prednisolone in Human Plasma. *J. Chromatogr. B Anal. Technol. Biomed. Life Sci.* **2011**, *879* (27), 2919–2927.

(12)   Lu, L.; Wang, J.; Xu, Y.; Wang, K.; Hu, Y.; Tian, R.; Yang, B.; Lai, Q.; Li, Y.; Zhang, W.; et al. A High-Resolution LC-MS-Based Secondary Metabolite Fingerprint Database of Marine Bacteria. *Sci. Rep.* **2014**, *4*, 6537.

(13)   Fernie, A. R.; Trethewey, R. N.; Krotzky, A. J. Metabolite Profiling: From Diagnostics to Systems Biology. *Nat. Rev. Mol. Cell Biol.* **2004**, *5* (September), 763–769.

(14)   Joyce, A. R.; Palsson, B. Ø. The Model Organism as a System: Integrating "omics" Data Sets. *Nat. Rev. Mol. Cell Biol.* **2006**, *7* (3), 198–210.

(15)   KELL, D. Metabolomics and Systems Biology: Making Sense of the Soup. *Curr. Opin. Microbiol.* **2004**, *7* (3), 296–307.

(16)   Immanuel, S. R. C.; Ghanate, A. D.; Parmar, D. S.; Marriage, F.; Panchagnula, V.; Day, P. J.; Raghunathan, A. Integrative Analysis of Rewired Central Metabolism in Temozolomide Resistant Cells. *Biochem. Biophys. Res. Commun.* **2018**, *495* (2), 2010–2016.

(17)   Ringnér, M. What Is Principal Component Analysis? *Nat Biotechnol* **2008**, *26* (3), 303–

304.

(18) Schatschneider, S.; Abdelrazig, S.; Safo, L.; Henstra, A. M.; Millat, T.; Kim, D. H.; Winzer, K.; Minton, N. P.; Barrett, D. A. Quantitative Isotope-Dilution High-Resolution-Mass-Spectrometry Analysis of Multiple Intracellular Metabolites in Clostridium Autoethanogenum with Uniformly13C-Labeled Standards Derived from Spirulina. *Anal. Chem.* **2018**, *90* (7), 4470–4477.

(19) Lu, W.; Clasquin, M. F.; Melamud, E.; Amador-Noguez, D.; Caudy, A. A.; Rabinowitz, J. D. Metabolomic Analysis via Reversed-Phase Ion-Pairing Liquid Chromatography Coupled to a Stand Alone Orbitrap Mass Spectrometer. *Anal. Chem.* **2010**, *82* (8), 3212–3221.

(20) Paglia, G.; Hrafnsdóttir, S.; Magnúsdóttir, M.; Fleming, R. M. T.; Thorlacius, S.; Palsson, B. Ø.; Thiele, I. Monitoring Metabolites Consumption and Secretion in Cultured Cells Using Ultra-Performance Liquid Chromatography Quadrupole-Time of Flight Mass Spectrometry (UPLC-Q-ToF-MS). *Anal. Bioanal. Chem.* **2012**, *402* (3), 1183–1198.

(21) Yuan, W.; Anderson, K. W.; Li, S.; Edwards, J. L. Subsecond Absolute Quantitation of Amine Metabolites Using Isobaric Tags for Discovery of Pathway Activation in Mammalian Cells. *Anal. Chem.* **2012**, *84* (6), 2892–2899.

(22) Ibáñez, C.; Simó, C.; García-Cañas, V.; Gómez-Martínez, Á.; Ferragut, J. A.; Cifuentes, A. CE/LC-MS Multiplatform for Broad Metabolomic Analysis of Dietary Polyphenols Effect on Colon Cancer Cells Proliferation. *Electrophoresis* **2012**, *33* (15), 2328–2336.

(23) Panopoulos, A. D.; Yanes, O.; Ruiz, S.; Kida, Y. S.; Diep, D.; Tautenhahn, R.; Herrerías, A.; Batchelder, E. M.; Plongthongkum, N.; Lutz, M.; et al. The Metabolome of Induced Pluripotent Stem Cells Reveals Metabolic Changes Occurring in Somatic Cell Reprogramming. *Nat. Publ. Gr.* **2011**, *22* (1), 168–177.

(24) Arnhard, K.; Pitterl, F.; Sperner-Unterweger, B.; Fuchs, D.; Koal, T.; Oberacher, H. A Validated Liquid Chromatography-High Resolution-Tandem Mass Spectrometry Method for the Simultaneous Quantitation of Tryptophan, Kynurenine, Kynurenic Acid, and Quinolinic Acid in Human Plasma. *Electrophoresis* **2018**, 1171–1180.

(25) Van Liempd, S.; Cabrera, D.; Mato, J. M.; Falcon-Perez, J. M. A Fast Method for the Quantitation of Key Metabolites of the Methionine Pathway in Liver Tissue by High-Resolution Mass Spectrometry and Hydrophilic Interaction Ultra-Performance Liquid Chromatography. *Anal. Bioanal. Chem.* **2013**, *405* (15), 5301–5310.

(26) Yang, Z. L.; Li, H.; Wang, B.; Liu, S. Y. An Optimized Method for Neurotransmitters and Their Metabolites Analysis in Mouse Hypothalamus by High Performance Liquid Chromatography-Q Exactive Hybrid Quadrupole-Orbitrap High-Resolution Accurate Mass Spectrometry. *J. Chromatogr. B Anal. Technol. Biomed. Life Sci.* **2016**, *1012–1013*, 79–88.

(27) Shlomi, T.; Fan, J.; Tang, B.; Kruger, W. D.; Rabinowitz, J. D. Quantitation of Cellular Metabolic Fluxes of Methionine. *Anal. Chem.* **2014**, *86* (3), 1583–1591.

(28) Murray, K. K.; Boyd, R. K.; Eberlin, M. N.; Langley, G. J.; Li, L.; Naito, Y. Definitions of Terms Relating to Mass Spectrometry (IUPAC Recommendations 2013)*. *Pure Appl. Chem* **2013**, *85* (7), 1515–1609.

(29) Singh, A.; Panchagnula, V. High Throughput Quantitative Analysis of Melamine and Triazines by MALDI-TOF MS. *Anal. Methods* **2011**, *3* (10), 2360.

(30) Wang, P.; Giese, R. W. Recommendations for Quantitative Analysis of Small Molecules by Matrix-Assisted Laser Desorption Ionization Mass Spectrometry. *J. Chromatogr. A* **2017**, *1486*, 35–41.

(31) Kadar, H.; Veyrand, B.; Antignac, J.-P.; Durand, S.; Monteau, F.; Le Bizec, B.

Comparative Study of Low- versus High-Resolution Liquid Chromatography-Mass Spectrometric Strategies for Measuring Perfluorinated Contaminants in Fish. *Food Addit. Contam. Part A. Chem. Anal. Control. Expo. Risk Assess.* **2011**, *28* (9), 1261–1273.

(32)   Stolker, A. a M.; Niesing, W.; Fuchs, R.; Vreeken, R. J.; Niessen, W. M. a; Brinkman, U. a T. Liquid Chromatography with Triple-Quadrupole and Quadrupole-Time-of-Flight Mass Spectrometry for the Determination of Micro-Constituents - A Comparison. *Anal. Bioanal. Chem.* **2004**, *378* (7), 1754–1761.

(33)   Botitsi, H. V; Garbis, S. D.; Economou, A.; Tsipi, D. F. Current Mass Spectrometry Strategies for the Analysis of Pesticides and Their Metabolites in Food and Water Matrices. *Mass Spectrom. Rev.* **2011**, *30* (5), 907–939.

(34)   Cordeiro, F. B.; Ferreira, C. R.; Sobreira, T. J. P.; Yannell, K. E.; Jarmusch, A. K.; Cedenho, A. P.; Lo Turco, E. G.; Cooks, R. G. Multiple Reaction Monitoring (MRM)-Profiling for Biomarker Discovery Applied to Human Polycystic Ovarian Syndrome. *Rapid Commun. Mass Spectrom.* **2017**, *31* (17), 1462–1470.

(35)   Hopfgartner, G.; Varesio, E.; Tschäppät, V.; Grivet, C.; Bourgogne, E.; Leuthold, L. A. Triple Quadrupole Linear Ion Trap Mass Spectrometer for the Analysis of Small Molecules and Macromolecules. *J. Mass Spectrom.* **2004**, *39* (8), 845–855.

(36)   Mol, H. G. J.; Van Dam, R. C. J.; Zomer, P.; Mulder, P. P. J. Screening of Plant Toxins in Food, Feed and Botanicals Using Full-Scan High-Resolution (Orbitrap) Mass Spectrometry. *Food Addit. Contam. Part A. Chem. Anal. Control. Expo. Risk Assess.* **2011**, *28* (10), 1405–1423.

(37)   Zhou, J.; Liu, H.; Liu, Y.; Liu, J.; Zhao, X.; Yin, Y. Development and Evaluation of a Parallel Reaction Monitoring Strategy for Large-Scale Targeted Metabolomics Quantification. *Anal. Chem.* **2016**, *88* (8), 4478–4486.

(38)   Periat, A.; Kohler, I.; Thomas, A.; Nicoli, R.; Boccard, J.; Veuthey, J. L.; Schappler, J.; Guillarme, D. Systematic Evaluation of Matrix Effects in Hydrophilic Interaction Chromatography versus Reversed Phase Liquid Chromatography Coupled to Mass Spectrometry. *J. Chromatogr. A* **2016**, *1439*, 42–53.

(39)   Schlittenbauer, L.; Seiwert, B.; Reemtsma, T. Matrix Effects in Human Urine Analysis Using Multi-Targeted Liquid Chromatography-Tandem Mass Spectrometry. *J. Chromatogr. A* **2015**, *1415*, 91–99.

(40)   Dams, R.; Huestis, M. A.; Lambert, W. E.; Murphy, C. M. Matrix Effect in Bio-Analysis of Illicit Drugs with LC-MS/MS: Influence of Ionization Type, Sample Preparation, and Biofluid. *J. Am. Soc. Mass Spectrom.* **2003**, *14* (11), 1290–1294.

(41)   Duckwall, C. S.; Murphy, T. A.; Young, J. D. Mapping Cancer Cell Metabolism with(13)C Flux Analysis: Recent Progress and Future Challenges. *J. Carcinog.* **2013**, *12*, 13.

(42)   Zhang, N. R.; Sean Yu; Tiller, P.; Yeh, S.; Mahan, E.; Emary, W. B. Quantitation of Small Molecules Using High-Resolution Accurate Mass Spectrometers – a Different Approach for Analysis of Biological Samples. *Rapid Commun. Mass Spectrom.* **2009**, *23*, 1085–1094.

(43)   Fedorova, G.; Randak, T.; Lindberg, R. H.; Grabic, R. Comparison of the Quantitative Performance of a Q-Exactive High-Resolution Mass Spectrometer with That of a Triple Quadrupole Tandem Mass Spectrometer for the Analysis of Illicit Drugs in Wastewater. *Rapid Commun. Mass Spectrom.* **2013**, *27* (15), 1751–1762.

(44)   Henry, H.; Sobhi, H. R.; Scheibner, O.; Bromirski, M.; Nimkar, S. B.; Rochat, B. Comparison between a High-Resolution Single-Stage Orbitrap and a Triple Quadrupole Mass Spectrometer for Quantitative Analyses of Drugs. *Rapid Commun. Mass*

Spectrom. **2012**, *26* (5), 499–509.

(45)   Tonoli, D.; Varesio, E.; Hopfgartner, G. Quantification of Acetaminophen and Two of Its Metabolites in Human Plasma by Ultra-High Performance Liquid Chromatography-Low and High Resolution Tandem Mass Spectrometry. *J. Chromatogr. B Anal. Technol. Biomed. Life Sci.* **2012**, *904*, 42–50.

(46)   Zelena, E.; Dunn, W. B.; Broadhurst, D.; Francis-McIntyre, S.; Carroll, K. M.; Begley, P.; O'Hagan, S.; Knowles, J. D.; Halsall, A.; Wilson, I. D.; et al. Development of a Robust and Repeatable UPLC-MS Method for the Long-Term Metabolomic Study of Human Serum. *Anal. Chem.* **2009**, *81* (4), 1357–1364.

(47)   U.S. Department of Health and Human Services Food and Drug Administration. Guidance for Industry Bioanalytical Method Validation Guidance for Industry Bioanalytical Method Validation (2001). *Food Drug Adm.* **2001**, 1–44.

(48)   Jang, C.; Chen, L.; Rabinowitz, J. D. Metabolomics and Isotope Tracing. *Cell* **2018**, *173* (4), 822–837.

(49)   Qi, Y.; Geib, T.; Schorr, P.; Meier, F.; Volmer, D. A. On the Isobaric Space of 25-Hydroxyvitamin D in Human Serum: Potential for Interferences in Liquid Chromatography/Tandem Mass Spectrometry, Systematic Errors and Accuracy Issues. *Rapid Commun. Mass Spectrom.* **2014**, *29* (1), 1–9.

(50)   Naz, S.; Moreira dos Santos, D. C.; García, A.; Barbas, C. Analytical Protocols Based on LC-MS, GC-MS and CE-MS for Nontargeted Metabolomics of Biological Tissues. *Bioanalysis* **2014**, *6* (12), 1657–1677.

(51)   Fenaille, F.; Barbier Saint-Hilaire, P.; Rousseau, K.; Junot, C. Data Acquisition Workflows in Liquid Chromatography Coupled to High Resolution Mass Spectrometry-Based Metabolomics: Where Do We Stand? *J. Chromatogr. A* **2017**, *1526*, 1–12.

Chapter 3

Targeted Metabolic Profiling Using Hydrophilic Interaction Liquid Chromatography - High Resolution Mass Spectrometry (HILIC-HRMS)

3A. Determination of polar metabolites from intracellular extracts of *Chromobacterium violaceum*

3.1 Introduction

HILIC was first coined by Alpert in 1990 who described it as "an alternative chromatographic procedure for separating highly polar compounds".[1] In the last decade, HILIC has been used in a wide variety of analyses of uncharged hydrophilic and amphiphilic compounds that are too polar to be retained in RPC but have insufficient charge to allow effective electrostatic retention in ion-exchange chromatography (IEC). This is evidently reflected by the substantial increase in the number of publications on HILIC as the need to analyze polar compounds such as metabolites from complex mixtures has been constantly growing.[2] HILIC employs traditional polar stationary phases such as silica (Si-OH), amino (-NH2), amide (-CONH2) or cyano (-CN) comparable to NPC with the mobile phases comparable to those employed in the RPC, albeit in a reverse gradient of polarity.[3–7] It is noteworthy that newer stationary phases are being constantly added to the HILIC portfolio, expanding the list of available phases for specific applications.[5,8–14] HILIC allows separation of compounds such as amino acids, organic acids, carbohydrates, oligonucleotide, polar pharmaceuticals, small peptides and natural products.[15–19]

HILIC offers several advantages in comparison to RPC and NPC. These include retention of analytes that generally elute at void volumes in RPC and the choice of aqueous phases that ensure solubility of polar compounds otherwise not feasible in case of conventional NPC. Additionally, HILIC removes the need for using ion pairing agents for polar separation. Complementary selectivity and compatibility with MS have resulted in a recent surge in its application for metabolomics. Current application of HILIC allows separation of compounds such as amino acids, organic acids, carbohydrates, oligonucleotide, polar pharmaceuticals, small peptides, natural products, et cetera.[15–19]

The threat of antibiotic-resistant human pathogens and infectious microorganisms is a global concern with portending grave human health outcomes. Improved methods are necessary to identify and understand genetic modifications that ultimately give rise to an adapted system with drug resistance. Changes associated with the functional machinery of

microorganisms can be studied across the levels of molecular hierarchy. Monitoring metabolic expression can provide significant directions towards functional changes potentially leading to valuable insights into the pathways that were altered while acquiring the resistance. Understanding functional changes in an infectious organism can thus provide a necessary roadmap to identifying potential drug targets. Here, we describe HILIC-HRMS analysis for targeted metabolomics of intracellular polar metabolites of *Chromobacterium violaceum* (CV) grown in nutrient-rich media followed by untargeted analysis using offline XCMS platform. Metabolic profiles obtained using HILIC-MS in the wild-type and adaptive laboratory evolution strains of *Chromobacterium violaceum* with drug resistance were compared. As an extension of this work, application on of HILIC-HRMS for the determination of isotopically labelled intracellular metabolites from Chinese hamster ovary has been reported in subsequent section **(3B)**. The work demonstrates and validates the potential utility of HILIC-HRMS in metabolomics.

3.2 Materials and methods

3.2.1 Materials

All amino acids, glucose, L-ascorbic acid, citric acid, glyceraldehyde-3-phosphate, ketoglutaric acid, lactic acid, citrulline, ornithine, malic acid, maleic acid, methylmalonic acid, malonic acid, oxo-adipic acid, pyruvic acid, sorbitol, and LC-MS grade formic acid were procured from (MO, USA). LC-MS grade acetonitrile and methanol were purchased from J T Baker (PA, USA). Deionized water (specific resistivity 18.2 MΩ) was obtained from Millipore Milli-Q water purification system. Verapamil and Atorvastatin, used as internal standards (IS), were received as gratis samples from Mylan, Hyderabad. Luria-Broth (LB, Hi-MediaM575) was procured from Hi-Media (Mumbai, India).

3.2.2 Sample collection and extraction

Cell culture experiments were carried out in the collaboration with Dr. Anu Raghunathan (by Deepanwita Banerjee). Chromobacterium violaceum strain ATCC 12472T, wild-type, (C. violaceum or WT) was obtained from the American Type Culture Collection Center (ATCC), USA. The wild-type C. violaceum was inoculated using 10% inoculum of

overnight starter culture in Luria-broth media. The culture was maintained at 30 °C with continuous aeration in a shaker incubator set at 180 revolutions per minute (rpm). 2 mL culture was harvested at the end of 0, 6, 12, 18, 24 and 30 h. The cell pellet was obtained by centrifugation at 12000 g at 4 °C. The pellets were reconstituted with ice-cold ethanol for quenching and extraction of metabolites as reported in previous studies. Subsequently, the suspension was centrifuged at 14000 g at 4 °C, the extracts were collected and stored at -80°C until further processed for LC-MS analysis. The intracellular ethanolic extract was dried in centrivap (Labconco) at 4°C, followed by reconstitution in 100 µL of 10% water in acetonitrile containing 2 µM atorvastatin (internal standard). The samples were maintained on ice in-between the sample preprocessing steps to preserve the metabolites as much as possible. Quality control (QC) samples were prepared by pooling 10 µL extract of all the time points of three cultures. The pooled QC sample was dried as described earlier and reconstituted to the initial mobile phase composition. 5 µL of pooled sample was analyzed after every 12 sample injection (6 hours 30 min) of data acquisition interval.

3.2.3 HILIC-HRMS analysis

The metabolites were separated using hydrophilic interaction liquid chromatographic setup on Accela 1250 chromatograph (Thermo) equipped with Sequent ZIC-HILIC column (100mm*2.1mm*5µm, Merck Millipore) column with a mobile phase gradient containing 0.1% formic acid in deionized water (Mobile phase 'A') and 0.08% formic acid in acetonitrile (Mobile phase 'B'). Gradient was set with 5% of mobile phase A (0-.0-5.0mins, 300 µL/min), 13% A (15.0, 300 µL/min), 45% A (20.0min, 300 µL/min), 90% A (23.0min-25.0min, 300 µL/min), 5%A (27.0-32.0min, 700 µL/min). Heated electrospray ionization (HESI) source was used as an interface between chromatograph and HRMS instrument. The spray voltage of the source was set at 3.7 kV with capillary temperature 300°C, sheath gas 45 units, auxiliary gas 10 units, heater temperature 390 °C and S-lens RF at 50 units. The data was acquired in a range of 70-1050 *m/z* at a resolution of 70,000 FWHM with AGC target 1e6 and injection time of 120 ms.

Prior to the sample analysis, HILIC column was stabilized using three preliminary injections of a pooled sample. Subsequently, 5 µL sample volume was injected during analysis in both positive and negative ion mode. Intermittently, QC samples were injected in between

the sample run in order to evaluate the reproducibility over the entire period of data acquisition. Accurate mass based extracted ion chromatograms (AM-XIC) of metabolites along with the internal standard (IS) were integrated based upon retention time profiles to generate area under peaks. The peak areas of all the metabolites were normalized to the uniformly spiked internal standard. The relative responses of 57 metabolites and absolute response of Atorvastatin (IS), along with retention time, were monitored in these QC runs to ensure stable system performance over the duration of the sample run. The metabolites were confirmed using retention time specific MS/MS (20ev, both ion modes) of metabolites in an HCD cell of the Q-Exactive™ mass spectrometer. The observed MS/MS profiles were compared with the METLIN database for confirmation. In cases the MS/MS spectra were not available in the database, the MS/MS profiles were confirmed against theoretical fragments generated using MassFrontier (Thermo) software.

3.3 Results and discussion

3.3.1 Evaluation of reproducibility of HILIC-HRMS

Initial method development was carried out using a cocktail containing standard metabolite mix and chemically defined media. C18 and ZIC-HILIC columns were compared with respect to the analyte retention times, peak shapes and separation resolution. The representative AM-XICs using RP and HILIC columns are shown in figure 3A.1. Unlike C18 columns, HILIC provided the enhanced retention of polar metabolites. Accurate mass and added parameter of retention time (R_t) improved the metabolite peak assignment. On C18 column, the analytes were not retained and eluted at dead volume even after trying different mobile phase compositions, pH(s) using buffers and gradient of mobile phases (data not shown). Evidently, the AM-XIC on C18 (RP) showcases the overlapping analyte peaks within the first 1 min. However, on HILIC columns, metabolites were retained and eluted over a period of 0-22 min (figure 3A.1) with a simple mobile phase composition containing 0.1% formic acid in water (phase A) and acetonitrile (phase B). Analyte peaks observed on HILIC were sharper with Gaussian profiles as compared to the C18 column for the same dilution levels of metabolite cocktail. This unambiguously demonstrates the improved separation of polar metabolites along with increment in the peaks areas using HILIC leading to potential

improvement in the sensitivity of the method for sample analysis. Sufficient chromatographic resolution between different analyte peaks was obtained by optimizing the elution gradient for HILIC (Figure 3A.2). These results are in agreement with previous report.[20]

(a) Reverse phase-C18 chromatography

(b) ZIC-HILIC column (HILIC chromatography)
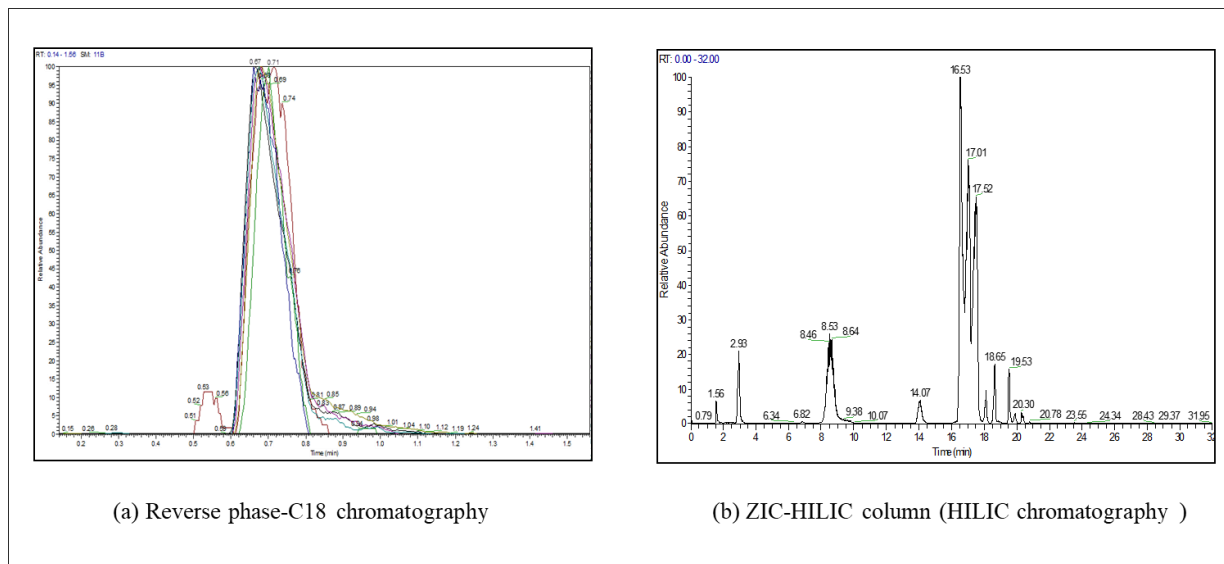
Figure 3A.1 AM-XIC chromatogram of polar metabolites on reverse phase-C18 (a) and ZIC-HILIC (b) columns. The mobile phases (aqueous and organic) used in both cases were unaltered. However, the gradient in the case of ZIC-HILIC was optimized for the best possible resolution of metabolite standard.
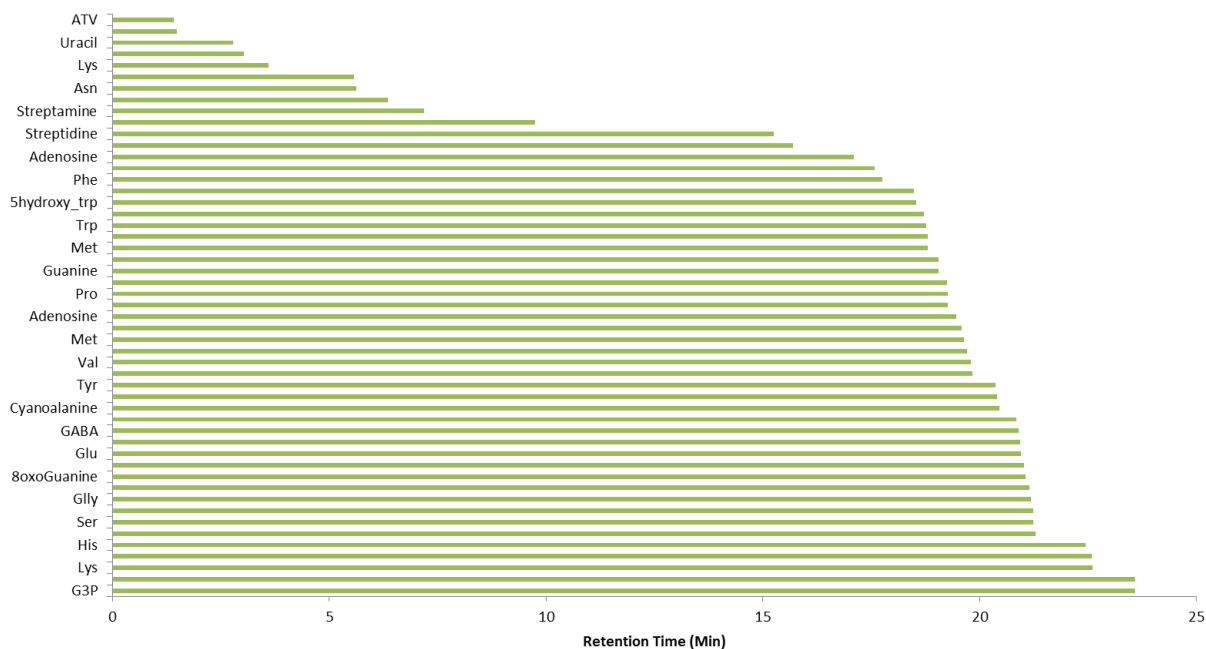
Figure3A.2 Schematic representation of metabolite retention time.
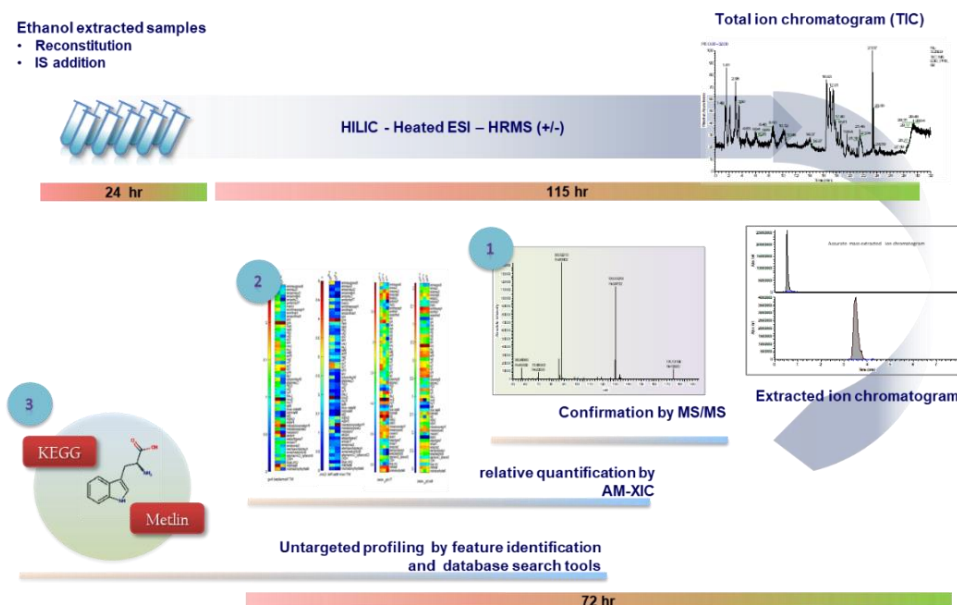
Figure 3A.3 Analytical workflow of HILIC-HRMS analysis of Chromobacterium violaceum metabolites. Various steps such as sample preparation, HILIC-HRMS analysis, data analysis, and MS/MS confirmation as showcased here, were carried out sequentially. Time taken for the analysis (post optimization) has been indicated.

Previously, HILIC columns have been reported to have poor reproducibility on account of lack of sufficient column stabilization that is necessary to allow the formation of the semi-immobilized aqueous rich layer to achieve reproducible retention behavior.[21] This limitation was overcome by stabilizing the HILIC column prior to initiating the sample analysis. The HILIC column was stabilized using 85% organic mobile phase for- 30 mins. This was followed by three analytical runs by injecting with mobile phase in its initial composition of the gradient (blank runs) prior to sample analysis. The schematic of the analytical workflow is shown in figure 3A.3. The blanks were repeated intermittently as well as at the end of the sample analysis and compared with the pre-sample blank runs. Reproducibility of the total ion chromatogram (TIC) profile was also monitored during the blank runs to evaluate column stability and any potential analyte carryover effects.

Figure 3A.4 represents the TIC profile of blank runs. The Blank-01 and Blank-07 represent the TIC profile at the beginning and end of the sample analysis, respectively. The rest of the blank TICs (indicated in the figure 3A.4) were acquired recurrently during sample runs. The reproducible TIC profiles of blank indicate consistent column performance. Additionally,

the retention time reproducibility of various metabolites was also monitored across the sample set and QC samples. The reproducibility of Rt was found to be within 1 percentage relative standard deviation (% RSD) of average retention time.
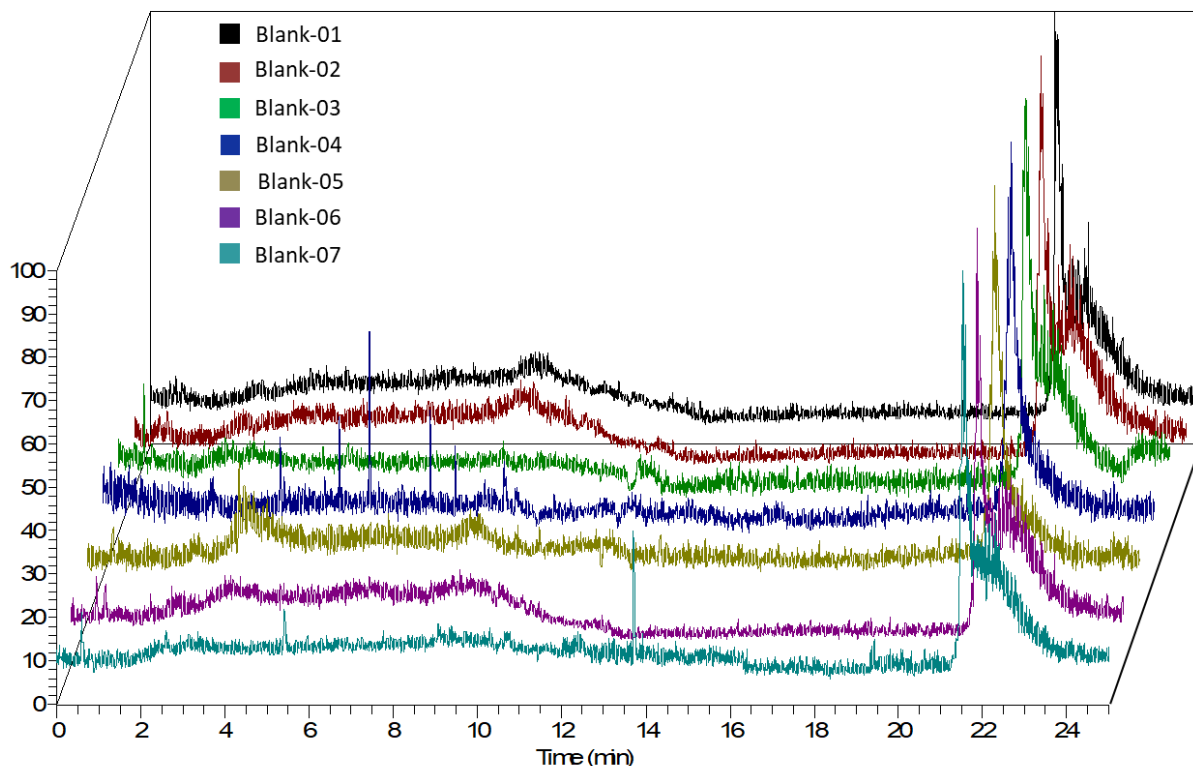
Figure 3A.4 Total ion chromatogram (TIC) profile of intermittent blank runs during the HILIC analysis. The blanks were interspersed before, within and after the sample runs. The reproducible TIC profiles indicate stable column performance during sample data acquisition.

The reproducibility of the sample data across the span of data acquisition was assessed using repeated injections of quality control samples. A total of 57 metabolites and atorvastatin (IS) were tracked in both ion modes using 16 QC runs. A plot of % RSD of analytes peak area is represented in figure 3A.5. As evident, for all the analytes reproducible peak area with <20 % RSD was observed. acetyl phosphate, bromobenzene, indole, mannitol, methylmalonic acid and uric acid were exceptions with % RSD values 21.9, 33.6, 41.7, 24.8, 21.2 and 28.9% respectively. The results indicate the robustness of the HILIC separation that is needed for using the analyte peak areas for further quantitative analysis (relative or absolute).
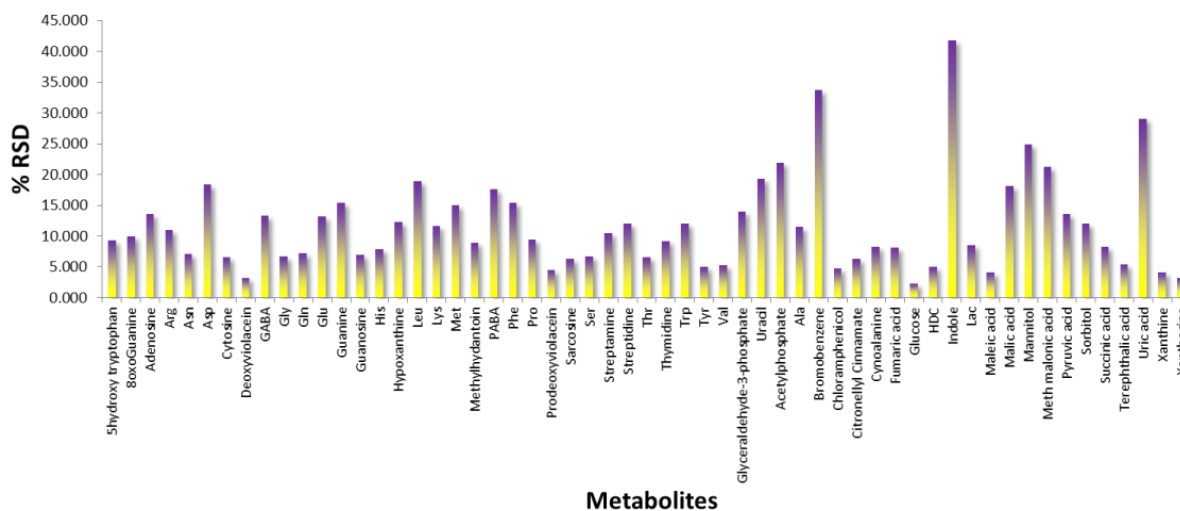
Figure 3A.5 Plot of %RSD of analyte peak areas obtained for the quality control samples is indicated against the respective metabolites. A representative sample was intermittently analyzed in both ionization modes. The retention time and peak areas were monitored to ensure the reproducibility of HILIC-HRMS.

Internal standard behavior was also monitored to check the reproducibility of the peak areas over 170 hr of run time. Two IS, namely, verapamil and atorvastatin were uniformly spiked in all samples for positive and negative ion mode, respectively. The trends in absolute peak area of internal standard observed during QC runs has been represented in figure 3A.6. The deviation in the peak areas of verapamil and atorvastatin were well below 15 % RSD, indicating acceptable reproducibility of internal standards. Verapamil is only ionized in the positive ion mode. However, atorvastatin can be ionized in both modes. The comparison of peak area for atorvastatin in positive and negative ion mode indicated a higher degree of reproducibility is observed for positive ion mode as compared to negative ion mode. This was also evident from the % RSD values for peak areas of the analytes analyzed in positive vs negative ion mode. The entire data for the samples were subsequently acquired after establishing the analytical robustness of the HILIC-HRMS as indicated by the standardization using QCs and ISs. A total of 254 analytical runs (QC + samples) for positive and negative mode analysis were performed.
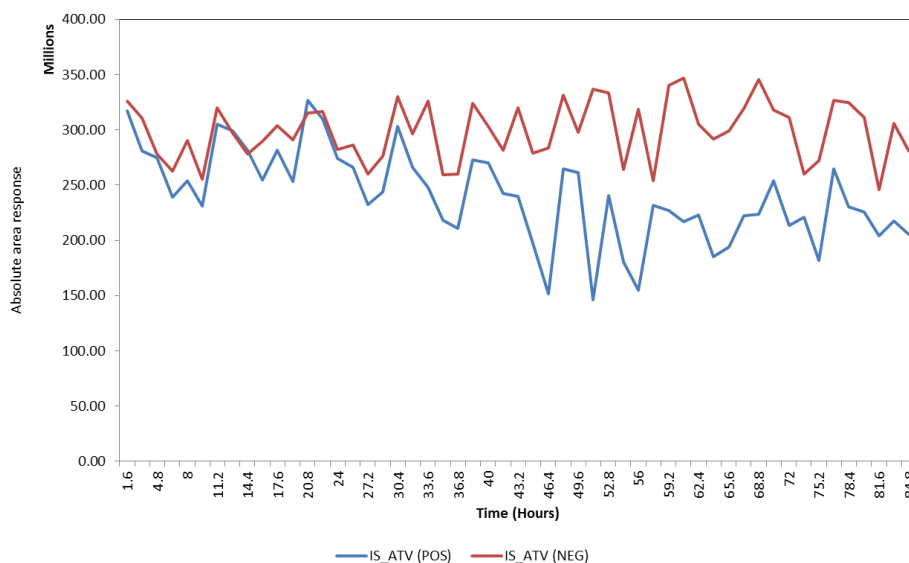
Figure 3A.6 Plot of absolute peak areas of two internal standards, verapamil (positive ion mode) and atorvastatin (negative ion mode) during the sample data acquisition. The % RSD was found to be <15% for both internal standards.

3.3.2 Metabolic profiling of Chromobacterium violaceum sample extracts

After evaluation of QC performance and establishing that the HILIC dataset had acceptable reproducibility in terms of retention time, peak profile and peak area, the sample data was analyzed to investigate the differences in the metabolic profile from various time points of wild-type (WT) and drug-resistant (ChlR, StrR) strains to elucidate the impact of acquired drug resistance on the phenotypic metabolite expression. Figure 3A.7 details the classification of samples and the time points of sample collection for the HILIC-HRMS analysis. The peak areas were identified using Quan-browser module of Xcalibur™ within 20 ppm mass extraction window. The internal standard normalized dataset was subjected to maximum value normalization before unsupervised principal component analysis (PCA). PCA models were built with the exclusion of QC data set. The analytes processed in both positive (+) and negative (-) ion mode were included. Figure 3A.8 shows the PC 1 scores plots from 5 time points of WT, ChlR, StrpR samples.
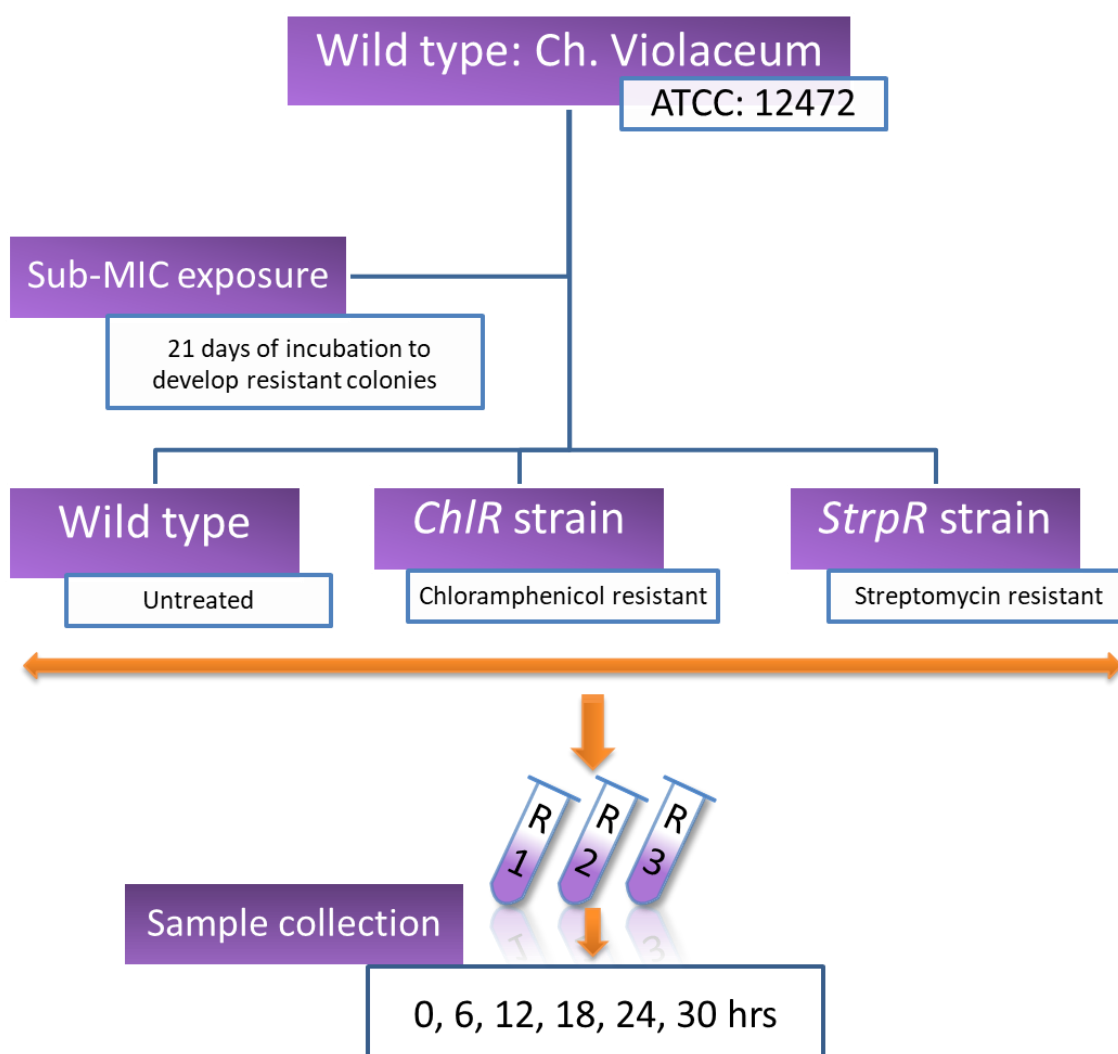
Figure3A.7 Representation of sample classification and time point of sample collection. 5 time point samples from three strains (WT, ChlR, StrpR) was collected in three biological replicates. The microbial cultures were performed at the collaborator (Dr. Anu Ragnunathan, NCL) laboratory.[22]

As shown in figure 3A.8, in the PC1 plot, 0, 6, 12, 18, 24 hr time points are easily distinguished from each other in all three sample types indicating clear metabolic differences arising over culture time from 0 to 24 hr. Upon comparing the data from all the three classes of samples using PC1 and PC3, differential clustering of various time points was observed. Notably, major differences were observed in time points post 6 hr. However, this is expected as the cellular growth and metabolic expression might have a latency phase. Also, there was no time point between 0 and 6 hr, it is difficult to pinpoint the exact time from where the visible metabolic differences starts to appear.
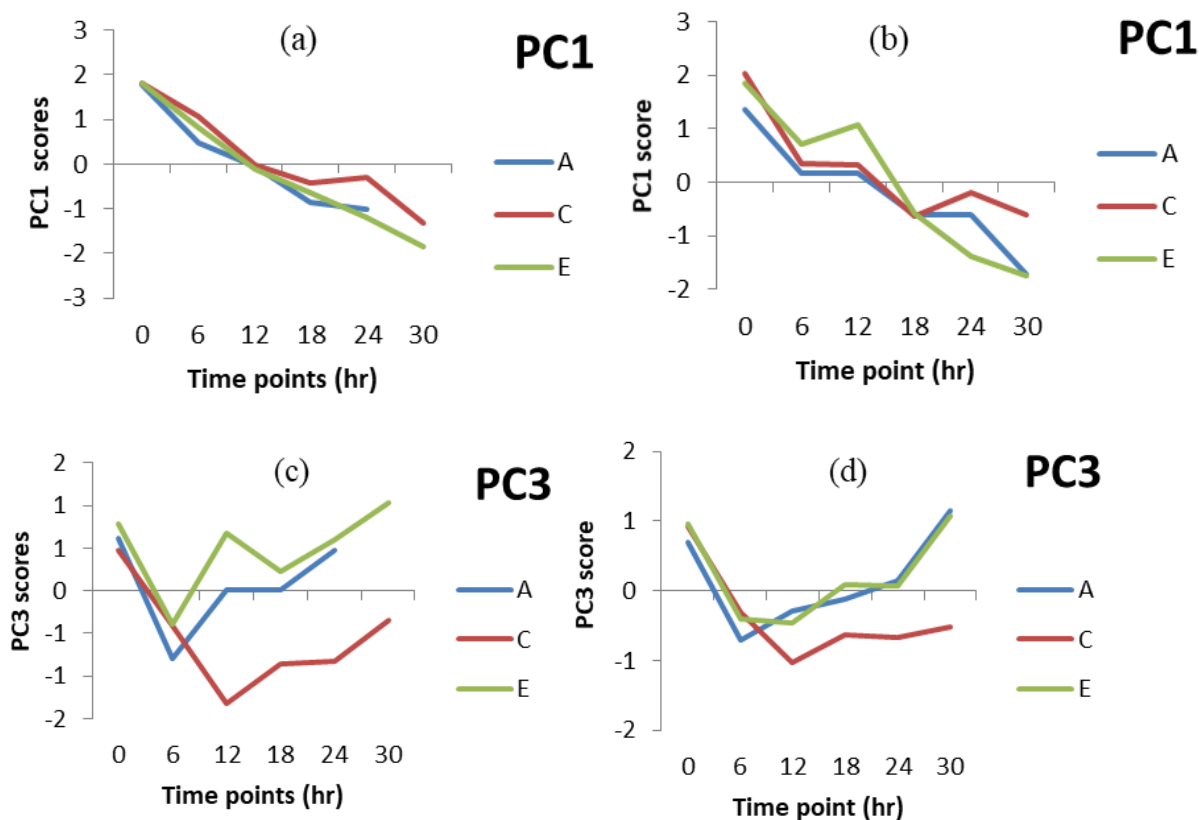
Figure 3A.8 PCA score plot of sample data derived from WT (A), ChlR (C), StrpR (E) strains of Chromobacterium violaceum. PC1 able to differentiate between the time point sample data. While PC3 identified the differences between the three strains. (a) PC1 biological replicate 1 (b) PC1 biological replicate 2 (c) PC3 biological replicate 1 (d) PC3 biological replicate 2. The differences were found to be consistent across biological replicates.

The top significantly contributing metabolites were identified from the PCA loading values. PC1 (34%) and PC3 (12%) were considered in this aspect as these were the two components which were able to identify the differences between various sample types and group them. These metabolites included deoxyviolacein, xanthine, cytosine, uric acid, indole, phenylalanine, fumaric acid, pyruvic acid, succinic acid, threonine, adenosine, lactic acid, aspartic acid, citronellyl cinnamate, tyrosine, indole, and prodeoxyviolacein.

In summary, a HILIC-HRMS based method was developed for polar metabolites extracted from *Chromobacterium Violaceum*. The ZIC-HILIC provided separation of the polar

metabolites from the CV's intracellular sample extracts. The quality controls indicated reliable reproducibility of HILIC with a reproducible retention time (Rt) and peak area, proving its merit for metabolomics applications from complex biological samples. Targeted analysis of metabolomics data revealed intracellular metabolic changes across the three different strains (WT, ChlR, StrpR) of CV demonstrating the utility of the developed HILIC-HRMS method.

3.4 Conclusions

Recent reports of HILIC separation in tandem with MS explore its applicability for various metabolomics investigations, especially to resolve the polar analytes and fatty acids from diverse biological samples.[23–27] ZIC-HILIC coupled with LTQ-Orbitrap mass spectrometer has been reported for the determination of polar metabolites in *Leishmania donovani*[28,29] wherein a proof-of-concept of untargeted metabolomics analysis by HILIC-HRMS has been demonstrated with a 40 min gradient method. In yet another comparable study, aqueous phase compatible silica column has been used for the metabolic profiling with the aim of biomarker identification in fungi, *Candida albicans*.[30] However, most of the previously reported literature have not delved deeper into various analytical aspects of HILIC-HRMS such as reproducibility, column performance, and retention behavior along with measurement of kinetic profiles. The work described herein has specifically looked at these aspects for targeted intracellular metabolomics from *Chromobacterium violaceum* using HILIC-HRMS presenting an advancement. As an outcome of this study, relative profiles based on internal standard normalized data was generated for three strains of Chromobacterium violaceum.[22] Significantly varying metabolites contributing maximally in differential metabolite expression were identified using unsupervised principal component analysis (PCA). The result indicated substantial changes in metabolic expression of resistant strains, especially chloramphenicol resistant (ChlR), post 6 hours. The metabolomics data provided an experimental base for the generation of the pathway network model of Chromobacterium using in a systems biology approach.[22] It also showcases the ability of the analysis method for delineating metabolic insights from in hypothesis-driven investigations such as the role of metabolic reprogramming in drug resistance.

3B. HILIC-HRMS of stable isotope labelled tricarboxylic acid cycle metabolites in Chinese hamster ovary (CHO) cells

3.5 Introduction

Various biological systems has been commercially used in industrial applications as a host for the production of valuable chemicals such as pharmaceuticals, foods and dairy products, and pigments. Continuous attempts are made to modify them in order to achieve enhanced yields or survival.[1–5] Inputs from metabolomics investigations offer valuable mechanistic insights into the phenotype of modified systems. It also allows cross-comparison against control (s) and aids in systematic optimization of synthetic strain designing experiments. Modification pertaining to specific pathways can be efficiently traced using stable isotopically labelled (SIL) tracers, for example through the cellular uptake of ^{13}C labelled glucose. Information from stable isotope labelling experiments has been pivotal in identification of cascade of downstream metabolic transformations and in filling the gaps about specific enzymes or metabolites.[6–9] SIL is an established and recommended technique for determination of fate of individual metabolites, delineate metabolic pathways and flux determination through targeted analysis by MS or ^{13}C NMR analysis.[10–14] SIL also offers easier and safer handling as compared to precedent radioactive labelling. So far, pathway networks in various systems such as bacteria, yeast, plant, and mammalian cells (cancer, Chinese hamster ovary) have been successfully elucidated with ^{13}C-labelling experiments.[14,15,24–28,16–23] Combined use of SIL and hyphenated HRMS in full-scan mode, provide an opportunity for network wide investigation of metabolic pathways. High mass accuracy offered by HRMS often allows reliable formula assignment for each detected mass.[29]

As an extension of the previous chapter, this work evaluated the suitability of HILIC-HRMS method for the accurate detection and estimation of targeted set of isotopically labelled

metabolites in the intracellular extracts of CHO cells. HILIC-HRMS analysis on metabolites from CHO cells has not been reported before. Co-elution of isotopologues and other metabolites (including isobaric) and associated ion suppression effects is a known challenge with SIL experiments.[30] Separation of the metabolites using HILIC column chemistry, reported herein, addresses this challenge for reliable use of the metabolite and isotopologue peak areas for relative profiling.

3.6 Materials and methods

3.6.1 Chemicals

All amino acids, glucose, citric acid, glyceraldehyde-3-phosphate, α-ketoglutaric acid, lactic acid, fumaric acid, succinic acid, malic acid (Mal), pyruvic acid, sorbitol, and LC-MS grade formic acid were procured from (MO, USA). LC-MS grade acetonitrile and methanol were purchased from J T Baker (PA, USA). Deionized water (specific resistivity 18.2 MΩ) was obtained from Millipore Milli-Q water purification system. Verapamil (Ver) and Atorvastatin (Atv), used as internal standards (IS), were received as gratis samples from Mylan, Hyderabad. Uniformly labelled ^{13}C-glucose was purchased from Cambridge isotope laboratories (MA, USA). CD CHO medium was purchased from Thermo Fisher Scientific Inc. (MA, USA). Unless otherwise stated all other chemicals were purchased from Sigma Aldrich (MO, USA).

3.6.2 Research Contributions

Cell culture experiments and associated metabolite extractions were carried by Vishwanathgouda Maralingannavar out as part of collaboration with Dr. Mugdha Gadgil (CSIR-NCL, Pune). The biological contexts of this work are part of a separate dissertation (Dr. Gadgil's group). Optimization of the HILIC-HRMS method, data acquisition on the extracted

samples, and LCMS data processing were performed by Dharmesh Parmar (Dr. Venkat Panchagnula group, CSIR-NCL Pune) and are reported as part of this dissertation. For further details of the complete study including cell culture experimental details, please see the published work.[31]

3.6.3 Sample collection and extraction

Briefly, after 24 hours CHO cells were harvested. Subsequently, cells (7.5×10^6) were extracted using two 100% -80 °C methanol (500 µL each) extractions followed by a single ice cold water extraction (250 µL). Internal standards were staged at two phases of samples preparation. 1 µM of verapamil, was added to the cell pellet before extraction. Recovery (%) of verapamil post extraction was used for estimating any variations during the extraction process. A second internal standard, 1 µM atorvastatin, was added during the reconstitution step and prior to the LC-HRMS analysis. The atorvastatin profile used to account for any instrumental variations during the course of data acquisition. The extracts were pooled and dried in a vacuum concentrator at 4 °C and stored at -80 °C. The sample extracts were reconstituted using 125 µL volume of 90% methanol by thorough mixing on vortex mixer for a period of 3 min. Atorvastatin prepared in acetonitrile: 20 mM ammonium acetate, pH 7.9 (90:10 v/v) was added to the reconstituted sample (0.8 µM in final solution) prior to the LC HRMS analysis. The samples were then transferred to the auto sampler maintained at 4 °C during the analysis. 5 µL of the final sample was injected for LC-HRMS analysis.

3.6.4 HILIC-HRMS analysis

LC-HRMS data was acquired on a Thermo Scientific Q-Exactive™ high resolution mass spectrometer equipped with a heated electrospray ionization (HESI) source, Accela auto sampler and quaternary pump, and. The instrumental setup was operated using Xcalibur™

(Thermo Scientific) software modules. A syncronis HILIC column, Thermo Fisher (100 mm*2.1 mm*1.7 µm) was used for the chromatographic separation of the metabolites. Mobile phase A and B consisted of 5% IPA isopropyl alcohol in acetonitrile (v/v) and 20 mM ammonium acetate buffer in water, pH adjusted to 7.9 using ammonium hydroxide, respectively. The mobile phase gradient consisted of 25% A initially maintained up to 2.0 min, followed by linear increase up to 35% A by 2.5 min, 80% A by 6.0 min and 90% A by 10 min further maintained up to 12.0 min. The column was restabilized with 25% A for 3 min period starting from 12.0 to 15 min. The gradient elution was carried out at a constant flow rate of 500 µL/min with a column temperature maintained at 35 °C using column oven. The spray voltage of the HESI source was set at 3 kV. Capillary temperature at 320 °C, heater temperature at 300 °C, sheath gas at 45 arbitrary units and auxiliary gas at 15 arbitrary units were maintained. The data was acquired in both negative and positive ion mode within m/z range of 70-750 at m/z resolution of 70,000 with automatic gain control (AGC) target 1e6 and maximum injection time of 120 ms.

Prior to the sample analysis, the HILIC column was stabilized for 30 minutes followed by three preliminary blank runs. Data for the samples was acquired in three technical replicates analysed in randomized fashion. Metabolites and atorvastatin were detected as [M-H] in negative ion mode. Further confirmation of the metabolites was achieved using retention time specific tandem MS of the observed precursor ion *m/z* (collision energy 20 NCE). Accurate mass-extracted ion chromatograms (AM-XIC) generated using a narrow mass extraction window (MEW) of 10 ppm was used to obtain the peak areas for the metabolites. The samples were also analysed in the positive ion mode to obtain the peak areas of the internal standard verapamil to assess extraction efficiency. The percentage relative standard deviation (%RSD)

of verapamil AM- XIC peak area across all samples was calculated. Measured isotopologue distributions were not corrected for the ^{13}C natural abundance.

3.7 Results and discussion

3.7.1 Reproducibility of HILIC-HRMS method
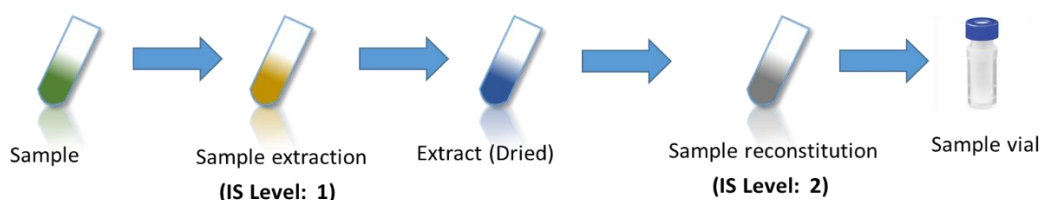
Figure 3B.1 Staging of internal standard

The method optimization, as described in the previous chapter, was used for the analysis of the samples after re-validating it with reference standards. Subsequently, the response of internal standards, verapamil and atorvastatin), spiked at two different stages, was evaluated to assess the robustness of the method and the instrument. Verapamil spiked before the metabolite extraction accounted for variations observed in the sample extraction process. Atorvastatin spiked in the sample extracts prior to the LCMS analysis was indicative of the reproducibility of HILIC-HRMS through the duration of the analysis. The staging of internal standard and the absolute responses obtained is shown in figure 3B.1 and 3B.2, respectively. The variation of verapamil (stage 1) and atorvastatin (stage 2) across samples was found to be at 19.2 and 10.9 % RSD. These values, <20 % RSD, indicated consistency in the extraction protocols and excellent instrumental reproducibility, respectively. The relatively higher %RSD in extraction could be a result of the manual extraction process.

Figure 3B.3 illustrates the HILIC separation obtained using reference standards of the metabolites from the TCA cycle. All the metabolites under investigation were well resolved within the 5 mins Rt as seen from the AM-XICs of the metabolites. The peak shapes for some of the metabolites (for example, aspartate) were non-ideal. However, these were consistent and were reproducibly obtained during the sample analysis and hence were used for metabolite profiling.
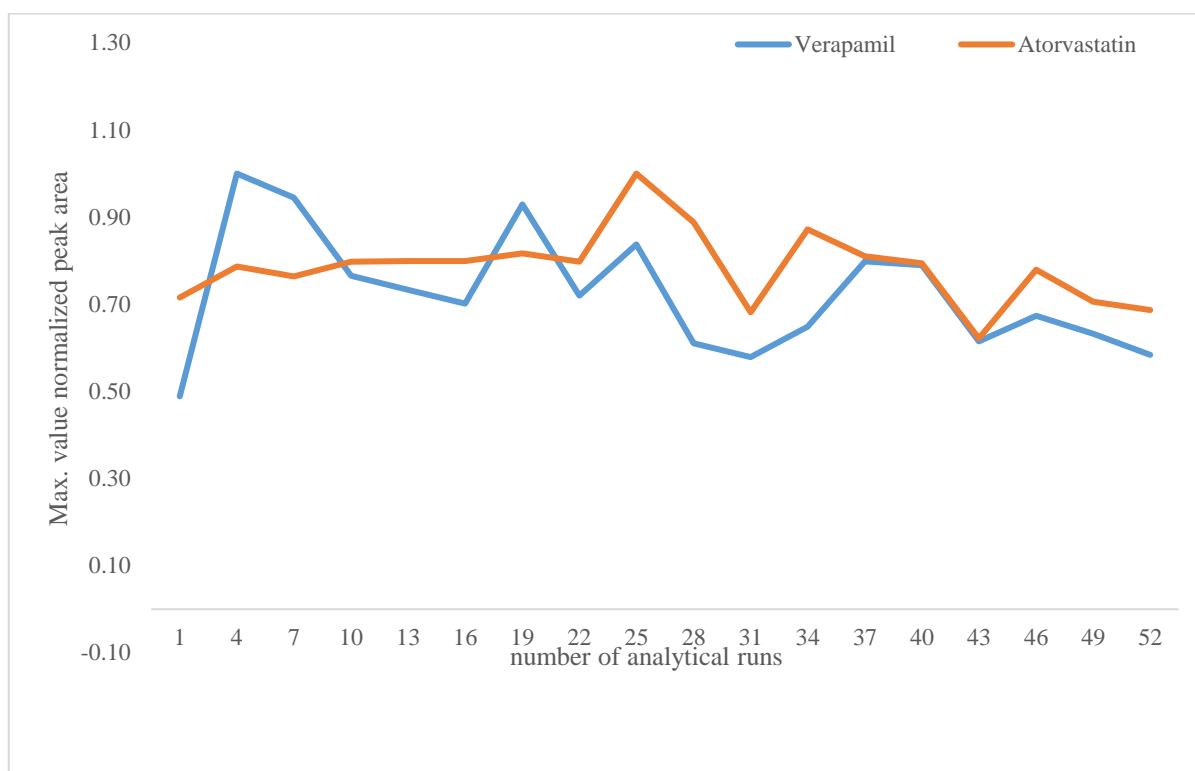
Figure 3B.2 Maximum value normalized peak areas of internal standards verapamil and atorvastatin across the analytical runs. Values represented are the average of technical replicates (n=3).

3.7.2 Isotopologues of 13C labelled TCA metabolites (succinate, fumarate, malate, asparate) from CHO cells

CHO cell lines are the model systems of choice for optimization of upstream bioreactor conditions for recombinant protein production. Two different cell types were considered for the SIL study that aimed to understand the effects of the phosphate limitation on upstream recombinant processes. Intracellular metabolites from CHO cells adapted to phosphate limited environment (PL) were compared with control cells (PC), both grown using ^{13}C labelled glucose. Different isotopologues could result from the path adopted by the ^{13}C incorporation for which other competing carbon sources could also contribute. Figure 3B.4 shows the complete intracellular incorporation of the ^{13}C labeled glucose in cells studies as compared to the cells grown in the absence of the labelled isotope. Glucose was predominantly observed in its M+6 isotopologue in both the control CHO cells (PC) and PL cells that were under investigation within the durations expected for the steady state to be achieved.[31]

Succinate, fumarate, malate, and aspartate are the key TCA metabolites that contributes into pyruvate carboxylase flux. These metabolites arise through various enzymatic reactions from acetyl-CoA, citrate/isocitrate, and α-ketoglutarate. The isotopologues for these metabolites in the cells grown under ^{13}C-labelled conditions were monitored for the two cell types. Figure 3B.5 showcases the peak areas for the various isotopologues for the metabolites in context as compared to the glucose uptake. The peak areas for all the isotopes for fumarate and malate were found to be greater in the PL cells as compared to the PC indicating a higher flux in the former. The corresponding peak areas for aspartate and succinate all the isotopes did not show significant changes in both the cells indicating that comparable fluxes in both the cell types for these metabolites.
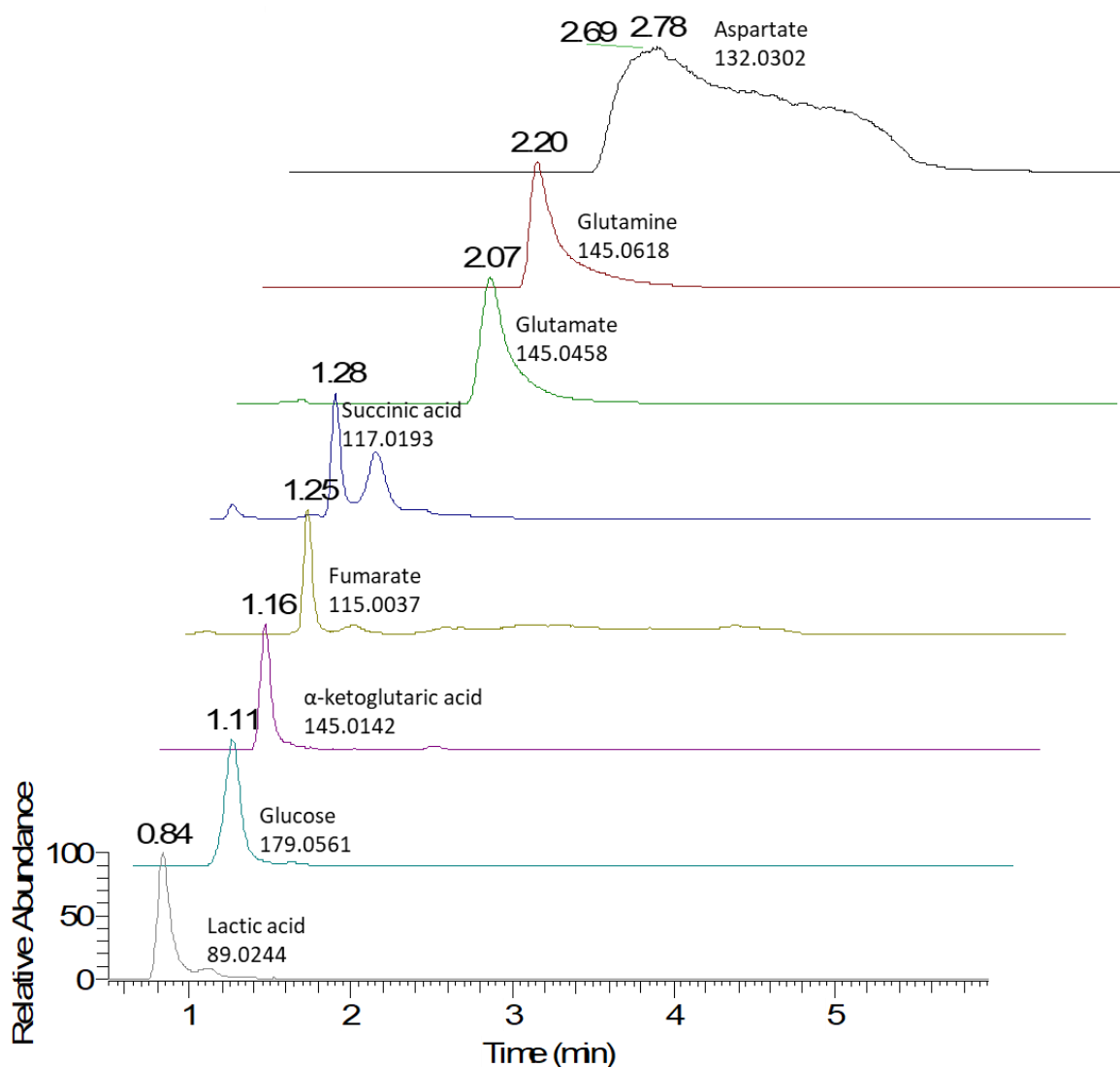
Figure 3B.3 Elution profiles of various polar metabolites (reference standards) on HILIC column.
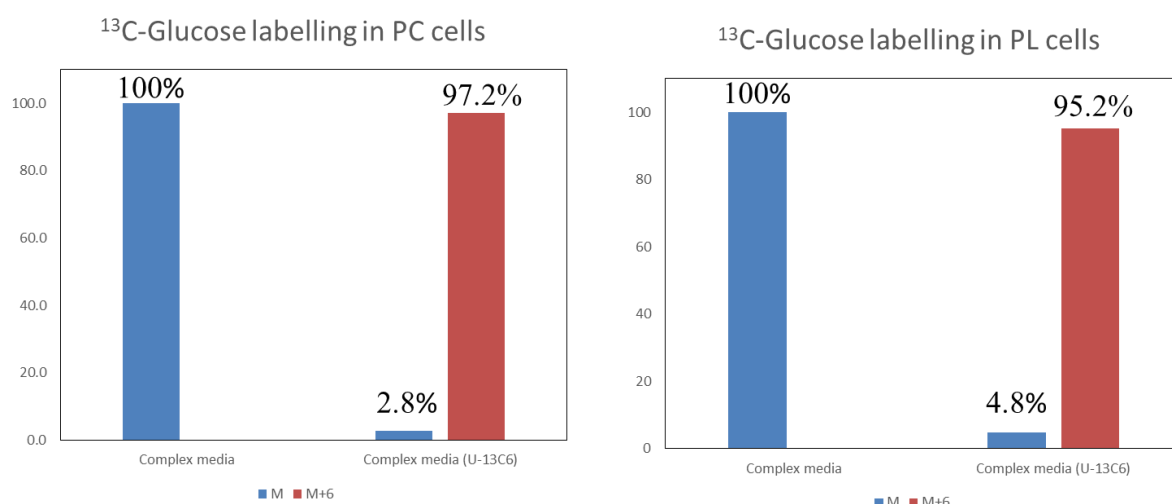
Figure 3B.4 The distribution of intracellular ^{13}C glucose in PC and PL after the cells were grown in complex media with glucose (U-$^{13}C6$) in comparison to unlabelled complex media.
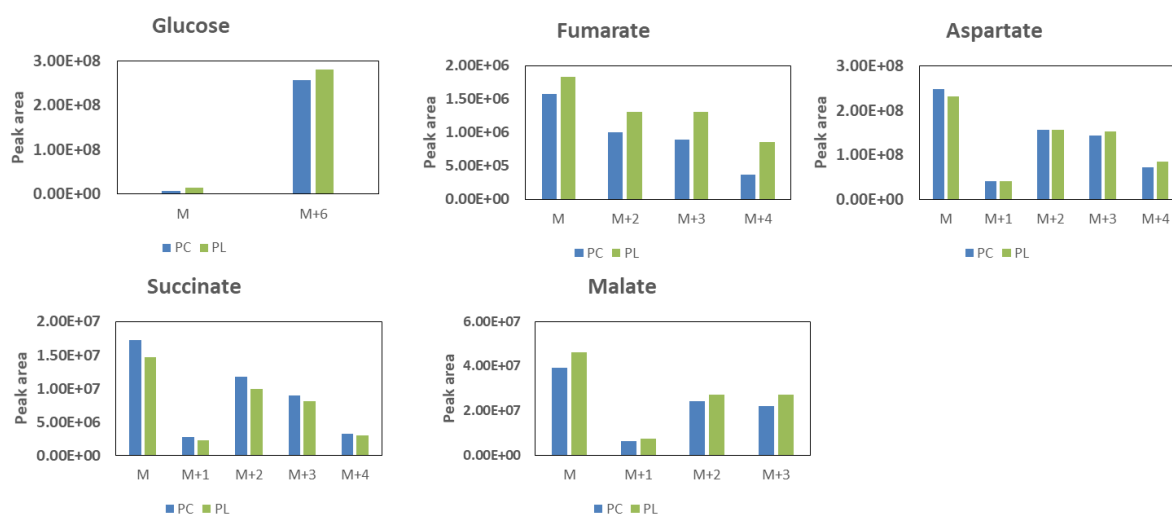
Figure 3B.5 Absolute peak area profile of various metabolite isotopologues in PL and PC cells in complex media with glucose (U-$^{13}C6$).

Table 3B.1 Variation in the peak areas of metabolites in a representative QC sample (12C-PC pooled)

QC Run	Atv	Asp	FA	Gluc	Lac	Suc	Mal
1	2.48E+07	4.27E+08	3.28E+06	2.25E+08	6.72E+08	1.56E+07	6.47E+07
2	2.63E+07	4.74E+08	3.79E+06	2.04E+08	6.17E+08	1.58E+07	8.74E+07
3	2.32E+07	3.74E+08	2.26E+06	1.48E+08	4.74E+08	1.15E+07	5.26E+07
Average	**2.48E+07**	**4.25E+08**	**3.11E+06**	**1.92E+08**	**5.88E+08**	**1.43E+07**	**6.83E+07**
%RSD	**6.3**	**11.8**	**25.1**	**20.8**	**17.3**	**17.1**	**25.9**

The HILIC-HRMS method was further evaluated using pooled QC samples for the duration of the analytical run. A common pooled sample was prepared by using three biological replicates of the PC cells. The metabolite extractions were carried out along with the samples as described above. Atorvastatin (IS) was added prior to the analysis. Table 3B.1 showcases the data obtained (peak areas) for three technical HILIC-HRMS analysis runs for the QC samples. These were analysed at the beginning, intermittently and at the end of the sample analysis. Any variation observed in these samples could help in the establishing the threshold of variations in the PL samples vis-à-vis PC that could be considered significant. Expectedly, atorvastatin showed the least of the peak area variations in terms of % RSD. The % RSDs for the rest of the metabolites were in the range of 11-26%. Bioanalyical method validation regulations generally allow a 15% variation for quantitative LC-MS analysis.[32] A higher allowance up to 30% RSD is indeed allowed in certain cases of metabolite analysis. The peak-area variations estimated in this study are relative indications of the metabolites present. Further normalizations, and calibration-based quantitative approaches will help bring down the

variations to acceptable ranges. Nevertheless, the results from the peak-areas alone are indicative of the comparative trends that could potentially give insights into the metabolic fluxes in operation for the varying environmental conditions investigated.

3.8 Conclusion

The measurement of metabolite level alone is insufficient to understand the direction or fluxes of biochemical reactions. Relative presence or abundance of any metabolite(s) is an output of multitude of pathways involving production/degradation, consumption/transformation as well as influx/efflux of metabolites. Therefore, pathways flux analysis is advised to be carried out in metabolic steady state.[33] As system reaches metabolic steady state, it has relatively stable pathway flux and renders reliable interpretation of metabolomics data. This preliminary study demonstrates the use of HILIC-HRMS as a valuable tool in the determination of ^{13}C labelled metabolites from mammalian cell culture samples. Excellent reproducibility of the HILIC-HRMS method offers reliable estimation of TCA intermediates even in a relative fashion instead of lengthy calibration-based quantitative regimes. High resolution-accurate mass detection of labelled isotopologues enabled determination of relative abundances of asprartate, fumarate, malate, and succinate. The contribution of various isotopologues allowed comparison of fluxes between control and adapted CHO cells. Furthermore, use of unlabelled IS and QC samples further increased the confidence of measurements and establishing the method associated variations that have to be taken into account for metabolic flux analysis using HILIC-HRMS.

3.9 References

Chapter 3A

(1)   Alpert, A. J. Hydrophilic-Interaction Chromatography for the Separation of Peptides, Nucleic Acids and Other Polar Compounds. J. Chromatogr. A 1990, 499 (C), 177–196.

(2)   Gama, M. R.; da Costa Silva, R. G.; Collins, C. H.; Bottoli, C. B. G. Hydrophilic Interaction Chromatography. TrAC - Trends Anal. Chem. 2012, 37, 48–60.

(3)   Guo, Y.; Gaiki, S. Retention Behavior of Small Polar Compounds on Polar Stationary Phases in Hydrophilic Interaction Chromatography. J. Chromatogr. A 2005, 1074 (1–2), 71–80.

(4)   McCalley, D. V. Understanding and Manipulating the Separation in Hydrophilic Interaction Liquid Chromatography. J. Chromatogr. A 2017, 1523, 49–71.

(5)   Jandera, P.; Janás, P. Recent Advances in Stationary Phases and Understanding of Retention in Hydrophilic Interaction Chromatography. A Review. Anal. Chim. Acta 2017, 967, 12–32.

(6)   Jandera, P. Stationary and Mobile Phases in Hydrophilic Interaction Chromatography: A Review. Anal. Chim. Acta 2011, 692 (1–2), 1–25.

(7)   Wang, C.; Jiang, C.; Armstrong, D. W. Considerations on HILIC and Polar Organic Solvent-Based Separations: Use of Cyclodextrin and Macrocyclic Glycopetide Stationary Phases. J. Sep. Sci. 2008, 31 (11), 1980–1990.

(8)   Shen, A.; Guo, Z.; Yu, L.; Cao, L.; Liang, X. A Novel Zwitterionic HILIC Stationary Phase Based on "Thiol-Ene" Click Chemistry between Cysteine and Vinyl Silica. Chem. Commun. 2011, 47 (15), 4550.

(9)   Qiao, L.; Dou, A.; Shi, X.; Li, H.; Shan, Y.; Lu, X.; Xu, G. Development and Evaluation of New Imidazolium-Based Zwitterionic Stationary Phases for Hydrophilic Interaction Chromatography. J. Chromatogr. A 2013, 1286, 137–145.

(10)   Cai, J.; Cheng, L.; Zhao, J.; Fu, Q.; Jin, Y.; Ke, Y.; Liang, X. A Polyacrylamide-Based Silica Stationary Phase for the Separation of Carbohydrates Using Alcohols as the Weak Eluent in Hydrophilic Interaction Liquid Chromatography. J. Chromatogr. A 2017, 1524, 153–159.

(11)   Qiao, L.; Lv, W.; Chang, M.; Shi, X.; Xu, G. Surface-Bonded Amide-Functionalized Imidazolium Ionic Liquid as Stationary Phase for Hydrophilic Interaction Liquid Chromatography. J. Chromatogr. A 2017, 12–14.

(12)   Qiao, L.; Li, H.; Shan, Y.; Wang, S.; Shi, X.; Lu, X.; Xu, G. Study of Surface-Bonded Dicationic Ionic Liquids as Stationary Phases for Hydrophilic Interaction Chromatography. J. Chromatogr. A 2014, 1330, 40–50.

(13)   Yin, W.; Chai, H.; Liu, R.; Chu, C.; Palasota, J. A.; Cai, X. Click N-Benzyl Iminodiacetic Acid: Novel Silica-Based Tridentate Zwitterionic Stationary Phase for Hydrophilic Interaction Liquid Chromatography. Talanta 2015, 132, 137–145.

(14)   Aral, H.; Çelik, K. S.; Altındağ, R.; Aral, T. Synthesis, Characterization, and Application of a Novel Multifunctional Stationary Phase for Hydrophilic Interaction/Reversed Phase Mixed-Mode Chromatography. Talanta 2017, 174 (June), 703–714.

(15)   Ikegami, T.; Tomomatsu, K.; Takubo, H.; Horie, K.; Tanaka, N. Separation Efficiencies in Hydrophilic Interaction Chromatography. J. Chromatogr. A 2008, 1184 (1–2), 474–503.

(16)   Chirita, R. I.; West, C.; Zubrzycki, S.; Finaru, A. L.; Elfakir, C. Investigations on the Chromatographic Behaviour of Zwitterionic Stationary Phases Used in Hydrophilic Interaction Chromatography. J. Chromatogr. A 2011, 1218 (35), 5939–5963.

(17)   Idborg, H.; Zamani, L.; Edlund, P. O.; Schuppe-Koistinen, I.; Jacobsson, S. P. Metabolic Fingerprinting of Rat Urine by LC/MS: Part 1. Analysis by Hydrophilic Interaction Liquid

Chromatography-Electrospray Ionization Mass Spectrometry. J. Chromatogr. B Anal. Technol. Biomed. Life Sci. 2005, 828 (1–2), 9–13.

(18) van Nuijs, A. L. N.; Tarcomnicu, I.; Covaci, A. Application of Hydrophilic Interaction Chromatography for the Analysis of Polar Contaminants in Food and Environmental Samples. J. Chromatogr. A 2011, 1218 (35), 5964–5974.

(19) Kahsay, G.; Song, H.; Van Schepdael, A.; Cabooter, D.; Adams, E. Hydrophilic Interaction Chromatography (HILIC) in the Analysis of Antibiotics. J. Pharm. Biomed. Anal. 2014, 87, 142–154.

(20) Cai, X.; Li, R. Concurrent Profiling of Polar Metabolites and Lipids in Human Plasma Using HILIC-FTMS. Sci. Rep. 2016, 6 (October), 1–10.

(21) Cubbon, S.; Antonio, C.; Wilson, J.; Thomas-oates, J. METABOLOMIC APPLICATIONS OF HILIC – LC – MS. 2010, No. November 2008, 671–684.

(22) Banerjee, D.; Parmar, D.; Bhattacharya, N.; Ghanate, A. D.; Panchagnula, V.; Raghunathan, A. A Scalable Metabolite Supplementation Strategy against Antibiotic Resistant Pathogen Chromobacterium Violaceum Induced by NAD+/NADH+imbalance. BMC Syst. Biol. 2017, 11 (51), 1–20.

(23) Spagou, K.; Tsoukali, H.; Raikos, N.; Gika, H.; Wilson, I. D.; Theodoridis, G. Hydrophilic Interaction Chromatography Coupled to MS for Metabonomic / Metabolomic Studies. J. Sep. Sci. 2010, 33, 716–727.

(24) Spagou, K.; Wilson, I. D.; Masson, P.; Theodoridis, G.; Raikos, N.; Coen, M.; Holmes, E.; Lindon, J. C.; Plumb, R. S.; Nicholson, J. K.; et al. HILIC-UPLC-MS for Exploratory Urinary Metabolic Profiling in Toxicological Studies. Anal. Chem. 2011, 83 (1), 382–390.

(25) Müller, D. C.; Degen, C.; Scherer, G.; Jahreis, G.; Niessner, R.; Scherer, M. Metabolomics Using GC-TOF-MS Followed by Subsequent GC-FID and HILIC-MS/MS Analysis Revealed Significantly Altered Fatty Acid and Phospholipid Species Profiles in Plasma of Smokers. J. Chromatogr. B 2014, 966, 117–126.

(26) Nizioł, J.; Bonifay, V.; Ossoliński, K.; Ossoliński, T.; Ossolińska, A.; Sunner, J.; Beech, I.; Arendowski, A.; Ruman, T. Metabolomic Study of Human Tissue and Urine in Clear Cell Renal Carcinoma by LC-HRMS and PLS-DA. Anal. Bioanal. Chem. 2018, 3859–3869.

(27) Marull, M.; Rochat, B. Fragmentation Study of Imatinib and Characterization of New Imatinib Metabolites by Liquid Chromatography-Triple-Quadrupole and Linear Ion Trap Mass Spectrometers. J. Mass Spectrom. 2006, 41 (3), 390–404.

(28) t'Kindt, R.; Jankevics, A.; Scheltema, R. a; Zheng, L.; Watson, D. G.; Dujardin, J.-C.; Breitling, R.; Coombs, G. H.; Decuypere, S. Towards an Unbiased Metabolic Profiling of Protozoan Parasites: Optimisation of a Leishmania Sampling Protocol for HILIC-Orbitrap Analysis. Anal. Bioanal. Chem. 2010, 398 (5), 2059–2069.

(29) Zheng, L.; T'Kindt, R.; Decuypere, S.; Freyend, S. J. von; Coombs, G. H.; Watson, D. G. Profiling of Lipids in Leishmania Donovani Using Hydrophilic Interaction Chromatography in Combination with Fourier Transform Mass Spectrometry. Rapid Commun. Mass Spectrom. 2010, 24, 2074–2082.

(30) Li, L.; Liao, Z.; Yang, Y.; Lv, L.; Cao, Y.; Zhu, Z. Metabolomic Profiling for the Identification of Potential Biomarkers Involved in a Laboratory Azole Resistance in Candida Albicans. PLoS One 2018, 13 (2), e0192328.

Chapter 3B

(1) Huber, R.; Roth, S.; Rahmen, N.; Büchs, J. Utilizing High-Throughput Experimentation to Enhance Specific Productivity of an E . Coli T7 Expression System by Phosphate Limitation. BMC Biotechnol. 2011, 11 (22), 1–11.

(2) Rasor, J. P.; Voss, E. Enzyme-Catalyzed Processes in Pharmaceutical Industry. Appl. Catal.

A Gen. **2001**, *221* (1–2), 145–158.

(3)   Wijesekara, I.; Kim, S. K. Angiotensin-I-Converting Enzyme (ACE) Inhibitors from Marine Resources: Prospects in the Pharmaceutical Industry. *Mar. Drugs* **2010**, *8* (4), 1080–1093.

(4)   Carpentier, B.; Chassaing, D. Interactions in Biofilms between Listeria Monocytogenes and Resident Microorganisms from Food Industry Premises. *Int. J. Food Microbiol.* **2004**, *97* (2), 111–122.

(5)   Nestl, B. M.; Nebel, B. A.; Hauer, B. Recent Progress in Industrial Biocatalysis. *Curr. Opin. Chem. Biol.* **2011**, *15* (2), 187–193.

(6)   Jang, C.; Chen, L.; Rabinowitz, J. D. Metabolomics and Isotope Tracing. *Cell* **2018**, *173* (4), 822–837.

(7)   Lu, W.; Clasquin, M. F.; Melamud, E.; Amador-Noguez, D.; Caudy, A. A.; Rabinowitz, J. D. Metabolomic Analysis via Reversed-Phase Ion-Pairing Liquid Chromatography Coupled to a Stand Alone Orbitrap Mass Spectrometer. *Anal. Chem.* **2010**, *82* (8), 3212–3221.

(8)   Orlando, R.; Lim, J. M.; Atwood, J. A.; Angel, P. M.; Fang, M.; Aoki, K.; Alvarez-Manilla, G.; Moremen, K. W.; York, W. S.; Tiemeyer, M.; et al. IDAWG: Metabolic Incorporation of Stable Isotope Labels for Quantitative Glycomics of Cultured Cells. *J. Proteome Res.* **2009**, *8* (8), 3816–3823.

(9)   Shlomi, T.; Fan, J.; Tang, B.; Kruger, W. D.; Rabinowitz, J. D. Quantitation of Cellular Metabolic Fluxes of Methionine. *Anal. Chem.* **2014**, *86* (3), 1583–1591.

(10) Tang, J. K.; You, L.; Blankenship, R. E.; Tang, Y. J. Recent Advances in Mapping Environmental Microbial Metabolisms through 13 C Isotopic Fingerprints. *J. R. Soc. Interface* **2012**, *9*, 2767–2780.

(11) Wiechert, W. 13C Metabolic Flux Analysis. *Metab. Eng.* **2001**, *3* (3), 195–206.

(12) Crown, S. B.; Ahn, W.; Antoniewicz, M. R.; Sauer, U.; Zamboni, N.; Fendt, S.; Ruhl, M.; Sauer, U.; Stephanopoulos, G.; Crown, S.; et al. Rational Design of 13C-Labeling Experiments for Metabolic Flux Analysis in Mammalian Cells. *BMC Syst. Biol.* **2012**, *6* (1), 43.

(13) Wiechert, W.; Nöh, K. Isotopically Non-Stationary Metabolic Flux Analysis: Complex yet Highly Informative. *Curr. Opin. Biotechnol.* **2013**, *24* (6), 979–986.

(14) Sriram, G.; Fulton, D. B.; Iyer, V. V; Peterson, J. M.; Zhou, R.; Westgate, M. E.; Spalding, M. H.; Shanks, J. V. Quantification of Compartmented Metabolic Fluxes in Developing Soybean Embryos by Employing Biosynthetically Directed Fractional 13 C Labeling , Two-Dimensional [13 C , 1 H] Nuclear Magnetic Resonance , and Comprehensive Isotopomer Balancing 1 [W]. *Plant Physiol.* **2004**, *136* (October), 3043–3057.

(15) Feng, X.; Mouttaki, H.; Lin, L.; Huang, R.; Wu, B.; Hemme, C. L.; He, Z.; Zhang, B.; Hicks, L. M.; Xu, J.; et al. Characterization of the Central Metabolic Pathways in Thermoanaerobacter Sp. Strain X514 via Isotopomer-Assisted Metabolite Analysis. *Appl. Environ. Microbiol.* **2009**, *75* (15), 5001–5008.

(16) Senn, H.; Werner, B.; Messerle, B. A.; Weber, C.; Traber, R.; Wiithrich, K. Stereospecific Assignment of the Methyl LH NMR Lines of Valine and Leucine in Polypeptides by Nonrandom 13C Labelling. *FEBS Lett.* **1989**, *249* (1), 113–118.

(17) Long, C. P.; Au, J.; Gonzalez, J. E.; Antoniewicz, M. R. C Metabolic Fl Ux Analysis of Microbial and Mammalian Systems Is Enhanced with GC-MS Measurements of Glycogen and RNA Labeling. *Metab. Eng.* **2016**, *38*, 65–72.

(18) Leighty, R. W.; Antoniewicz, M. R. Parallel Labeling Experiments with [U- 13 C] Glucose Validate E . Coli Metabolic Network Model for 13 C Metabolic Flux Analysis. *Metab. Eng.* **2012**, *14* (5), 533–541.

(19) Scandellari, F.; Hobbie, E. A.; Ouimette, A. P.; Stucker, V. K. Tracing Metabolic Pathways of Lipid Biosynthesis in Ectomycorrhizal Fungi from Position-Specific C-Labelling in Glucose. *Environ. Microbiol.* **2009**, *11*, 3087–3095.

(20) Tcherkez, G.; Cornic, G.; Ghashghaie, J. Respiratory Carbon Metabolism Following

Illumination in Intact French Bean Leaves Using 13 C / 12 C Isotope Labeling 1. *Plant Physiol.* **2004**, *136* (October), 3245–3254.

(21) Avice, J. C.; Ourry, A.; Lemaire, C.; Boucaud, J. Nitrogen and Carbon Flows Estimated by 15N and 13C Pulse-Chase Labeling during Regrowth of Alfalfa. *Plant Physiol.* **1996**, *112*, 281–290.

(22) Roessner-tunali, U.; Liu, J.; Leisse, A.; Balbo, I.; Perez-melis, A.; Willmitzer, L. Kinetics of Labelling of Organic and Amino Acids in Potato Tubers by Gas Chromatography-Mass Spectrometry Following Incubation in 13 C Labelled Isotopes. *Plant J.* **2004**, *39*, 668–679.

(23) Lane, A. N.; Tan, J.; Wang, Y.; Yan, J.; Higashi, R. M.; Fan, T. W. Probing the Metabolic Phenotype of Breast Cancer Cells by Multiple Tracer Stable Isotope Resolved Metabolomics. *Metab. Eng.* **2017**, *43* (February), 125–136.

(24) Dong, W.; Keibler, M. A.; Stephanopoulos, G. Review of Metabolic Pathways Activated in Cancer Cells as Determined through Isotopic Labeling and Network Analysis. *Metab. Eng.* **2017**, *43* (February), 113–124.

(25) Achreja, A.; Zhao, H.; Yang, L.; Hyun, T.; Marini, J. Exo-MFA – A 13C Metabolic Fl Ux Analysis Framework to Dissect Tumor Microenvironment-Secreted Exosome Contributions towards Cancer Cell Metabolism. *Metab. Eng.* **2017**, *43* (December 2016), 156–172.

(26) Lakshmanan, M.; Ho, Y. S.; Bardor, M.; Nagarajan, N.; Lee, D.; Noor, F.; Yusufi, K.; Lakshmanan, M.; Ho, Y. S.; Liat, B.; et al. Cellular Adaptations in a Recombinant CHO Cell Line Mammalian Systems Biotechnology Reveals Global Cellular Adaptations in a Recombinant CHO Cell Line. *Cell Syst.* **2017**, *4* (5), 530–542.e6.

(27) Goudar, C.; Biener, R.; Boisart, C.; Heidemann, R.; Piret, J.; de Graaf, A.; Konstantinov, K. Metabolic Flux Analysis of CHO Cells in Perfusion Culture by Metabolite Balancing and 2D [13C,1H] COSY NMR Spectroscopy. *Metab. Eng.* **2010**, *12* (2), 138–149.

(28) Woo Suk, A.; Antoniewicz, M. R. Parallel Labeling Experiments with [1,2-13C]Glucose and [U-13C]Glutamine Provide New Insights into CHO Cell Metabolism. *Metab. Eng.* **2013**, *15* (1), 34–47.

(29) Creek, D. J.; Chokkathukalam, A.; Jankevics, A.; Burgess, K. E. V.; Breitling, R.; Barrett, M. P. Stable Isotope-Assisted Metabolomics for Network-Wide Metabolic Pathway Elucidation. *Anal. Chem.* **2012**, *84* (20), 8442–8447.

(30) Chokkathukalam, A.; Kim, D.-H.; Barrett, M. P.; Breitling, R.; Creek, D. J. Stable Isotope-Labeling Studies in Metabolomics: New Insights into Structure and Dynamics of Metabolic Networks. *Bioanalysis* **2014**, *6* (4), 511–524.

(31) Maralingannavar, V.; Parmar, D.; Pant, T.; Gadgil, C.; Panchagnula, V.; Gadgil, M. CHO Cells Adapted to Inorganic Phosphate Limitation Show Higher Growth and Higher Pyruvate Carboxylase Flux in Phosphate Replete Conditions. *Biotechnol. Prog.* **2017**, *33* (3), 749–758.

(32) U.S. Department of Health and Human Services Food and Drug Administration. Guidance for Industry Bioanalytical Method Validation Guidance for Industry Bioanalytical Method Validation (2001). *Food Drug Adm.* **2001**, 1–44.

(33) Egorova-Zachernyuk, T. A.; Bosman, G. J. C. G. M.; Degrip, W. J. Uniform Stable-Isotope Labeling in Mammalian Cells: Formulation of a Cost-Effective Culture Medium. *Appl. Microbiol. Biotechnol.* **2011**, *89* (2), 397–406.

Chapter 4

Performance evaluation of MALDI-TOF MS/MS estimation of asymmetric to symmetric dimethylarginine ratio

4.1 Introduction

Development of MALDI-MS methods for small molecule analysis has been significantly thwarted because of interferences from UV absorptive MALDI matrices that introduce complex high-intensity background signals in the region below 500 *m/z*, often confounding with analyte peaks. Many attempts have been made to overcome matrix interference through the introduction of novel matrices and other ion suppression strategies in the last two decades.[1–6] However, these approaches led to limited success often restricting the analysis to specific molecules that could be efficiently ionized in the presence of novel matrices. Analysis using MALDI MS/MS, on the other hand, offers a potential alternative to overcome matrix peak interferences without a need for novel matrices. Monitoring specific diagnostic ions in tandem mass spectrometry resulting from fragmentation of analytes can be used for simultaneous selective qualification as well as quantification purposes.[7] It is noteworthy that monitoring MS/MS transitions has been rather quintessential with triple-quadruple MS analyses, albeit in combination with liquid chromatography. This mode of analysis has provided sensitivity and selectivity for quantitative LC-MS workflows. MALDI-MS/MS approach as an alternative to tackle matrix interferences has been emphasized previously by Karas *et al.* [8] However, this work has not yet seen the wider adaptation. MALDI-MS data is acquired following discrete laser shots on a specific sample surface that is exhausted rapidly unlike LC-MS that enables longer-duration continuous sample injection and data acquisition. Hence, the number of metabolites that can be simultaneously monitored on a single spot can be limited. Nevertheless, MALDI MS/MS provides superior selectivity over single stage MS while still retaining high throughput nature. This can be especially advantageous for the measurement of structural isomers from complex biological samples.

Dimethylarginine (DMA) exists in two isomeric forms, namely, asymmetric dimethylarginine (ADMA) and symmetric dimethylarginine (SDMA). These structural isomers are formed as a result of lysis of proteins with methylated arginine residues.[9,10] Increased plasma levels of ADMA has a direct inhibitory effect on nitric oxide synthase (NOS) causing impaired nitric oxide generation.[11–13] This subsequently results in endothelial dysfunction and several physiological complications such as hypertension and immune dysfunction in chronic renal failure patients.[14–18] While SDMA does not have direct inhibitory effect on NOS, its competitive nature towards arginine transporters has been postulated to induce indirect NOS inhibition.[19] Altered asymmetric to symmetric dimethylarginine ratio

(ASR) in blood plasma has been observed in the case of cardiovascular diseases (CVD), diabetes, chronic kidney disease(CKD), chronic active hepatitis, muscular dystrophy and end-stage renal failure patients.[11,20–22] Methods to detect the DMAs are thus important in clinical studies across a wide spectrum of diseases. As of now, determination of ADMA and SDMA involves various analytical strategies that invariably use liquid chromatography and calibrations from biological matrix-matched standards for absolute quantitation.[23–29] We have previously demonstrated the precise determination and absolute quantitation of isomeric dimethylarginines (DMA) using MALDI-TOF MS approach [30]. Calibration curves from reference standards in matrix-matched simulated urine were generated and used for single stage MALDI-TOF MS quantitation of isomeric DMAs from urine samples from healthy individuals in the reported work[30]. However, estimation of isomeric DMAs from urine in disease conditions presents significant challenges limiting the applicability of the previous method. Urinary concentrations of the DMA markers can significantly vary with individual hydration levels, among other patient and environment specific factors, rendering urine an unreliable sample matrix for physiological estimations and to draw meaningful disease correlations. Urine from proteinuric individuals could also induce protein binding and resultant inefficient extractions. This invariably leads to measurement inaccuracies that would make it difficult to compare estimated absolute concentrations both within a particular group and between disease and control groups.

In this work, we describe the selective MALDI-TOF MS/MS detection and estimation of urinary asymmetric and symmetric dimethylarginine ratio (ASR) as an alternative to absolute quantitation. We further demonstrate the potential prognostic use of urinary ASR measured using MALDI-TOF MS/MS in diabetes complications. The method was validated against LC-MS/MS data using a subset of 25 samples drawn from diabetic individuals at different stages of progression towards nephropathy. Inter-day reproducibility of the method was investigated using healthy and macroalbuminuric urine samples as quality controls during implementation in a randomized clinical study (n=555) over several days of sample data acquisitions. This method of measuring ratios using MALDI-TOF MS/MS overcomes the inherent limitations of absolute quantitative MS methods from urine samples. The high throughput MALDI-TOF MS/MS approach is devoid of chromatographic or derivatization steps and eliminates the need for isotopically labeled reference standards.

4.2 Materials and methods

4.2.1 Materials

Ultrapure α-cyano-4-hydroxycinnamic acid (CHCA), NG, NG'-dimethyl L-arginine di(p-hydroxyazobenzene-p'-sulphonate) salt (SDMA), NG, NG-dimethylarginine hydrochloride (ADMA), bovine serum albumin (BSA) and trifluoroacetic acid (TFA) were purchased from Sigma Aldrich (MA, USA). LC-MS grade acetonitrile (ACN) and methanol were purchased from J T Baker (PA, USA). Deionized water with a specific resistivity of 18.2 MΩ cm^{-1} (Merck-Millipore) was used for analysis.

4.2.2 Recruitment of study participants

Participant recruitment, sample collection, and processing was performed by Madras Diabetes Research Foundation (MDRF, Chennai, India) after appropriate approvals of the study from Institutional Ethics Committee. A written informed consent was obtained from all individuals prior to the sample collection. A total of 25 individuals were recruited for the method standardization and cross-platform validation. The individuals were assigned to 5 different categories as (1) normal glucose tolerance (NGT), (2) impaired glucose tolerance (IGT), (3) newly diagnosed diabetes (NDD), (4) Type 2 diabetes with microalbuminuria (MIC), and (5) Type 2 diabetes with macroalbuminuria (MAC). The categories were made according to the World Health Organization consulting group criteria. Each category consisted of 5 individuals.

4.2.3 Standards, sample processing, and method validation

Standard calibration levels were prepared by serial dilution. The levels included 0.06, 0.125, 0.25, 5, and 9 µM solution for both ADMA and SDMA. Two standard QCs at 7 and 3 µM were also prepared. Urine samples were collected, aliquoted and immediately stored at -80°C until further processing. Samples were thawed on ice prior to further processing. 400µL cold methanol was added to 100 µL aliquot of each urine sample. The contents were thoroughly mixed using vortex mixer followed by centrifugation at 13,200 rpm, 4°C for 15 minutes. ~250 µL supernatant was subsequently collected, divided into aliquots and used for MS analysis. For cross-platform comparison, identical aliquots of all the 25 processed samples were prepared as above and used for MALDI-MS/MS and LC-MS/MS analyses. These samples were analyzed to obtain the ASR from the respective methods.

Detailed performance evaluation of the MALDI-TOF MS/MS method to measure ASR was undertaken in a series of experiments described below. Sample matrix effects that might have a bearing on ion suppression or enhancement and analyte recovery were evaluated using pooled samples and surrogate matrices. Pooled samples were prepared by mixing 100µL of 5 representative NGT and MAC individual urine samples, randomly chosen from a sample set of 555 clinical samples collected. The sample processing for pooled samples was also performed as described above. (i) Separate QC samples to estimate the ion suppression effects were prepared by spiking three concentration levels of ADMA and SDMA (1:1), 9 µM, 30 µM and 45 µM, in pooled NGT and MAC samples. A corresponding control solution of these without the sample matrix was also similarly analyzed. (ii) Additionally, influence of varying (excess) amounts SDMA on endogenous ADMA levels was investigated by spiking pooled NGT and MAC samples with the three levels of SDMA (9 µM, 30 µM and 45 µM) and measuring ADMA alone (diagnostic peak *m/z* 46). Similar experiment to investigate the effect of excess ADMA on endogenous SDMA was also performed by spiking the pooled NGT and MAC matrices with three concentration levels of ADMA (9 µM, 30 µM and 45 µM) and measuring SDMA alone (diagnostic peak *m/z* 172). (iii) To estimate the effect of albumin content on the ASR measurement, spiked NGT* 1 and 2 were prepared with the variable concentration of albumin representing the MIC and MAC, respectively. Further, albumin spiked NTG* 3 and 4 were prepared with excess on albumin content. Spiked samples were extracted using the protocol described above. (iv) Two randomly selected samples, one each from NGT and MAC categories were used as quality control samples (QC1 and QC2) throughout the course of data acquisitions for the 555 clinical samples.

4.2.4 MALDI-MS/MS analysis

96-well MALDI target plate was pre-spotted with 0.5µL CHCA matrix (10mg/mL). After drying, 0.5 µL of each sample or QC were applied on to the target plate. The target plate was dried overnight before being analyzed. MALDI-MS/MS was performed on AB Sciex 5800 MALDI TOF/TOF instrument with a collision-induced dissociation (CID) cell. The instrument is equipped with Nd-YAG laser operating at 345 nm, pulse length - 500 ps and repetition rate - 1000 Hz. CID was performed at 1 kV in positive ion mode and the pressure was maintained at 1 X 10e-6 Torr. Optimized laser fluence at 5200 units, delayed extraction (DE) time at 200 ns, 2000 laser shots and a precursor selection window 203.15±0.5 *m/z* were used for MS/MS analysis. Detector voltage was optimized at 2.69 eV for small molecule analysis. Entire

analysis was performed in automated mode. Data analysis was performed using Data Explorer (AB Sciex) and an in-house developed data processing algorithm MQ [(http://www.ldi-ms.com/services/software) respectively. Briefly, raw instrumental files (T2D) were converted to ASCII format using T2Dconverter (software version 1.0) prior to processing using 'MQ'. was estimated Ratio of peak intensities, within mass extraction window (MEW) of 50 ppm, of the diagnostic product ions of ADMA and SDMA at *m/z* 46 and *m/z* 172 respectively were estimated using the 'relative quantitation' module of MQ and reported as ADMA: SDMA ratio (ASR). The above optimized method was used for the 25 standardization samples used for cross-platform validation as well as the remaining clinical samples (n=555) and other QC samples.

4.2.5 LC-MS/MS analysis

LC-MS/MS of the 25 samples intended for cross-platform validation was performed on an Agilent 6420 triple quadrupole mass spectrometer with electrospray ionization (ESI) interface. The samples were reconstituted in 160 µl of ACN: water (50:50) and maintained at 4˚C in the autosampler. Injection volume was set to 5 µL. The separation was achieved using Agilent ZORBAX HILIC PLUS column (100mm*4.6mm*3.5µm) with isocratic mobile phase consisting of ACN:water (90:10) with 0.3% acetic acid and 0.0125% trifluoroacetic acid, flow rate 600 µL/min, and total run time of 9 min. The column temperature was maintained at 28±2.5 ˚C. The ESI capillary temperature, sheath gas, and auxiliary gas were set at 300 ˚C, 45, 15 arbitrary units, respectively. The mass spectrometer was operated in positive ion mode with ionization voltage 4000 V. Ion transitions, *m/z* 203.1→46.1 for ADMA and m/z 203.1→172.1 for SDMA, were monitored in multiple reaction monitoring mode (MRM). MS/MS for ADMA and SDMA was performed at 20 eV, 13 eV, respectively. MassHunter software, version B.07.00, was used for data analysis.

4.3 Results and Discussion

MALDI MS/MS of the precursor ion at *m/z* 203 from the urine samples yielded the expected diagnostic product ion peaks for ADMA and SDMA at *m/z* 46 and 172 (*m/z* 46.0641 and 172.1048 in NGT, and *m/z* 46.0643 and 172.1031 in MAC). Measurement of ADMA and SDMA by diagnostic product ions in healthy urine samples has been demonstrated previously.[30] The observed MS/MS product ions from both the control and the diabetic samples

were in agreement with previous results. MS/MS peaks were observed within 25 ppm mass accuracy. Figure 4.1 shows representative annotated *m/z* data for NGT and MAC urine samples subjected to MALD-TOF MS/MS. Preliminary inspection of the MS/MS data from the NGT and MAC samples showed marked differences in the relative peak intensities of the diagnostic ADMA and SDMA peaks. Both the metabolites were unequivocally detected from the urine samples of NGT, IGT, NDD, MIC and MAC individuals simultaneously detecting and confirming the presence of ADMA and SDMA. Detection of the DMA metabolites from the urine samples by MALDI-TOF MS/MS within a narrowly defined *m/z* window ensured a high degree of selectivity that would be retained with the ASR measurements as well.[8,31]
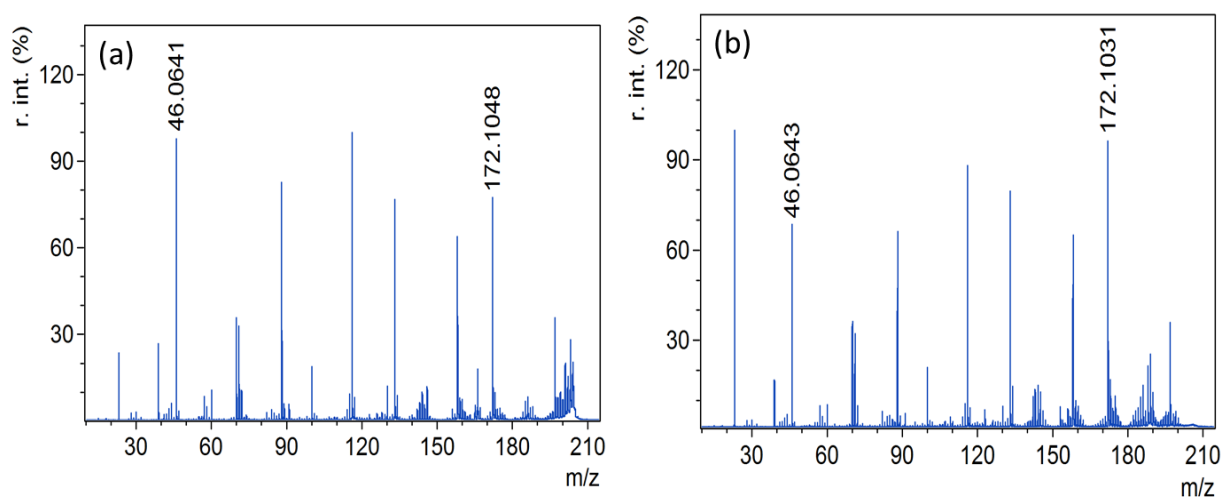
Figure 4.1 Representative MALDI-TOF MS/MS of urinary isomeric dimethylarginine (m/z 203) from (a) normoglycemic (NGT) and (b) type 2 diabetes with macroalbuminuria (MAC) samples. The diagnostic product ions at m/z 46 and m/z 172 represent ADMA and SDMA, respectively.

Calibration curves for ADMA and SDMA were prepared using an absolute intensity of 46 and 172 ions. Excellent linearity with R^2 0.99 was observed for both ADMA and SDMA. The QC recoveries were within ± 20%, except in case of one QC (SDMA 3 µM), where the recovery was 123.96%. Subsequently, the calibration curve was used to measure the ADMA and SDMA concentration in representative pool samples from NGT and MAC categories. The samples concertation were within the reported urinary concentration of ADMA and SDMA metabolites

as per HMDB database.[32] The slopes of both isomers, ADMA and SDMA, were comparable indicating similar ionization behavior.

Table 4.1 Details of the calibration curve and QC recoveries. The absolute concentration of ADMA and SDMA measured in pooled samples is shown.

Analyte	Ion (*m/z*)	Calibration range (µM)	Calibration Equation; R^2	Sample	Measured Concentration (% Recovery)
ADMA	46	(0.06-9)	y=299.76X+15.444; 0.99	QC 7 µM	6.87 µM (98.13)
				QC 3 µM	2.65 µM (88.48)
				NGT[a]	23.3 µM
				MAC[a]	6.1 µM
SDMA	172	(0.06-9)	y=215.92X-7.976; 0.99	QC 7 µM	6.74 µM (96.24)
				QC 3 µM	3.72 µM (123.96)
				NGT[a]	28.95 µM
				MAC[a]	13.5 µM

[a] Pooled sample; values indicated factored in a 5X dilution to fit the calibration range

The MALDI-TOF MS/MS method was further evaluated prior to using the ratios of peak-intensities of the detected diagnostic ions as a measure for the ASR from the urine samples. Sample matrix-associated ion suppression effects, variability owing to the presence of protein (in MIC and MAC urine samples), inter and intra assay reproducibility were investigated. Figure 4.2 and table 4.2 summarize the results obtained. ADMA and SDMA reference standards spiked (1:1) in pooled NGT and MAC at 9 µM, 30 µM, and 45 µM showed a proportional and linear increase in the peak intensity for the respective diagnostic ions (Figure 4.2 (b) and (c)). The increase is similar to that of the reference standards (Figure 4.2 (a)) in the absence of any biological matrix. The peak intensities of ADMA and SDMA were overlapping at each of the spiked levels. The corresponding ASR (*m/z* 46/172) estimated from the peak intensities (seen in figure. 4.2 a, b & c) was nearly constant (Figure 4.2 (d)). The ASR was relatively uninfluenced by the three different concentration levels and from the urine sample

matrix that had the analyte spiked (NGT, MAC, and the control reference standard solution; figure 4.2 (d)). These results indicate that the MS/MS ionization efficiencies were similar for both the isomers, responses were linear and the urine matrix-associated ion suppression effects (represented by two extremes of the urine samples NGT and MAC) were negligible.
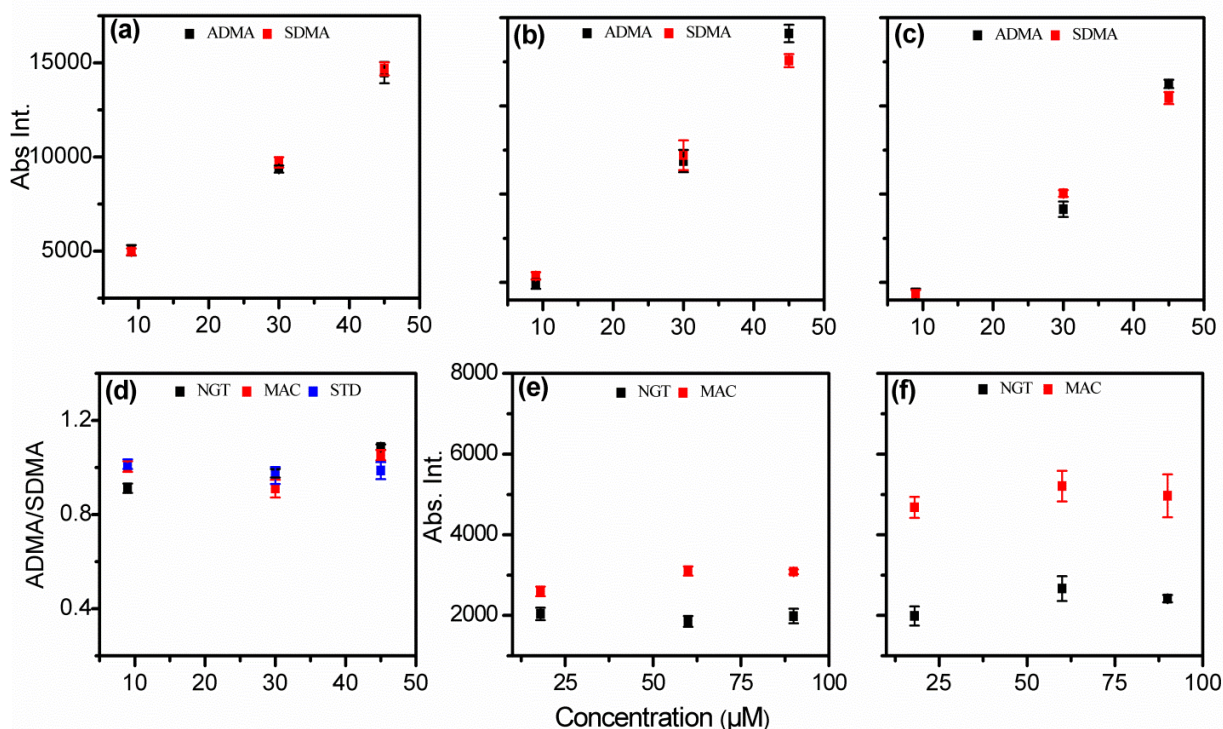
Figure 4.2 MALDI-TOF MS/MS peak intensity profiles of ADMA (m/z 46) and SDMA (m/z 172) as measured in standard solution (a) are shown. Three concentration levels of ADMA and SDMA (1:1) were used – 9 µM, 30 µM and 45 µM and a proportional increase in the intensity for the respective diagnostic ions was observed. ADMA and SDMA standards were also spiked in pooled NGT (b) and MAC (c) samples with similar trends observed. The corresponding m/z 46/172 ASR estimated as a ratio of peak intensities (from a, b & c) is relatively uninfluenced by the three concentration levels (d). Influence of varying amounts SDMA (spiked in excess) on endogenous ADMA levels (e) and varying amounts of ADMA (spiked in excess) on endogenous SDMA (f) indicate no significant ion suppression or enhancement effects in both the pooled NGT and MAC matrices.

Low abundant analytes could potentially encounter inefficient ionization and resultant signal suppression in the presence of highly abundant analytes of similar *m/z* and chemical nature. To rule out any competitive ionization between ADMA and SDMA with potential

resultant ion population losses, the effect of excess analyte (spiked) on the endogenous (non-spiked) counterpart was investigated. In the first case, three concentration levels of SDMA were spiked in the NGT and MAC samples (in significant excess, 18 µM, 60 µM and 90 µM in the final solution) and the endogenous ADMA levels were monitored using MALDI TOF MS/MS. The marginal increase in the absolute peak intensities was observed for ADMA in the MAC pooled sample in the presence of 60 and 90 µM spiked SDMA (figure 4.2 (e)). There was no significant peak intensity change at 9 µM spiked SDMA in MAC and all the three levels of spiked SDMA in NGT sample. Likewise, SDMA measured in the presence of excess spiked ADMA at the three levels (18 µM, 60 µM and 90 µM) showed no significant enhancement or suppression in both NGT and MAC samples (figure 4.2 (f)).All the peak intensities were observed reproducibly with low standard deviations as indicated by the error bars. The outcomes of these investigations indicate an absence of abundant analyte associated competitive or selective ionization of ADMA and SDMA from NGT and MAC samples. Thus, any variations of ASR measured from urine samples would in all likelihood be free from ion suppression effects and uninfluenced by relative abundancies of the respective metabolites.

To understand the impact of higher protein content in micro and macro-albuminuria, the change in ASR was monitored in albumin spiked pooled NGT sample (n=5). The average normal concentration of albumin in human urine is 30 µg/mg of creatinine. This corresponds to an absolute concentration of albumin being 377.25 µM. As per the NKF-KDOQI (National Kidney Foundation–Kidney Disease Outcomes Quality Initiative) guidelines, the albumin excretion rate (AER) for MIC and MAC are 30-300 µg/mg and >300 µg/mg creatinine, respectively.[33,34] Corresponding to the guidelines, pooled NGT samples were spiked with albumin to obtain a representative albumin concentration for MIC and MAC categories. To understand the influence of variable albumin concentration on the measurement of ASR, 100 µL pooled NGT urine was spiked with albumin to bring the albuminuria content level to MIC and MAC, respectively. The final concentration of albumin in the spiked sample was 4.263 µM (spiked NGT* 1), 9.1 µM (spiked NGT* 2), 1.4 mM (spiked NGT* 3), and 4.3 mM (spiked NGT* 4). Spiked sample NGT* 1 and NGT* 2 represented albumin level within the range of MIC and MAC samples. Table 1 contains the details of replicate data for control and albumin spiked NGT* samples. The RSD of technical replicates was found to be <10 % RSD, indicating acceptable reproducibility. The changes in the ASR in control and spiked samples showed <10% variation from the control sample indicating the negligible influence of albumin content

on ASR measurement using MALDI-MS/MS. Spiked sample NGT* 3 and NGT* 4 were prepared in extreme excess albumin content to further evaluate the influence of albumin on ASR measurement. The albumin content in spiked sample 3 and 4 is in practically impossible in real life scenario. Despite of extreme levels of albumin, the reproducibility of ASR measurement remained unaffected. The changes in ASR values were at 10%.

NGT sample was dried and reconstituted with albumin equivalent to 5 and 15 µg / 50 µL sample volume, representative of albumin content in microalbuminuric and macroalbuminuric urine, respectively (Spiked NGT*1 and 2). Whereas, post extraction, ADMA/SDMA ratio in control and albumin spiked samples were measured using MALDI-TOF MS/MS.

Reproducibility of MALDI-MS/MS measurement was evaluated by monitoring QC control samples. In a clinical study comprised of 555 participants, data for all samples were acquired in triplicate using 18 iterations of 96-well MALDI target plate. Each plate was spotted with duplicate spots of 2 QC samples from NGT and MAC categories. The ASR in these two QCs was monitored over the span of the entire MALDI-TOF MS/MS analysis of the 18 target plates. This generated 36 data points for each of the QCs that were used to estimate the intra and inter-day reproducibility of the ASR measurement.

The box-whiskers plot of replicate data of QC1 and QC2 is showcased in figure 4.3. The reproducibility measured as % RSD of QC1 and QC2 over 18 days was found to be 8.8 % (average ASR 0.85) and 15.9 % (average ASR 0.39) respectively, both within acceptable values of 15%. The lower RSD for the NGT (QC1) that indicates the baseline control values in comparison to the MAC (QC 2) might indicate slightly more variability in the latter. The data encompassing 18 MALDI target plates indicate that the ASR can be reproducibly measured in a clinical sample using MALDI-MS/MS over a period of several days and the data comparisons can be drawn. Any prolonged use of MALDI-MS/MS for the measurement of ASR in a study of larger sample set may require the use of QC checks and monitoring of reproducibility to ensure any time-associated variations.

Table 4.2 ADMA / SDMA ratio measured as a peak intensity ratio (m/z 46/172) in NGT (control) and albumin spiked NGT samples (spiked NGT* 1 to 4) to estimate the influence of protein content on ASR measurement.

Sample Name	Replicate	*m/z* 46	*m/z* 172	*m/z* 46/172	Replicate avg. (%RSD)	% Variation from control
	R1	7.53E+03	6.19E+03	1.22		
NGT* (control)	R2	4.97E+03	3.97E+03	1.25	1.20 (4.7)	00.00
	R3	5.16E+03	4.53E+03	1.14		
Spiked NGT* 1	R1	1.73E+03	1.52E+03	1.13		
(4.2 µM of	R2	1.80E+03	1.71E+03	1.05	1.11(5.30)	-7.09
albumin)	R3	1.32E+03	1.14E+03	1.16		
Spiked NGT* 2	R1	1.13E+03	9.28E+02	1.22		
(9.1 µM of	R2	1.07E+03	9.74E+02	1.10	1.13 (7.51)	-6.19
albumin)	R3	1.04E+03	9.78E+02	1.06		
Spiked NGT* 3	R1	2.67E+03	2.54E+03	1.05		
(1.4 mM	R2	2.74E+03	2.47E+03	1.11	1.08 (2.8)	-10.00
albumin)	R3	2.36E+03	2.19E+03	1.08		
Spiked NGT* 4	R1	5.70E+03	4.71E+03	1.21		
(4.3 mM	R2	4.26E+03	3.20E+03	1.33	1.33 (8.7)	+10.83
albumin)	R3	3.19E+03	2.21E+03	1.44		

NGT* = Pooled sample (n=5)
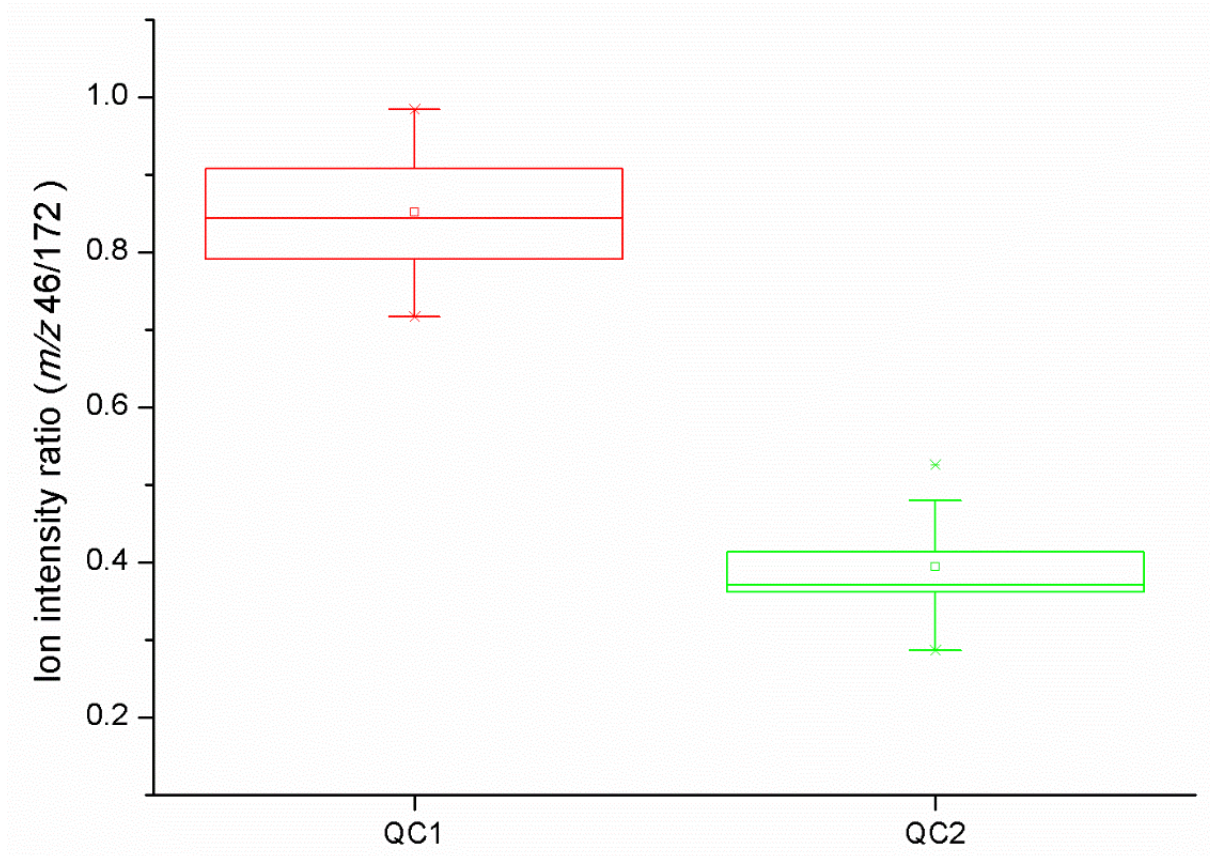
Figure 4.3 Box-Whiskers plot representing inter-day reproducibility of two quality control (QC1 and QC2) samples used over the course of MALDI-TOF MS/MS analysis of 555 clinical samples. The data was acquired in duplicates on each occasion and compiled for 18 MALDI target plates (analyzed over several days; 36 data points for each QC). A variation of 8.8 % (average=0.85) and 15.9 % (average=0.39) were observed for QC1 and QC2 respectively.
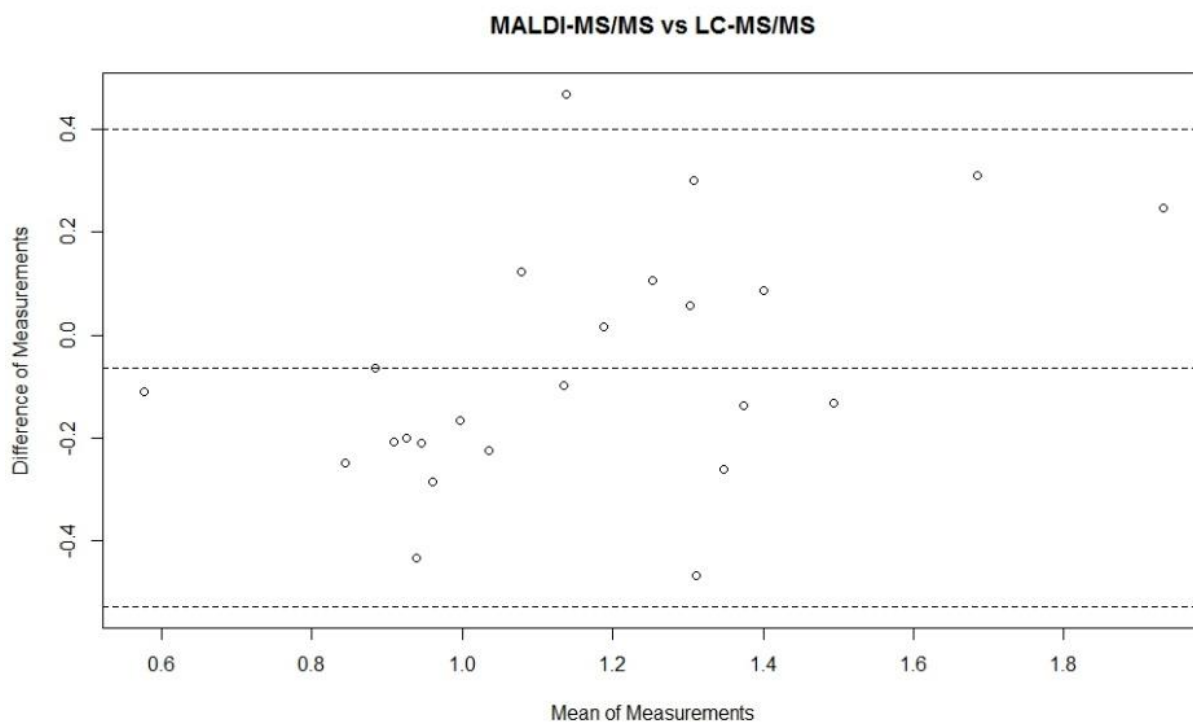
Figure 4.4 Bland-Altman plot for the ADMA/SDMA ratio measured in 24 samples from the 5 different diabetes classes of samples studied (NGT, IGT, NDD, MIC, and MAC) using MALDI-MS/MS and LC-MS/MS. ADMA/SDMA ratio measured for 23 out of 24 samples showed agreement between both methods within 95% confidence interval.

LC-MS/MS, widely accepted as the gold standard in quantitative analysis, was used to cross-validate the results obtained from MALDI MS/MS. A subset of 25 urine samples, five each encompassing the control and all the categories of the diabetic samples in the study were used for the validation. The transitions *m/z* 203 to 46 and 203 to 172 indicative of the presence of ADMA and SDMA were monitored from the urine samples as well as reference standards. ASR in the 25 urine samples from five clinical categories was measured on both the platforms. The data was acquired in triplicate on both platforms and is tabulated in Table 4.3. Intra-assay repeatability for the technical replicates (n=3) was found to be well within 15 % RSD for MALDI MS/MS and 3% RSD for LC-MS/MS. Both data indicated a high degree of reproducibility across the sample sets with notably lower RSDs observed in case of LC-MS/MS. Subsequently, the agreement between the two methods was tested using a Bland-Altman plot.[35] Figure 4.4 showcases the Bland-Altman plot of replicate average data from both platforms.

Table 4.3 ASR (%RSD) values of 24 samples measured on MALDI MS/MS and LC-MS/MS.

Category	Sample No.	MALDI MS/MS	LC-MS/MS
NGT	1	1.077(4.9%)	1.546(1.3%)
	2	1.196(12.2%)	1.180(0.3%)
	3	1.144(1.9%)	1.017(0.4%)
	4	1.427(8.0%)	1.560(0.4%)
	5	1.332(5.5%)	1.275(0.5%)
IGT	1	1.305(2.5%)	1.442(1.7%)
	2	1.842(5.4%)	1.530(0.4%)
	3	1.086(1.2%)	1.184(0.4%)
	4	1.372(5.2%)	0.903(0.4%)
	5	0.818(1.7%)	1.104(0.7%)
NDD	1	1.216(5.6%)	1.478(2.2%)
	2	2.055(8.3%)	1.808(0.7%)
	3	1.444(14.5%)	1.358(0.5%)
	4	0.924(6.0%)	1.148(0.7%)
	5	1.306(9.6%)	1.201(0.3%)
MIC	1	1.457(5.1%)	1.157(0.5%)
	2	0.915(5.3%)	1.080(0.2%)
	3	0.723(2.8%)	1.156(1.0%)
	4	0.825(2.1%)	1.026(1.2%)
	5	0.852(2.0%)	0.916(1.0%)
MAC	1	0.720(3.1%)	0.968(0.8%)
	2	0.841(3.0%)	1.033(2.5%)
	3	0.805(7.7%)	1.012(0.5%)
	4	0.521(22.5%)	0.632(0.5%)

The agreement was measured with an α value of 0.05, which signifies agreement interval of 95% with respect to LC-MS/MS measurements. 24 out of 25 samples analyzed for this comparison were found to be within the 95% interval limit. These results indicate agreement with the LC-MS/MS validating the MALDI MS/MS measurement of ASR.

4.4 Conclusions

MALDI MS/MS estimation of ASR in diabetic urine sample is reliable and analytically robust approach which involves minimal sample preparation. The validated method described herein would significantly simplify and render high throughput investigations involving large numbers of samples feasible. This work presents advancement over the previously reported absolute quantitation of isomeric DMAs using MALDI MS.[30] MALDI MS/MS allows precise, accurate and simultaneous confirmation and relative estimation of the DMA isomers without the need for absolute quantitation. MALDI MS/MS measurement of ion ratios also allows a chromatography-free analysis, which is a marked departure from absolute small molecule quantitation from urine and dialysates reported previously.[36,37] As ASR is the ratio of two metabolites and not individual concentration being measured, the effect of dilution or instrumental variation will be negligible on measurements. Hence, a necessity of creatinine estimation during urine testing can potentially be avoided. MALDI MS/MS as a method offers a viable alternative for diagnostic measurement of isomeric DMA metabolites in other class of samples such as serum/plasma and tissues.

Urinary ADMA to SDMA distribution has been detected earlier from various disease conditions.[26,38,39] However, to our knowledge this is the first report that measures the urinary DMA distribution from different stages of diabetes. Physiologically, urinary ASR reflects impaired arginine metabolism in progressive diabetes mellitus.[27,40] Decreasing trends of this ratio can correlate to worsening pathological condition and can serve as a potential biomarker of diabetic renal complication. There have also been no reports, till date, of implementation and validation of the analytical performance of MALDI-TOF MS/MS method for the measurement of ASR in clinical samples from diabetic and proteinuric individuals. Further investigations measuring ASR from a statistically relevant cohort are necessary to establish any correlations of ASR with the onset and progression of renal disease.

4.5 References

(1)   Cohen, L. H.; Gusev, A. I. Small Molecule Analysis by MALDI Mass Spectrometry. *Anal. Bioanal. Chem.* **2002**, *373* (7), 571–586.

(2)   Zhang, S.; Liu, J.; Chen, Y.; Xiong, S.; Wang, G.; Chen, J.; Yang, G. A Novel Strategy for MALDI-TOF MS Analysis of Small Molecules. *J. Am. Soc. Mass Spectrom.* **2010**, *21* (1), 154–160.

(3)   Soltzberg, L. J.; Patel, P. Small Molecule Matrix-Assisted Laser Desorption/Ionization Time-of-Flight Mass Spectrometry Using a Polymer Matrix. *Rapid Commun. Mass Spectrom.* **2004**, *18* (13), 1455–1458.

(4)   Lin, Z.; Zheng, J.; Bian, W.; Cai, Z. $CuFe_2O_4$ Magnetic Nanocrystal Clusters as a Matrix for the Analysis of Small Molecules by Negative-Ion Matrix-Assisted Laser Desorption/Ionization Time-of-Flight Mass Spectrometry. *Analyst* **2015**, *140* (15), 5287–5294.

(5)   Giampà, M.; Lissel, M. B.; Patschkowski, T.; Fuchser, J.; Hans, V. H.; Gembruch, O.; Bednarz, H.; Niehaus, K. Maleic Anhydride Proton Sponge as a Novel MALDI Matrix for the Visualization of Small Molecules (<250 m/z) in Brain Tumors by Routine MALDI ToF Imaging Mass Spectrometry. *Chem. Commun.* **2016**, *52* (63), 9801–9804.

(6)   Ugarov, M. V; Khabashesku, D. V; Peng, H.; Khabashesku, V. N.; Furutani, H.; Prather, K. S.; Schultz, J. A.; Woods, A. S. New MALDI Matrices for Biomolecular Analysis Based on Functionalized Carbon Nanomaterials. *Anal. Chem.* **2004**, *76* (22), 1–2.

(7)   Schwartz, S. a.; Reyzer, M. L.; Caprioli, R. M. Direct Tissue Analysis Using Matrix-Assisted Laser Desorption/Ionization Mass Spectrometry: Practical Aspects of Sample Preparation. *J. Mass Spectrom.* **2003**, *38* (7), 699–708.

(8)   Ejsing, C. S.; Moehring, T.; Bahr, U.; Duchoslav, E.; Karas, M.; Simons, K.; Shevchenko, A. Collision-Induced Dissociation Pathways of Yeast Sphingolipids and Their Molecular Profiling in Total Lipid Extracts: A Study by Quadrupole TOF and Linear Ion Trap–orbitrap Mass Spectrometry. *J. Mass Spectrom.* **2006**, *41* (3), 372–389.

(9)   Kakimoto, Y.; Akazawa, S. Isolation and Identification and Hydroxylysine from Human of NG3 NG- and NG3 WG-Dimethyl- Urine. *J. Biol. Chem.* **1970**, *245* (21), 5751–5758.

(10)   Markiw, R. T. Isolation of N-Methylated Basic Amino Acids from Physiological Fluids and Protein Hydrolysates. *Biochem. Med.* **1975**, *13* (1), 23–27.

(11)   Leone, A.; Moncada, S.; Vallance, P.; Calver, A.; Collier, J. Accumulation of an Endogenous Inhibitor of Nitric Oxide Synthesis in Chronic Renal Failure. *Lancet* **1992**, *339* (8793), 572–575.

(12)   Böger, R. H.; Vallance, P.; Cooke, J. P. Asymmetric Dimethylarginine (ADMA): A Key Regulator of Nitric Oxide Synthase. *Atheroscler. Suppl.* **2003**, *4*, 1–3.

(13)   Böger, R. H. Asymmetric Dimethylarginine, an Endogenous Inhibitor of Nitric Oxide Synthase, Explains the "L-Arginine Paradox" and Acts as a Novel Cardiovascular Risk Factor. *J. Nutr.* **2004**, *134* (10 Suppl), 2842S–2847S.

(14)   Sibal, L.; Agarwal, S. C.; Home, P. D.; Boger, R. H. The Role of Asymmetric Dimethylarginine (ADMA) in Endothelial Dysfunction and Cardiovascular Disease. *Curr. Cardiol. Rev.* **2010**, *6*, 82–90.

(15)   Lin, K. Y.; Ito, A.; Asagami, T.; Tsao, P. S.; Adimoolam, S.; Kimoto, M.; Tsuji, H.; Reaven, G. M.; Cooke, J. P. Impaired Nitric Oxide Synthase Pathway in Diabetes Mellitus: Role of Asymmetric Dimethylarginine and Dimethylarginine Dimethylaminohydrolase. *Circulation* **2002**, *106* (8), 987–992.

(16)   Franco, M. Di; Lucchino, B.; Conti, F.; Valesini, G.; Spinelli, F. R. Review Article Asymmetric Dimethyl Arginine as a Biomarker of Atherosclerosis in Rheumatoid Arthritis. *Mediators Inflamm.* **2018**, *2018*, 1–13.

(17)   Stühlinger, M. C.; Tsao, P. S.; Her, J. H.; Kimoto, M.; Balint, R. F.; Cooke, J. P. Homocysteine Impairs the Nitric Oxide Synthase Pathway Role of Asymmetric Dimethylarginine. *Circulation* **2001**, *104* (21), 2569–2575.

(18) Lu, T.-M.; Ding, Y.-A.; Charng, M.-J.; Lin, S.-J. Asymmetrical Dimethylarginine: A Novel Risk Factor for Coronary Artery Disease. *Clin. Cardiol.* **2003**, *26* (10), 458–464.

(19) Closs, E. I.; Basha, F. Z.; Habermeier, A.; Förstermann, U. Interference of L-Arginine Analogues with L-Arginine Transport Mediated by the Y+ Carrier HCAT-2B. *Nitric Oxide Biol. Chem.* **1997**, *1* (1), 65–73.

(20) Lou, M. F. Human Muscular Dystrophy: Elevation of Urinary Dimethylarginines. *Science (80- .).* **1979**, *203* (4381), 668–670.

(21) MacAllister, R. J.; Rambausek, M. H.; Vallance, P.; Williams, D.; Hoffmann, K. H.; Ritz, E. Concentration of Dimethyl-L-Arginine in the Plasma of Patients with End-Stage Renal Failure. *Nephrol. Dial. Transplant* **1996**, *11* (12), 2449–2452.

(22) Marescau, B.; Nagels, G.; Possemiers, I.; De Broe, M. E.; Becaus, I.; Billiouw, J. M.; Lornoy, W.; De Deyn, P. P. Guanidino Compounds in Serum and Urine of Nondialyzed Patients with Chronic Renal Insufficiency. *Metabolism.* **1997**, *46* (9), 1024–1031.

(23) Schwedhelm, E. Quantification of ADMA: Analytical Approaches. *Vasc. Med.* **2005**, *10* (SUPPL. 1), 89–95.

(24) Schwedhelm, E.; Maas, R.; Tan-Andresen, J.; Schulze, F.; Riederer, U.; Böger, R. H. High-Throughput Liquid Chromatographic-Tandem Mass Spectrometric Determination of Arginine and Dimethylated Arginine Derivatives in Human and Mouse Plasma. *J. Chromatogr. B Anal. Technol. Biomed. Life Sci.* **2007**, *851* (1–2), 211–219.

(25) Teerlink, T.; Nijveldt, R. J.; De Jong, S.; Van Leeuwen, P. A. M. Determination of Arginine, Asymmetric Dimethylarginine, and Symmetric Dimethylarginine in Human Plasma and Other Biological Samples by High-Performance Liquid Chromatography. *Anal. Biochem.* **2002**, *303* (2), 131–137.

(26) Davids, M.; Swieringa, E.; Palm, F.; Smith, D. E. C.; Smulders, Y. M.; Scheffer, P. G.; Blom, H. J.; Teerlink, T. Simultaneous Determination of Asymmetric and Symmetric Dimethylarginine, l-Monomethylarginine, l-Arginine, and l-Homoarginine in Biological Samples Using Stable Isotope Dilution Liquid Chromatography Tandem Mass Spectrometry. *J. Chromatogr. B Anal. Technol. Biomed. Life Sci.* **2012**, *900*, 38–47.

(27) Martens-Lobenhoffer, J.; Bode-Böger, S. M. Measurement of Asymmetric Dimethylarginine (ADMA) in Human Plasma: From Liquid Chromatography Estimation to Liquid Chromatography-Mass Spectrometry Quantification. *Eur. J. Clin. Pharmacol.* **2006**, *62* (SUPPL. 13), 61–68.

(28) Martens-Lobenhoffer, J.; Bode-Böger, S. M. Mass Spectrometric Quantification of L-Arginine and Its Pathway Related Substances in Biofluids: The Road to Maturity. *J. Chromatogr. B Anal. Technol. Biomed. Life Sci.* **2014**, *964*, 89–102.

(29) Martens-Lobenhoffer, J.; Bode-Böger, S. M. Quantification of L-Arginine, Asymmetric Dimethylarginine and Symmetric Dimethylarginine in Human Plasma: A Step Improvement in Precision by Stable Isotope Dilution Mass Spectrometry. *J. Chromatogr. B Anal. Technol. Biomed. Life Sci.* **2012**, *904*, 140–143.

(30) Bhattacharya, N.; Singh, A.; Ghanate, A.; Phadke, G.; Parmar, D.; Dhaware, D.; Basak, T.; Sengupta, S.; Panchagnula, V. Matrix-Assisted Laser Desorption/Ionization Mass Spectrometry Analysis of Dimethyl Arginine Isomers from Urine. *Anal. Methods* **2014**, *6* (13), 4602–4609.

(31) Arnold, A.; Persike, M.; Gorka, J.; Dommett, E. J.; Zimmermann, M.; Karas, M. Fast Quantitative Determination of Methylphenidate Levels in Rat Plasma and Brain Ex Vivo by MALDI-MS/MS. *J. Mass Spectrom.* **2015**, *50* (8), 963–971.

(32) Bouatra, S.; Aziat, F.; Mandal, R.; Guo, A. C.; Wilson, M. R.; Knox, C.; Bjorndahl, T. C.; Krishnamurthy, R.; Saleem, F.; Liu, P.; et al. The Human Urine Metabolome. *PLoS One* **2013**, *8* (9).

(33) Inker, L. A.; Astor, B. C.; Fox, C. H.; Isakova, T.; Lash, J. P.; Peralta, C. A.; Kurella Tamura, M.; Feldman, H. I. KDOQI US Commentary on the 2012 KDIGO Clinical Practice Guideline for the Evaluation and Management of CKD. *Am. J. Kidney Dis.* **2014**, *63* (5), 713–735.

(34) Uhlig, K.; Eckardt, K. U. A Decade after the KDOQI CKD Guidelines: Impact on CKD Guidelines. *Am. J. Kidney Dis.* **2012**, *60* (5), 705–706.

(35) Bland, J. M.; Altman, D. G. Statistical Methods for Assessing Agreement Between Two Methods of Clinical Measurement. *Lancet* **1986**, *327*, 307–310.

(36) Chen, S.; Chen, L.; Wang, J.; Hou, J.; He, Q.; Liu, J.; Wang, J.; Xiong, S.; Yang, G.; Nie, Z. 2,3,4,5-Tetrakis(3′,4′-Dihydroxylphenyl)Thiophene: A New Matrix for the Selective Analysis of Low Molecular Weight Amines and Direct Determination of Creatinine in Urine by MALDI-TOF MS. *Anal. Chem.* **2012**, *84* (23), 10291–10297.

(37) Persike, M.; Zimmermann, M.; Klein, J.; Karas, M. Quantitative Determination of Acetylcholine and Choline in Microdialysis Samples by MALDI-TOF MS. *Anal. Chem.* **2010**, *82* (3), 922–929.

(38) Hsu, C. N.; Huang, L. T.; Lau, Y. T.; Lin, C. Y.; Tain, Y. L. The Combined Ratios of L-Arginine and Asymmetric and Symmetric Dimethylarginine as Biomarkers in Spontaneously Hypertensive Rats. *Transl. Res.* **2012**, *159* (2), 90–98.

(39) Bode-Böger, S. M.; Scalera, F.; Kielstein, J. T.; Martens-Lobenhoffer, J.; Breithardt, G.; Fobker, M.; Reinecke, H. Symmetrical Dimethylarginine: A New Combined Parameter for Renal Function and Extent of Coronary Artery Disease. *J. Am. Soc. Nephrol.* **2006**, *17* (4), 1128–1134.

(40) Jayachandran, I.; Sundararajan, S.; Paramasivam, P.; Venkatesan, B.; Subramanian, S. C.; Balasubramanyam, M.; Mohan, V.; Manickam, N. Association of Circulatory Asymmetric Dimethylarginine (ADMA) with Diabetic Nephropathy in Asian Indians and Its Causative Role in Renal Cell Injury. *Clin. Biochem.* **2017**, *50* (15), 835–842.

Chapter 5

Urinary isomeric dimethylarginine ratio and its plausible diagnostic value for diabetic nephropathy

5.1 Introduction

Diabetic nephropathy (DN) is one of the most important long-term complications of diabetes mellitus. Indeed, diabetes is estimated to increase the risk of end-stage renal disease (ESRD) approximately 12-fold, leading to premature morbidity and mortality.[1] A recent epidemiological study reported a significant increase in mortality rates associated with renal complications in diabetes.[2] Microalbuminuria (MAU) is an early sign of incipient renal disease and a marker of its progression. Furthermore, it is a key indicator of the need for intensified treatment of diabetes and hypertension, the most powerful predictor of cardiovascular and atherosclerotic risk and a prognostic marker in the development of ESRD and mortality.[3] Although MAU is the best available noninvasive predictor for risk of diabetic nephropathy, it occurs after several years of diabetes. Some patients with MAU have quite advanced renal pathological changes, for which therapies are less effective than the earlier stages of the disease.[4] Therefore, along with MAU, more sensitive markers and alternative approaches are essential for the diagnosis of early stages of diabetic nephropathy. Such diagnostic markers are also vital for assessing the renal state, optimizing diabetes care and for monitoring the success of therapy.

Asymmetric dimethylarginine (ADMA) and its structural isomer symmetric dimethylarginine (SDMA) are formed in the protein methylation biosynthetic pathway when methylated protein arginine residues are hydrolyzed and released [5,6]. They were originally discovered from urine in relatively high abundance [5]. Studies have reported that over 90% of ADMA entering the kidney is metabolized by DDAH1 (dimethylarginine dimethylamino hydrolase) isoform located primarily in the proximal tubule of renal tissue [7]., while the remaining 10% is removed by urinary excretion [8]. Thus kidney plays a major role in eliminating ADMA and injury to renal tissue leads to the alteration in the metabolism of ADMA. Studies have demonstrated that SDMA may indirectly reduce nitric oxide (NO) production by inducing intracellular arginine deficiency, as SDMA competes with the cationic amino acid transporter in the endothelial cell membrane [9]. Accumulation of plasma ADMA, an inhibitor of nitric oxide synthase (NOS), is caused primarily by the disruption of the DDAH pathway that metabolizes ADMA to citrulline and dimethylamine [10,11]. Overexpression of renal DDAH and increased urinary elimination of ADMA reduces renal injury in diabetic nephropathy [12]. Longitudinal

studies reported that patients with elevated plasma ADMA and SDMA are at higher risk of CKD progression and incident atherosclerotic cardiovascular events [13,14]. Altered asymmetric to symmetric dimethylarginine ratio (ASR) was found in patients with end-stage renal failure [15–17] and suggest that ASR may be a potential mediator and early biomarker of nephropathy in T2DM. Hence, we hypothesize that the altered ASR level in the urine could serve as a potent early biomarker for diabetic nephropathy.

Validated MALDI MS/MS method (described in chapter 4) to directly measure urinary ASR using diagnostic ion ratios of the isomeric DMA metabolites. Measuring the ASR, a ratio is an alternative to absolute quantification for the isomeric metabolite measurement and overcomes a multitude of variations that could arise from urine. To the best of our knowledge, direct MALDI MS/MS relative estimation of the DMA (dimethylarginine) isomers in relation to type 2 diabetes and nephropathy has not been previously reported. This high throughput MALDI MS/MS approach was validated using LC-MS/MS, is devoid of either chromatographic or derivatization steps and eliminates the need for isotopically labeled internal standards.

As Asian Indians are known to be more insulin resistant [18]. and more susceptible to cardio-metabolic diseases and DN [19–21]. There is a lack of data on ASR in relation to nephropathy in this high-risk population. Therefore, we aimed to study the efficacy of ASR, measured by the high throughput MALDI MS/MS approach, as a marker of early nephropathy and to evaluate ASR in Asian Indians with different degrees of glucose intolerance and type 2 diabetes mellitus (T2DM) subjects with and without diabetic nephropathy. Methods

5.2 Research Design and Methods

Study participants were recruited from, a large tertiary diabetes care center at Chennai in South India. Individuals with (a) normal glucose tolerance (NGT; $n=95$), (b) impaired glucose tolerance (IGT; $n=80$), (c) newly diagnosed diabetes (NDD; $n=120$), (d) T2DM with microalbuminuria (MIC; $n=140$), and (e) T2DM with macroalbuminuria (MAC; $n=120$) were recruited. Oral glucose tolerance test (OGTT) was done in those without self-reported diabetes. Institutional Ethics Committee (IEC) approval (from the Madras Diabetes Research

Foundation, Chennai, and National Chemical Laboratory, Pune) was obtained prior to the start of the study and written informed consent was obtained from the study participants.

Anthropometric measurements including weight, height, and waist circumference, were obtained by trained data collectors using standardized methods.[22] Body mass index (BMI) was calculated as weight (kg)/height (m)^2. Blood pressure was recorded from the right arm in a sitting position to the nearest 2 mmHg with a mercury sphygmomanometer (Diamond Deluxe BP apparatus, Pune, India). Two readings were taken 5 minutes apart and the mean of the two was taken as the blood pressure. Fasting plasma glucose (hexokinase method), serum cholesterol (cholesterol oxidase-peroxidase-amidopyrine method), serum triglycerides (glycerol phosphate oxidase-peroxidase-amidopyrine method) and HDL cholesterol (direct method-polyethylene glycol-pretreated enzymes), were measured using Hitachi-912 Autoanalyser (Hitachi, Mannheim, Germany). Low-density lipoprotein (LDL) cholesterol was calculated using the Friedewald formula. Glycated hemoglobin (HbA1c) was measured by high-pressure liquid chromatography using the Variant machine (Bio-Rad, Hercules, Calif., USA). Serum insulin concentration was estimated using the electrochemiluminescence method (COBAS E 411; Roche Diagnostics). Blood urea and serum creatinine (CRE) (Jaffe's method) were measured using a Hitachi-912 Autoanalyser (Hitachi, Mannheim, Germany). The intra- and inter-assay coefficients of variation for the biochemical assays ranged between 3.1% and 7.6%.

Urinary albumin was measured in fasting urine sample using immunoturbidimetric assay (Hitachi 902 autoanalyzer; Roche Diagnostics). eGFR was calculated by using CKD-epi equation. The CKD-EPI equation was calculated as GFR (ml/min/1.73 m2) = 141× min (serum creatinine/k, 1)α ×max (serum creatinine/k, 1)−1.209 ×0.993Age ×1.018 (if women) × 1.159 (if black), where k is 0.7 for women and 0.9 for men, α is −0.329 for women and −0.411 for men; 'min' indicates minimum serum creatinine/k or 1, and 'max' indicates maximum serum creatinine/k or 1.[23] All measurements were performed in a laboratory that is certified by the College of American Pathologists (Northfield, IL) and the National Accreditation Board for Testing and Calibration of Laboratories (New Delhi, India).

5.2.1 Statistical analysis

We compared anthropometric, clinical, and biochemical characteristics of groups using one-way ANOVA [with Tukey's HSD] for continuous variables and Chi-square test or Fisher's exact test to compare proportions. We performed Pearson correlation analysis to examine the correlation of various risk factors with ASR. Standardized polytomous regression analysis was done to assess how incremental changes in ASR were associated with MIC and MAC. We adjusted models for any demographic, anthropometric, clinical, or biochemical characteristics that were significantly different across groups.

Receiver operating characteristic curves (ROC) were plotted for ASR to identify MIC and MAC. Sensitivity, specificity, positive and negative predictive values and accuracy for predicting MIC and MAC were calculated for various ASR cut points. C statistic or the area under the ROC (AROC) was estimated and by interpolation from the area under the curve, the point closest to the upper-left corner, which maximized sensitivity and specificity, was selected as the optimal cut point; this identified the highest number of subjects with or without MIC or MAC.[25] All analyses was done using Windows-based SPSS statistical package (version 12.0, Chicago, IL).

5.3 Results and discussion

Table 6.1 shows the clinical and biochemical characteristics of the study participants. Age, Waist circumference, systolic and diastolic blood pressure, total cholesterol and serum triglycerides were significantly higher in patients with MIC ($p<0.05$) and MAC ($p<0.05$) compared to NDD, IGT, and NGT. Serum creatinine ($p<0.05$) was higher and eGFR ($p<0.05$) was lower in patients with MIC and MAC compared to NDD or NGT.

ASR was measured for the 555 urine samples across all the sample groups. As shown in figure 6.1, ASR was significantly lower in MIC (0.909; $p<0.01$) and MAC (0.741; $p<0.01$) in comparison to the NGT and NDD groups while there were no significant differences between NGT, IGT and NDD groups.
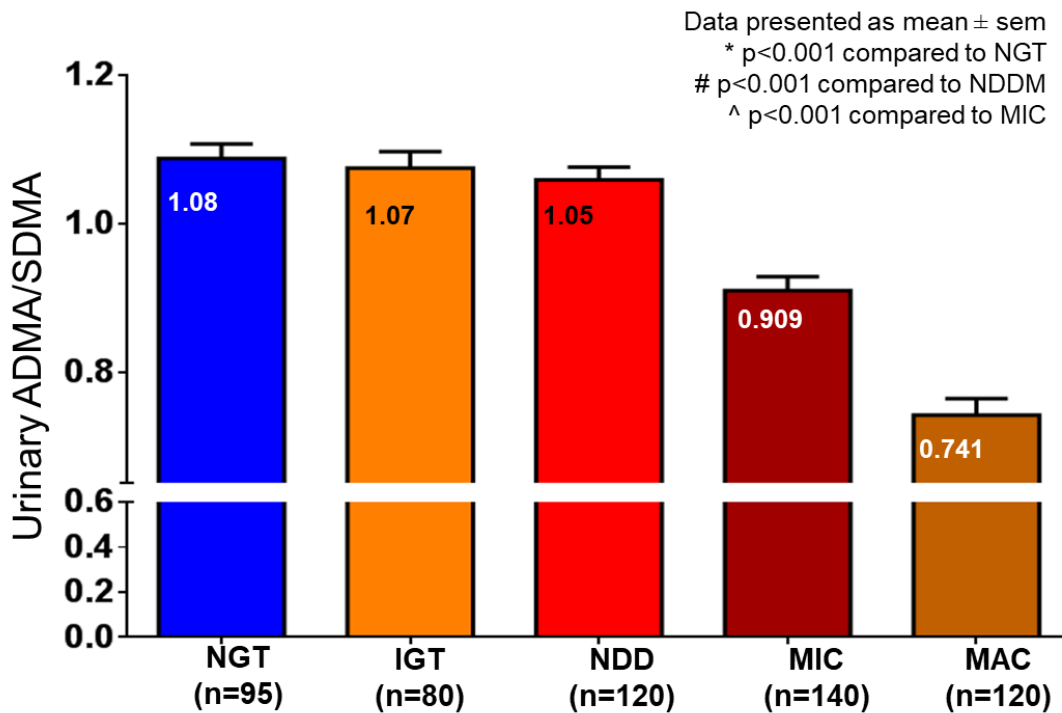
Figure 5.1 Category wise representation of ASR. A number of the candidates in each category has been shown.

To examine the influence of gender on the association of ASR with MIC and MAC, study subjects were stratified by gender. There were no significant differences in the ASR by gender in individuals with NDD, MIC, and MAC [Data not shown]. ASR was negatively correlated with age (p<0.001), systolic blood pressure (p<0.001), fasting plasma glucose (p=0.004) and glycated hemoglobin (p<0.001), total cholesterol (p<0.01), blood urea (p<0.001), serum creatinine (p<0.001) and microalbuminuria (p<0.001). ASR showed a positive correlation with HDL cholesterol (p<0.001) and eGFR (p<0.001) (Table 6.2)

Table 5.1 Clinical and biochemical characterization of study subjects.

Variables	NGT(n=95)	IGT(n=80)	NDD (n=120)	MIC (n=140)	MAC (n=120)
Male/Female	49/46	34/46	68/52	96/44	84/36
Age (years)	44 ± 10	48 ± 9.3	47 ± 10	54 ± 10 *#	56 ± 11*#
Waist circumference (cm)	90 ± 11.0	95 ± 11.0*	96 ± 10*	96 ± 11*	98 ± 10*
Body mass index (kg/m2)	27 ± 4.6	29 ± 7.0	28 ± 4.1	27 ± 4.3	27 ± 4.5
Systolic blood pressure (mmHg)	124 ± 16	125 ± 15	124 ± 16	136 ± 19*#	139 ± 18*#
Diastolic blood pressure (mmHg)	79 ± 11	79 ± 9.0	80 ± 9.0	82 ± 9.0*	81 ± 12^
Fasting plasma glucose (mg/dl)	90 ± 13	107 ± 23	175 ± 63*	179 ± 77*	182 ± 85*
HbA1c (%)	5.6 ± 0.4	6.1 ± 0.6	8.4 ± 2.2*	8.8 ± 2.0*	8.6 ± 2.2*
Total cholesterol (mg/dl)	178 ± 31	187 ± 37	197 ± 46*	169 ± 45#	173 ± 53#
Serum triglycerides (mg/dl)	127 ± 59	145 ± 85	169 ± 116	186 ± 115*	217 ± 188*#
Serum HDL cholesterol (mg/dl)	42 ± 9.3	42 ± 9.1	39 ± 9.0	37 ± 7.6*	38 ± 8.8*
Serum LDL cholesterol (mg/dl)	112 ± 25	118 ± 34	126 ± 42	96 ± 35 *#	94 ± 40 *#
Blood urea (mg/dl)	21 ± 5.2	21 ± 5.1	22 ± 6.1	27 ± 11*#	40 ± 23*#^
Serum creatinine (mg/dl)	0.72 ± 0.17	0.73 ± 0.16	0.76 ± 0.17	0.98 ± 0.33 *	1.5 ± 1.0*#^
eGFR (mL/min/1.73m^2)	107 ± 33	102 ± 23	102 ± 21	92 ± 31*#	63 ± 32*#^
Hypertension n (%)	8 (8.4)	21 (26.3)	37 (30.8)	81 (57.9)	88 (73.3)
Retinopathy n (%)	0	1 (1.3)	4 (3.3)	34 (24.3)	34 (28.3)
CAD n (%)	0	1 (1.3)	5 (4.2)	7 (5.0)	13 (10.8)
Insulin + OHA n (%)	0	0	0	82 (58.6)	99 (82.5)
OHA n (%)	0	0	0	58 (41.4)	21 (17.5)
Antihypertensive drug n (%)	6 (6.3)	16 (20.0)	32 (26.7)	75 (53.6)	81 (67.5)
Aspirin n (%)	0	0	5 (4.2)	10 (7.1)	16 (13.3)
Fenofibrate n (%)	7 (7.4)	11 (13.8)	26 (21.7)	34 (24.3)	27 (17.5)
Statin n (%)	16 (16.5)	28 (35.0)	52 (43.3)	89 (63.6)	77 (64.2)

**p<0.05 compared to NGT; # p<0.05 compared to NDD; ^ p<0.05 compared to MI*

Table 5.2 Correlation analysis of ASR with metabolic risk factors

	ADMA/SDMA	
	r-value	**p-value**
Age	-0.267	**p<0.001**
Body Mass Index	0.047	0.278
Waist	-0.091	0.056
Systolic blood pressure	-0.189	**p<0.001**
Diastolic blood pressure	0.001	0.981
Fasting plasma glucose	-0.136	**p= 0.004**
HbA1c	-0.176	**p<0.001**
Serum cholesterol	0.165	**p<0.001**
Serum triglycerides	-0.077	**0.088**
High density lipoprotein	0.161	**p<0.001**
Low density lipoprotein	0.214	**p<0.001**
Urea	-0.323	**p<0.001**
Creatinine	-0.321	**p<0.001**
eGFR	0.334	**p<0.001**
Microalbumin	-0.519	**p<0.001**

Table 5.3 Standardized polytomous logistic regression estimates for the risk of MIC and MAC

VARIABLES	NDD	MIC	MAC
	Ref.	OR (CI)	OR (CI)
ADMA/SDMA Ratio – Independent variable*			
ADMA/SDMA ratio unadjusted	1	0.307 (0.213 –0.444)*	0.138 (0.090 – 0.211)*
Model 1: Adjusted for age and gender	1	0.316 (0.213 – 0.468)*	0.147 (0.094 - 0.230)*
Model 2: Model 1 plus systolic, diastolic blood pressure and glycated hemoglobin		0.304 (0.196 – 0.473)*	0.145 (0.088 – 0.240)*
Model 3: Model 2 plus serum cholesterol, triglycerides, HDL and LDL cholesterol		0.287 (0.171 – 0.483)*	0.117 (0.064 – 0.215)*
Model 4: Model 3 plus Urea, Serum Creatinine, and eGFR		0.287 (0.162 – 0.508)*	0.152 (0.076 – 0.302)*

* $p<0.01$ compared to NDD
*per standard deviation changes in ADMA/SDMA

Standardized polytomous logistic regression analysis was performed with NDD as the dependent variable and ASR as the independent variable (Table 6.3). Every one standard deviation decrease in ASR was independently associated MIC [odds ratio (OR): 0.307, 95% confidence interval (CI): 0.213 – 0.444; $p<0.01$]. This association remained statistically significant even after adjusting for age, gender, blood pressure, glycated hemoglobin serum cholesterol, triglycerides, HDL and LDL cholesterol, Urea, serum Creatinine and eGFR [OR: 0.287; 95% CI: 0.162 – 0.508; $p<0.01$]. ASR was independently associated with MAC [OR per standard deviation: 0.138; 95% CI: 0.090 – 0.211; $p<0.01$]. Adjustment for age, gender, blood pressure, glycated hemoglobin serum cholesterol, triglycerides, HDL and LDL

cholesterol, Urea, serum Creatinine and eGFR did not substantially change the association between ASR and MAC [OR per standard deviation: 0.152; 95% CI: 0.076 – 0.302; p<0.01].
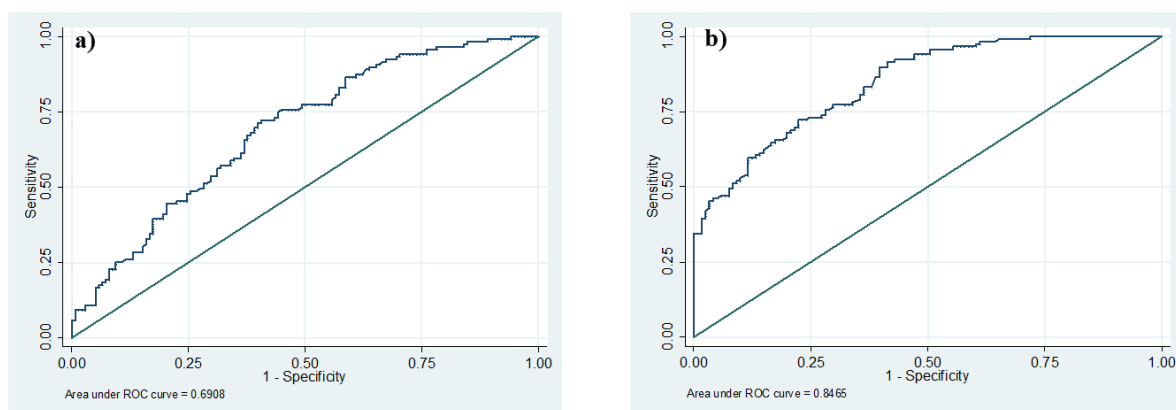
Sr.No	ASR cut point	Sensitivity	Specificity	PPV	NPV	LR +ve	LR-ve
Microalbuminuria							
1	0.95	0.72	0.60	60.5	71.30	1.78	0.43
Macroalbuminuria							
2	0.82	0.91	0.72	68.55	87.6	2.2	0.14

PPV-positive predictive value, NPV- negative predictive value, LR- likelihood ratio

Figure 5.2 ROC curves and details of sensitivity and specificity of ASR between individuals with (a) Microalbuminuria and (b) Macroalbuminuria.

Receiver operating characteristic curves (ROC) were constructed to derive the cut-point for ASR with the best sensitivity and specificity to identify MIC and MAC. Figure 6.2 shows the C statistic for the ASR in predicting MIC and MAC. An ASR cut-point of 0.95 had C statistic of 0.691 (95% CI: 0.627-0.755; p<0.001) indicating the high ability of ASR to discriminate MIC from NDD. The sensitivity and specificity of this ASR cut-off of ≥ 0.95 were 72% and 60%, respectively, for identifying patients with MIC. The positive predictive value was 60.5%, and the negative predictive value, 71.3%. An ASR cut-point of 0.82 had C statistic of 0.846 (95% CI: 0.800 - 0.893, p<0.001) had a sensitivity of 91% and specificity of 72%, for identifying MAC. The positive predictive and the negative predictive values were 68.5% and 87.6% respectively.

The natural history of DN is characterized by albuminuria, overt nephropathy, and eventually renal insufficiency with declining glomerular filtration rate (GFR), ultimately leading to ESRD.[26] We earlier reported that the prevalence of overt nephropathy and microalbuminuria was 2.2 and 26.9%, respectively in urban Asian Indians.[21] Studies have shown that low-grade albuminuria (microalbuminuria) is a poor predictor of diabetic nephropathy and high-grade albuminuria, which is a strong predictor of disease progression, only develops at advanced diabetic nephropathy, a stage when less can be done to prevent the development of end-stage kidney failure. It is, therefore, necessary to detect at an early stage of the condition to prevent the progression into overt nephropathy. Thus a sensitive biomarker could be helpful to detect earlier stages in the natural history of diabetes and this could be useful to prevent or delay the onset of nephropathy at an early stage. In this context, our study reports the following significant findings: 1) ASR is lower in patients with MIC and MAC compared to NGT or NDD. 2) ASR shows a significant inverse correlation with age, systolic blood pressure, blood urea, serum creatinine and microalbuminuria and positively correlated with HDL cholesterol and eGFR. 3) ASR is independently associated with higher risk of MIC and MAC even after adjusting for other risk variables known to be associated with nephropathy. 4) An ASR cut-points of 0.95 and 0.82 had a best sensitivity and specificity for identifying MIC and MAC respectively among Asian Indians.

ADMA and SDMA are important disease markers implicated in clinical findings across a spectrum of diseases that include cardiovascular, renal disorders, hypertension and diabetes [27–30] ADMA and SDMA, having a nominal mass of 203, are generated as a consequence of the protein methylation biosynthetic pathway and subsequent hydrolysis. Both ADMA and SDMA are released during the proteolytic breakdown of nuclear proteins and both have been studied as biomarkers for kidney disease.[31,32] SDMA is primarily excreted through the kidney and is strongly associated with renal function.[33] ADMA to SDMA ratio (ASR), also known as catabolism index, has been implicated in hypertension, malnutrition, and inflammation.[34–36] A direct correlation between malnutrition, the inflammatory marker C-reactive protein, and the ASR was also established in patients undergoing hemodialysis.[36] In this context, the decreased ASR in patients with MIC and MAC in our study is an important finding. Additionally, our data suggest that an ASR cut-point of 0.95 and 0.82 could be used to correctly identify 72% of MIC and 91% of MAC respectively in this Asian Indian population.

Clinical trial studies that included patients with diabetic and non-diabetic CKD (chronic kidney disease) have demonstrated an association of ADMA and SDMA levels with declining renal function after stratification of patients according to glomerular filtration rate. The prognostic value of ADMA in patients with CKD has been evaluated by Fliser et al., in the 'Mild to Moderate Kidney Disease Study' and reported that plasma ADMA levels were the independent predictor of progression of renal disease. [37] Similar findings were made by Ravani et al., in which ADMA emerged as an independent predictor of progression to dialysis. [38] These studies support the potential role of ADMA and SDMA to predict the severity of renal disease. In this context, we found a negative correlation between ASR and glycemic parameters including fasting glucose and Glycated hemoglobulin. This supports our hypothesis that an increase in glucose can cause kidney injury and in turn, leads to the decrease in ASR. The inverse correlation between ASR and established kidney injury markers such as serum creatinine and microalbuminuria suggests a diagnostic as well as the prognostic value of ASR. The significant positive correlation of ASR with eGFR also substantiates the role of ASR in assessing diabetic kidney injury. Interestingly, the association of ASR with MIC or MAC is significant even after adjusting the conventional risk factors for diabetic nephropathy and emphasizes a potential risk factor role of ASR. Decreased ASR may, therefore, represent a biomarker for MIC and MAC but this needs to be confirmed by longitudinal studies. Identification of new biomarkers such as ASR would open up new avenues for assessing progressive diabetic nephropathy and our work is a proof of concept in this direction.

5.4 Conclusion

Direct estimation of the ASR overcomes the inherent challenges of metabolite variations in urine samples and allows for comparisons to be made across disease conditions. We report that in Asian Indians, the ASR profile is lower in MIC and MAC suggesting that it has the potential to be used as an early diagnostic marker for MIC or MAC. ASR cut-points of 0.95 and 0.82 could be used to correctly identify 72% of MIC and 91% of MAC respectively among Asian Indians a population which is currently the epicenter of the global diabetes epidemic. Further prospective studies are needed to understand the mechanisms that contribute to decreased ASR and the factors that could be beneficially used to neutralize their cellular action both from the

prevention aspect as well as for novel therapeutic measures in the management of diabetic nephropathy.

To our knowledge, this is the first report that measures the urinary DMA distribution from different stages of diabetes. The strengths of the study are that the cases (MIC, MAC/NDD) and IGT and controls (NGT) were classified using standard methods. One of the limitations of this study is that being a cross-sectional study, no cause and effect relationship between ASR and NDD, MIC or MAC could be established, for which prospective studies are needed. Furthermore, while the ASR cut-points of 0.95 and 0.82 may be useful in South Asians, this cut points may well differ in other ethnic groups. The current study is a proof of concept demonstrating the method using a cross-sectional cohort. To translate the findings into a meaningful diagnostic test or to help understand the underlying disease mechanisms, prospective studies with clinical follow up are indeed necessary. The study nevertheless showcases the robustness of the high throughput method for any prospective studies that often span longer durations of investigations.

5.5 References

(1)   Brancati, F. L.; Whelton, P. K.; Randall, B. L.; Neaton, J. D.; Stamler, J.; Klag, M. J. Risk of End-Stage Renal Disease in Diabetes Mellitus: A Prospective Cohort Study of Men Screened for MRFIT. *Jama* **1997**, *278* (23), 2069–2074.

(2)   Gregg, E. W.; Cheng, Y. J.; Srinivasan, M.; Lin, J.; Geiss, L. S.; Albright, A. L.; Imperatore, G. Trends in Cause-Specific Mortality among Adults with and without Diagnosed Diabetes in the USA: An Epidemiological Analysis of Linked National Survey and Vital Statistics Data. *Lancet* **2018**, *391*, 2430–2440.

(3)   Stehouwer, C. D. a; Henry, R. M. a; Dekker, J. M.; Nijpels, G.; Heine, R. J.; Bouter, L. M. Microalbuminuria Is Associated with Impaired Brachial Artery, Flow-Mediated Vasodilation in Elderly Individuals without and with Diabetes: Further Evidence for a Link between Microalbuminuria and Endothelial Dysfunction - The Hoorn Study. *Kidney Int. Suppl.* **2004**, *66* (92), 42–44.

(4)   Perkins, B. A.; Ficociello, L. H.; Ostrander, B. E.; Silva, K. H.; Weinberg, J.; Warram, J. H.; Krolewski, A. S. Microalbuminuria and the Risk for Early Progressive Renal Function Decline in Type 1 Diabetes. *J. Am. Soc. Nephrol.* **2007**, *18*, 1353–1361.

(5)   Kakimoto, Y.; Akazawa, S. Isolation and Identification and Hydroxylysine from Human of NG3 NG- and NG3 WG-Dimethyl- Urine. *J. Biol. Chem.* **1970**, *245* (21), 5751–5758.

(6)   Markiw, R. T. Isolation of N-Methylated Basic Amino Acids from Physiological Fluids and Protein Hydrolysates. *Biochem. Med.* **1975**, *13* (1), 23–27.

(7)   Palm, F.; Onozato, M. L.; Luo, Z.; Wilcox, C. S. Dimethylarginine Dimethylaminohydrolase (DDAH): Expression, Regulation, and Function in the Cardiovascular and Renal Systems. *Am. J. Physiol. Heart Circ. Physiol.* **2007**, *293* (6), H3227-45.

(8)   Zakrzewicz, D.; Eickelberg, O. From Arginine Methylation to ADMA: A Novel Mechanism with Therapeutic Potential in Chronic Lung Diseases. *BMC Pulm. Med.* **2009**, *9*, 1–7.

(9)   Bode-Böger, S. M.; Scalera, F.; Kielstein, J. T.; Martens-Lobenhoffer, J.; Breithardt, G.; Fobker, M.; Reinecke, H. Symmetrical Dimethylarginine: A New Combined Parameter for Renal Function and Extent of Coronary Artery Disease. *J. Am. Soc. Nephrol.* **2006**, *17* (4), 1128–1134.

(10)   Tran, C. T. .; Leiper, J. M.; Vallance, P. The DDAH/ADMA/NOS Pathway. *Atheroscler. Suppl.* **2003**, *4* (4), 33–40.

(11)   Davids, M.; Richir, M. C.; Visser, M.; Ellger, B.; Van Den Berghe, G.; Van Leeuwen, P. A. M.; Teerlink, T. Role of Dimethylarginine Dimethylaminohydrolase Activity in Regulation of Tissue and Plasma Concentrations of Asymmetric Dimethylarginine in an Animal Model of Prolonged Critical Illness. *Metabolism.* **2012**, *61* (4), 482–490.

(12)   Shibata, R.; Ueda, S.; Yamagishi, S. I.; Kaida, Y.; Matsumoto, Y.; Fukami, K.; Hayashida, A.; Matsuoka, H.; Kato, S.; Kimoto, M.; et al. Involvement of Asymmetric Dimethylarginine (ADMA) in Tubulointerstitial Ischaemia in the Early Phase of Diabetic Nephropathy. *Nephrol. Dial. Transplant.* **2009**, *24* (4), 1162–1169.

(13)   Schlesinger, S.; Sonntag, S. R.; Lieb, W.; Maas, R. Asymmetric and Symmetric Dimethylarginine as Risk Markers for Total Mortality and Cardiovascular Outcomes: A Systematic Review and Meta-Analysis of Prospective Studies. *PLoS One* **2016**, *11* (11), 1–26.

(14)   Willeit, P.; Freitag, D. F.; Laukkanen, J. A.; Chowdhury, S.; Gobin, R.; Mayr, M.; Di Angelantonio, E.; Chowdhury, R. Asymmetric Dimethylarginine and Cardiovascular Risk: Systematic Review and Meta-Analysis of 22 Prospective Studies. *J. Am. Heart Assoc.* **2015**, *4* (6), e001833.

(15)   Carnegie, P. R.; Fellows, F. C. I.; Symington, G. R. Urinary Excretion of Methylarginine in Human Diseases. *Metabolism* **1977**, *26* (May), 531–537.

(16)   Lou, M. F. Human Muscular Dystrophy: Elevation of Urinary Dimethylarginines. *Science (80-*

.). **1979**, *203* (4381), 668–670.

(17) MacAllister, R. J.; Rambausek, M. H.; Vallance, P.; Williams, D.; Hoffmann, K. H.; Ritz, E. Concentration of Dimethyl-L-Arginine in the Plasma of Patients with End-Stage Renal Failure. *Nephrol Dial.Transplant.* **1996**, *11* (0931–0509 (Print)), 2449–2452.

(18) Anjana, R. M.; Pradeepa, R.; Deepa, M.; Datta, M.; Sudha, V.; Unnikrishnan, R.; Bhansali, A.; Joshi, S. R.; Joshi, P. P.; Yajnik, C. S.; et al. Prevalence of Diabetes and Prediabetes (Impaired Fasting Glucose and/or Impaired Glucose Tolerance) in Urban and Rural India: Phase i Results of the Indian Council of Medical Research-INdia DIABetes (ICMR-INDIAB) Study. *Diabetologia* **2011**, *54* (12), 3022–3027.

(19) Unnikrishnan, R.; Anjana, R. M.; Mohan, V. Diabetes Mellitus and Its Complications in India. *Nat. Rev. Endocrinol.* **2016**, *12* (6), 357–370.

(20) Anand, S.; Shivashankar, R.; Ali, M. K.; Kondal, D.; Binukumar, B.; Montez-Rath, M. E.; Ajay, V. S.; Pradeepa, R.; Deepa, M.; Gupta, R.; et al. Prevalence of Chronic Kidney Disease in Two Major Indian Cities and Projections for Associated Cardiovascular Disease. *Kidney Int.* **2015**, *88* (1), 178–185.

(21) Unnikrishnan, R. I.; Rema, M.; Pradeepa, R.; Deepa, M.; Shanthirani, C. S.; Deepa, R.; Mohan, V. Prevalence and Risk Factors of Diabetic Nephropathy in an Urban South Indian Population: The Chennai Urban Rural Epidemiology Study (CURES 45). *Diabetes Care* **2007**, *30* (8), 2019–2024.

(22) Deepa, M.; Pradeepa, R.; Rema, M.; Mohan, A.; Deepa, R.; Shanthirani, S.; Mohan, V. The Chennai Urban Rural Epidemiology Study (CURES) - Study Design and Methodology (Urban Component) (CURES - 1). *J. Assoc. Physicians India* **2003**, *51* (SEP), 863–870.

(23) Levey, A. S.; Stevens, L. A.; Schmid, C. H.; Zhang, Y. L.; Castro, A. F.; Feldman, H. I.; Kusek, J. W.; Eggers, P.; Van Lente, F.; Greene, T.; et al. A New Equation to Estimate Glomerular Filtration Rate. *Ann. Intern. Med.* **2009**, *150* (9), 604–612.

(24) Alberti, K. G. M. M.; Zimmet, P. Z. Definition, Diagnosis and Classification of Diabetes Mellitus and Its Complications. Part 1: Diagnosis and Classification of Diabetes Mellitus Provisional Report of a WHO Consultation. *Diabet. Med.* **1998**, *15* (7), 539–553.

(25) Hanley, A. J.; McNeil, J. B. The Meaning and Use of the Area under a Receiver Operating Characteristic (ROC) Curve. *Radiology* **1982**, *143*, 29–36.

(26) Chowdhury, T. a; Barnett, a H.; Bain, S. C. Pathogenesis of Diabetic Nephropathy. *Trends Endocrinol. Metab.* **1996**, *7* (9), 320–323.

(27) Surdacki, A.; Kruszelnicka, O.; Rakowski, T.; Jaźwińska-Kozuba, A.; Dubiel, J. S. Asymmetric Dimethylarginine Predicts Decline of Glucose Tolerance in Men with Stable Coronary Artery Disease: A 4.5-Year Follow-up Study. *Cardiovasc. Diabetol.* **2013**, *12* (1), 1–9.

(28) Wolf, C.; Lorenzen, J. M.; Stein, S.; Tsikas, D.; Störk, S.; Weidemann, F.; Ertl, G.; Anker, S. D.; Bauersachs, J.; Thum, T. Urinary Asymmetric Dimethylarginine (ADMA) Is a Predictor of Mortality Risk in Patients with Coronary Artery Disease. *Int. J. Cardiol.* **2012**, *156* (3), 289–294.

(29) Ueda, S.; Yamagishi, S.-I.; Kaida, Y.; Okuda, S. Asymmetric Dimethylarginine May Be a Missing Link between Cardiovascular Disease and Chronic Kidney Disease (Review Article). *Nephrology* **2007**, *12* (6), 582–590.

(30) Scott, J. A.; North, M. L.; Rafii, M.; Huang, H.; Pencharz, P.; Subbarao, P.; Belik, J.; Grasemann, H. Asymmetric Dimethylarginine Is Increased in Asthma. *Am. J. Respir. Crit. Care Med.* **2011**, *184* (7), 779–785.

(31) Siegerink, B.; Maas, R.; Vossen, C. Y.; Schwedhelm, E.; Koenig, W.; Böger, R.; Rothenbacher, D.; Brenner, H.; Breitling, L. P. Asymmetric and Symmetric Dimethylarginine and Risk of Secondary Cardiovascular Disease Events and Mortality in Patients with Stable Coronary Heart Disease: The KAROLA Follow-up Study. *Clin. Res. Cardiol.* **2013**, *102* (3), 193–202.

(32) Gore, M. O.; Lüneburg, N.; Schwedhelm, E.; Ayers, C. R.; Anderssohn, M.; Khera, A.; Atzler,

D.; De Lemos, J. A.; Grant, P. J.; McGuire, D. K.; et al. Symmetrical Dimethylarginine Predicts Mortality in the General Population: Observations from the Dallas Heart Study. *Arterioscler. Thromb. Vasc. Biol.* **2013**, *33* (11), 2682–2688.

(33)   Meinitzer, A.; Kielstein, J. T.; Pilz, S.; Drechsler, C.; Ritz, E.; Boehm, B. O.; Winkelmann, B. R.; März, W. Symmetrical and Asymmetrical Dimethylarginine as Predictors for Mortality in Patients Referred for Coronary Angiography: The Ludwigshafen Risk and Cardiovascular Health Study. *Clin. Chem.* **2011**, *57* (1), 112–121.

(34)   Hsu, C. N.; Huang, L. T.; Lau, Y. T.; Lin, C. Y.; Tain, Y. L. The Combined Ratios of L-Arginine and Asymmetric and Symmetric Dimethylarginine as Biomarkers in Spontaneously Hypertensive Rats. *Transl. Res.* **2012**, *159* (2), 90–98.

(35)   Iapichino, G.; Umbrello, M.; Albicini, M.; Spanu, P.; Bellani, G.; Polli, F.; Pavlovic, R.; Cugno, M.; Fermo, I.; Paroni, R. Alpha-Keto-Beta-Methyl-n-Valeric Acid Diminishes Reactive Oxygen Species and Alters Endoplasmic Reticulum Ca(2+) Stores. *Minerva Anestesiol.* **2010**, *76* (5), 325–333.

(36)   Cupisti, A.; Saba, A.; D'Alessandro, C.; Meola, M.; Panicucci, E.; Panichi, V.; Raffaelli, A.; Barsotti, G. Dimethylarginine Levels and Nutritional Status in Hemodialysis Patients. *J. Nephrol.* **2009**, *22* (5), 623–629.

(37)   Fliser, D. Asymmetric Dimethylarginine and Progression of Chronic Kidney Disease: The Mild to Moderate Kidney Disease Study. *J. Am. Soc. Nephrol.* **2005**, *16* (8), 2456–2461.

(38)   Ravani, P. Asymmetrical Dimethylarginine Predicts Progression to Dialysis and Death in Patients with Chronic Kidney Disease: A Competing Risks Modeling Approach. *J. Am. Soc. Nephrol.* **2005**, *16* (8), 2449–2455.